



UNIVERSITÀ
DI SIENA
1240

UNIVERSITY OF SIENA
DEPARTMENT OF BIOTHECNOLOGY, CHEMISTRY AND
PHARMACY

DOCTORATE IN
CHEMICAL AND PHARMACEUTICAL SCIENCES
XXXIV Cycle

COORDINATOR: Prof. Maurizio Taddei

**TOWARDS STRUCTURE DETERMINATION OF PROTEIN-LIGAND
COMPLEXES OF TrkA AND TrkB RECEPTORS:
from protein production to crystal optimization**

SSD: CHIM/03

TUTOR:

Prof. Stefano Mangani

CO-TUTOR:

Prof. Cecilia Pozzi

CANDIDATE:
Federica Carucci

ACCADEMIC YEAR: 2022-2033

CONTENTS

ABBREVIATIONS	5
1. INTRODUCTION	9
1.1. NEUROTROPHINS AND NEUROTROPHIN RECEPTOR: GENERAL OVERVIEW.....	9
1.2. NEUROTROPHINS BIOSYNTHESIS AND STRUCTURE	11
1.3. STRUCTURE OF TRK RECEPTORS.....	14
1.4. TRKS ACTIVATION MECHANISM	18
1.5. SIGNALING PATHWAYS VIA TRK RECEPTORS	19
2. THESIS OVERVIEW AND OBJECTIVES	23
3. THE D5 DOMAIN OF TRKA AND TRKB RECEPTORS.....	25
3.1. PRODUCTION OF TRKA D5 DOMAIN: MATERIAL AND METHODS.....	25
3.1.1. <i>Construct design</i>	25
3.1.2. <i>Transformation</i>	27
3.1.3. <i>Expression and purification of pMAL-c5E/TrkA d5</i>	28
3.1.4. <i>Expression test pET-28a(+)-TEV/TrkA d5</i>	30
3.1.5. <i>Expression and purification of His₆-TrkA-d5</i>	32
3.1.6. <i>Expression and purification of NMR-TrkA-d5 construct</i>	36
3.1.7. <i>Circular dichroism spectroscopy</i>	37
3.2. PRODUCTION OF TRKA D5 DOMAIN: RESULTS	38
3.2.1. <i>Expression and purification of MBP-TrkA-d5 construct</i>	38
3.2.2. <i>His₆-TrkA-d5 expression tests</i>	42
3.2.3. <i>His₆-TrkA-d5 purification</i>	47
3.2.4. <i>Expression and purification of NMR-TrkA-d5 construct</i>	54
3.3. PRODUCTION OF TRKB D5 DOMAIN: MATERIAL AND METHODS.....	57
3.3.1. <i>Construct design</i>	57
3.3.2. <i>TrkB-d5 and BDNF co-expression tests</i>	57
3.3.3. <i>Expression and purification of TrkB-d5 and BDNF</i>	58
3.3.4. <i>Mass spectrometry and circular dichroism analysis</i>	59
3.3.5. <i>Crystallization screen of TrkB-d5</i>	59
3.4. PRODUCTION OF TRKB D5 DOMAIN: RESULTS	60
3.4.1. <i>TrkB-d5 and BDNF co-expression tests</i>	60
3.4.2. <i>Expression and purification of TrkB-d5 and BDNF</i>	62
4. THE EXTRACELLULAR DOMAIN OF TRKA AND TRKB RECEPTORS	70

4.1.	PRODUCTION OF TRKA AND TRKB ECTODOMAINS: MATERIAL AND METHODS	70
4.1.1.	<i>Gibson Cloning</i>	70
4.1.2.	<i>Transient transfection of TrkA and TrkB in mammalian cells</i>	72
4.1.3.	<i>Purification of TrkA and TrkB ectodomains</i>	73
4.1.4.	<i>In vitro deglycosylation</i>	73
4.1.5.	<i>Size exclusion chromatography</i>	74
4.1.6.	<i>Neurotrophin and Trk receptors complexes purification</i>	74
4.2.	PRODUCTION OF TRKA AND TRKB ECTODOMAINS: RESULTS	75
4.2.1.	<i>Gibson Cloning</i>	75
4.2.2.	<i>Expression and purification of TrkA-ECD and TrkB-ECD</i>	80
4.2.3.	<i>In vitro deglycosylation</i>	85
4.2.4.	<i>Neurotrophin and Trk receptors complexes purification</i>	89
4.3.	CRYSTALLOGRAPHY	94
4.3.1.	<i>TkA-NGF and TrkB-BDNF complexes crystallization screening</i>	94
4.3.2.	<i>Co-crystallization screening</i>	98
4.4.	CRYO ELECTRON MICROSCOPY	101
4.5.	GRATING COUPLED INTERFEROMETRY.....	104
5.	CONCLUDING REMARKS	108
	BIBLIOGRAPHY	112

ABBREVIATIONS

Abs280	Absorbance at 280 nm
Amp	ampicillin
ATP	adenosine triphosphate
BDNF	brain-derived neurotrophic factor
BDNFpd	BDNF pro-domain
CD	circular dichroism
Ch1	channel 1
Ch2	channel 2
CNS	central nervous system
CREB	cyclic adenosine monophosphate response-element binding protein
Cryo EM	Cryo Electron Microscopy
CVs	column volumes
DAG	diacylglycerol
DMSO	dimethyl sulfoxide
ECD	extracellular domain
eJTM	extracellular juxtamembrane
Ek	Enterokinase
ESI-MS	electron-spray ionization mass spectrometry
EtOH	ethanol
FBS	fetal bovine serum
FRS2	fibroblast receptor substrate-2
GCI	Grating Coupled Interferometry
GSH	reduced L-glutathione
GSSG	oxidized L-glutathione

Hek293	Human embryonic kidney 293
IBs	inclusion bodies
ICD	intracellular domain
IDPs	intrinsically disordered proteins
IP3	inositol trisphosphate
IPTG	isopropyl β -D-1-thiogalactopyranoside
kan	kanamycin
LB	Luria Bertani
MBP	maltose binding protein
MCS	multiple cloning site
MMS	microseeding matrix screening
MWCO	molecular weight cut off
NGF	nerve growth factor
NGFpd	NGF pro-domain
NMR	nuclear magnetic resonance
NS	negative stain
NT	neurotrophin
NT3	neurotrophin 3
NT4-5	neurotrophin 4
NTRK	neurotrophin receptor
OD ₆₀₀	optical density at 600 nm
PBS-T	PBS Tween buffer
PCR	polymerase chain reaction
PEG	polyethylene glycol
PEI	polyethilenimine
PI3K	phosphoinositide 3-kinase
PKC	protein kinase C

PLC γ	phospholipase-C γ
PNS	peripheral nervous system
PTB	phosphotyrosine-binding
PtdIns(4,5)P ₂	phosphatidylinositol 4,5-bisphosphate
PTM	post-translational modification
pY	phosphotyrosine residue
RTK	tyrosine kinase receptor
SB	super broth
SDS-PAGE	sodium dodecyl sulphate polyacrylamide gel electrophoresis
SH2	Src-homology-2
Shc	Src homology collagen-like
SPR	surface plasmon resonance
STD NMR	saturation transfer difference NMR
TAE	tris-acetate EDTA
TEM	transmission electron microscopy
TMD	transmembrane domain
Trk	tropomyosin kinase receptors
WB	Western blot

1. Introduction

This chapter will provide an overview of the current knowledge on neurotrophins and neurotrophin receptors, highlighting the structure-function relationships of the tropomyosin kinase receptors (Trk), their central role in neurobiology, and how their dysregulation is related to the pathogenesis of many neurodegenerative diseases, making the neurotrophin-Trk system an attractive target for the development of new drugs.

1.1. Neurotrophins and Neurotrophin receptor: general overview

In the late 1950s, nerve growth factor (NGF) was identified by Rita Levi Montalcini as “growth promoting material” able to induce “exceptional outgrowth of nerve fibers”^{1,2} in sensory and sympathetic ganglia of chick embryos. Starting from this discovery, other members of the neurotrophin family were found, consisting of brain-derived neurotrophic factor (BDNF)³, neurotrophin 3 (NT3)⁴, and neurotrophin 4 (NT4-5)^{5,6}.

Neurotrophins (NTs) are key growth factors in both central and peripheral nervous system (CNS, PNS), that promotes neuronal proliferation, differentiation and survival, as well as cellular apoptosis and synaptic plasticity, in distinct but overlapping neuronal populations. In addition, tissue-specific neurotrophin expression outside the nervous system has been shown in bladder, cardio and myocytes, mammalian ovary and B lymphocytes^{7,8,9,10}.

Once released in the synaptic cleft, as either autocrine and paracrine factors, neurotrophins implement their pleiotropic effects through binding to two distinct receptors. On one side, the tropomyosin kinase receptors are single-pass transmembrane receptors with intrinsic catalytic activity, which activation upon neurotrophin binding generally mediates pro-survival signals¹¹. The Trks family includes TrkA, TrkB, and TrkC receptors that selectively interact with specific cognate neurotrophin, resulting in the following signaling pairs: TrkA and NGF, TrkB and BDNF or NT4, TrkC and NT3¹² (figure 1.1).

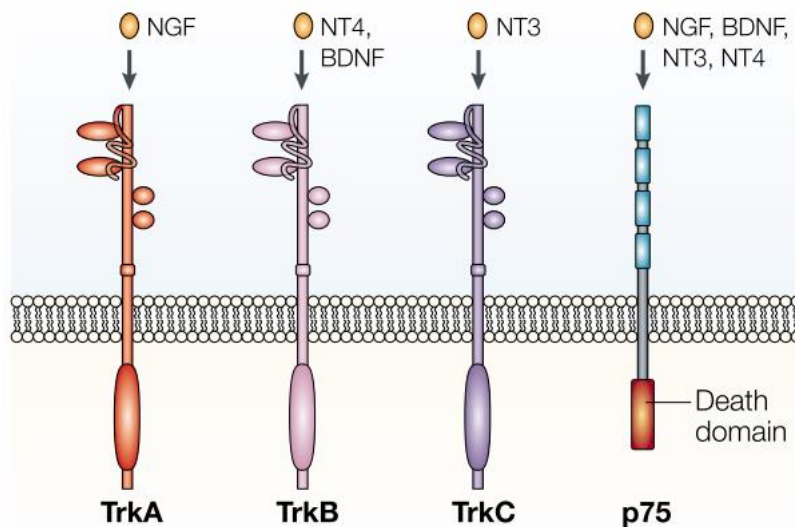


Figure 1.1. Neurotrophin and Neurotrophin receptors. Schematic illustration of the neurotrophin and neurotrophin receptors pairs. Neurotrophins selectively bind the tropomyosin kinase receptors (TrkA, TrkB and TrkC), forming NGF-TrkA, TrkB-BDNF or NT4 and TrkC-NT3 signaling systems, as well as promiscuously activate the common receptor p75, which intracellular death domain initiates apoptotic cascades. Figure taken from Chao et al, 2003¹².

However, some promiscuity exists, as NT-3 can also bind to TrkA and TrkB isoforms, that contain an additional short insert in the extracellular juxtamembrane¹³. On the other side the p75 neurotrophin receptor, a member of tumor necrosis factor superfamily, consists of a death domain in the intracellular domain, which activation leads to pro-apoptotic cascades¹⁴.

Depending on the differentiation, cellular stage, as well as neuronal populations, the specific expression level of the NTs and their receptors determines the signaling pathways activated, finely regulating the balance between trophic and apoptotic signals, critical for the functionality and maintenance of the nervous system. Dysregulation of this homeostasis results in pathological conditions, neuropsychiatric and neurodegenerative diseases, such as Alzheimer's^{15,16}, Parkinson's¹⁷, Multiple Sclerosis¹⁸ and depression¹⁹, schizophrenia²⁰ and bipolar disorders²¹. In addition, chromosomal rearrangements²² or mutations²³ of Trk genes (NTRKs) are involved in the oncogenesis of different carcinomas, as well as increased receptors surface expression correlates with proliferation, aggressiveness and metastasis in many cancers, such as brain tumors²⁴, glioblastoma²⁵ and lung adenocarcinomas²⁶.

1.2. Neurotrophins biosynthesis and structure

Neurotrophins are synthesized as pre-proneurotrophin precursors, that are progressively processed in mature forms²⁷. At the N-terminal, a 18 amino acids signal peptide for protein secretion (24 in NT4) drives the nascent polypeptide chain from the rough endoplasmic reticulum into the Golgi apparatus, where post-translational modifications occur, such as signal peptide cleavage and N-glycosylation at asparagine residues (Asn, N) of pro-domains^{28,29} (highlighted in orange in Figure 1.2).

The pro-domains act as intramolecular chaperons and are pivotal for proper protein folding. Indeed, studies showed that the pro-domain of NGF increases the protein yields during *in vitro* refolding³⁰, shielding hydrophobic patches of folding intermediates and assisting the mature neurotrophin fold formation (see below), as well as mutagenesis of the pro-domain sequence prevents maturation of biologically active NGF³¹. Moreover, it has been recently shown that the Asn127 residue of BDNF pro-domain is glycosylated with rare glycans modified by terminal sulfation²⁹, as well as Asn148 of NGF pro-domain²⁸, and inhibition of such post-translational modifications prevents the intracellular maturation and neurotrophin secretion.

After signal peptide cleavage, the pro-neurotrophins (proNTs) are trafficked to the trans Golgi network and in turn cleaved into the mature forms by furin and proconvertase at a highly conserved dibasic motif^{32,33}. The proteolytical cleavage can take place extracellularly by plasmin and matrix metalloproteinases³⁴ and secreted proNTs can act as ligands *per se*, forming ternary complexes with sortilin and the p75 receptors, which activation induces cell death^{35,36}.

Additionally, recent studies showed independent activity of the pro-domains³⁷ (NGFpd, BDNFpd), that together with mature and proNTs are stored in dense vesicles in the presynaptic terminals³⁸ and released in an activation dependent manner^{39,40}.

Nuclear magnetic resonance (NMR) spectroscopy studies revealed a intrinsically disordered structure of both NGFpd⁴¹ and BDNFpd⁴², that undergoes onto transient α -helices structures, while *in vitro* experiment showed intrinsic activity of the NGF and BDNF pro-domains, able to induced growth cone retraction of hippocampal neurons, and hence suggesting a potential role in morphological organization of synaptic networks.

The four mature neurotrophins share an overall sequence identity of about 50%, where the conserved residues are predominantly in homologous secondary structures, forming the characteristic neurotrophic fold (Figure 1.2).



Figure 1.2. Alignment of the human pre-proneurotrophin sequences and structure of neurotrophin protomer. **A)** Sequences of human NGF, BDNF, NT3 and NT4 align by ClustalΩ. The N-terminal signal peptides are shown in light pink, the glycosylated asparagine residues of the pro-domains are highlighted in orange, while in yellow and green are shown the residues forming the β-strands scaffold and the cysteine-knot motif, respectively. **B)** Crystal structure of NGF protomer⁴³ (PDB: 1BET) showing the cysteine knot in gold and the orientation of loop 3 (L3), N- and C-termini. Image created with PyMol Molecular Graphics System, Version 2.0 Schrcrödinger, LL.

Although BDNF-NT3 and BDNF-NT4⁴⁴ heterodimers have been formed *in vitro* and structurally characterized by x-ray crystallography, their physiological role has not been investigated and generally native neurotrophins fold in symmetrical homodimers. Each protomer consists in two antiparallel pairs of twisted β-strands in an elongated shape, stabilized by a cysteine-knot motif of three highly conserved disulfide bonds (Figure 1.2). The two monomers interface by hydrogen bonds and side-chain interactions between conserved hydrophobic residues in the β-strands, compacting around a central twofold axis (Figure 1.3).

A neurotrophin dimer forms a quaternary complex with the extracellular domain of two single-pass transmembrane Trk receptors, more specifically with the immunoglobulin-like II or so called d5 sub-domains, that mutagenesis and deletion studies showed to be necessary and sufficient for neurotrophin binding^{45,46}.

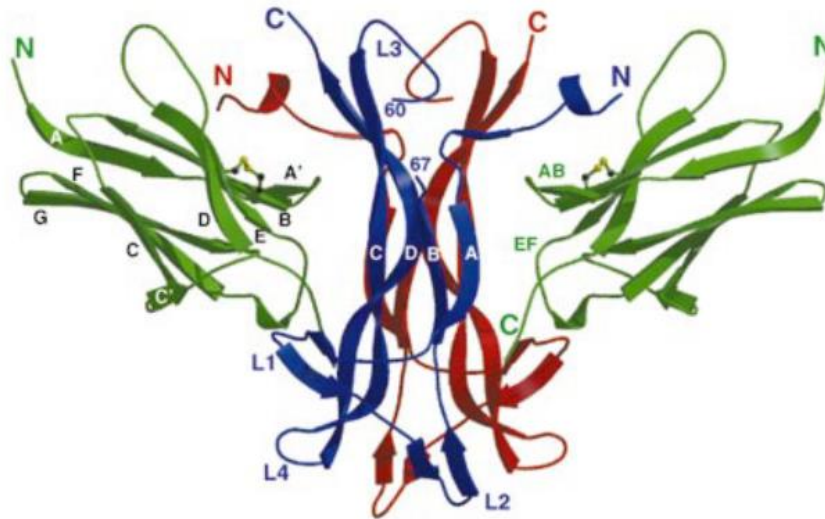


Figure 1.3. Crystal structure of NGF and TrkA-d5 complex. The complex is formed by the NGF dimer interacting with the d5 subdomains of two TrkA receptors. The protomers of the NGF homodimer are shown in red and blue, while the two TrkA-d5 are shown in green. The orientation of L3 NGF loop, the N- and C-termini of both NGF and TrkA-d5 dimers are reported, as well as the β -strands nomenclature. Image of 1WWW PDB entry taken from Wiesmann et al, 1999⁴⁷.

As shown in the crystal structures of the complex between NGF and TrkA receptor⁴⁷, the elongated NGF dimer is oriented with the N and C termini and the loop 3 (L3) on the opposite side of the plasma membrane, facing the N-terminal region of the TrkA receptor. The interaction with the d5 domains takes place through two distinct patches, a conserved patch of residues protruding from the central β -sheet scaffold, and a specificity patch in the flexible loop regions, consisting of residues with a low degree of conservation, whose interactions confer the binding selectivity. Particularly, the specificity patches takes highly specific contacts with the N-terminal of neurotrophin leading to ordering these disordered regions. For instance, upon α -helix formation of NGF N-terminal residues, the side chain of a Isoleucine residue (Ile 6) is accommodated into an hydrophobic pocket of TrkA-d5 surface, while the same pocket is less

hydrophobic in TrkB-d5, by the substitution of valine and methionine residues (294 and 296 in TrkA-d5) in threonine and aspartate residues (296 and 298 in TrkB-d5), forming in contrast a specific salt bridge with an arginine residue of NT-4/5 in the same location⁴⁸

1.3. Structure of Trk receptors

The Trk receptors are a subfamily of tyrosine kinase receptor (RTK) that share a common architecture, consisting of an extracellular domain (ECD), followed by extracellular juxtamembrane linker (eJTM), a single pass transmembrane domain (TMD) and an intracellular domain (ICD) with intrinsic kinase activity (Figure 1.4).

The extracellular or ectodomain consists of about 120 amino acid residues, folded in three leucin-rich repeats flanked by two cysteine-rich clusters (called d1 - d3 domains) and two immunoglobulin-like II domains (d4 and d5 domains). It is heavily glycosylated and the glycans moieties seem to be important for both receptor activity and structural integrity, packing inside interdomains grooves⁴².

As previously described, the neurotrophin homodimer binds the Trk receptors in a 2:2 stoichiometry through interactions with the d5 domains and, as shown in the crystal structure of the whole ectodomain of TrkA^{46,49}, the overall structure resembles a crab-shape, where the NGF dimer composes the core body, while the two TrkA extracellular domains the pinchers (Figure 1.4).

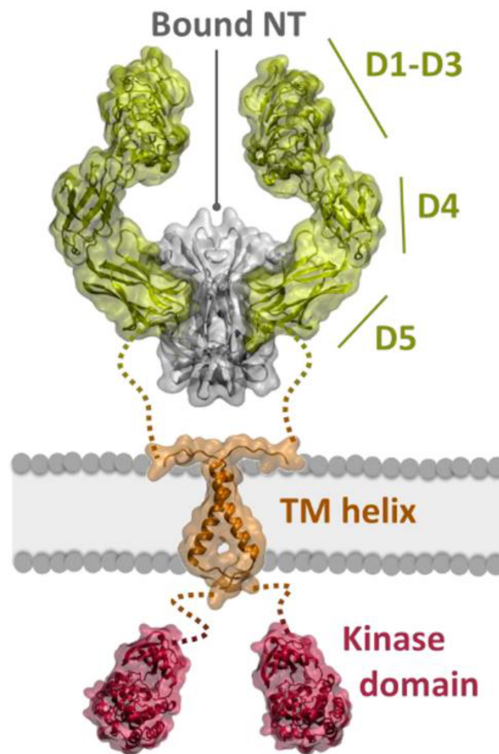


Figure 1.4. Structure model of the NT-Trk receptor complex. Schematic representation of the NT-Trk complex based on the crystal structure of the TrkA extracellular domain in complex with NGF (PDB: 2IFG), the NMR structure of TrkA-TMD dimer in DPC micelles (PDB: 2N90) and crystal structure of the apo-TrkA kinase domain (PDB:4F0I). The juxtamembrane regions are shown as dot lines.

The juxtamembrane region comprises around 30 amino acid residues, that connect the extracellular domain to the transmembrane domain. This linker consists of an intrinsically disorder region, rich in proline residues, which are known to promote disorder but also important for protein-protein interactions of intrinsically disordered proteins (IDPs)⁵⁰. Recently, functional assays showed that deletion of the eJTM of TrkA prevents NGF binding and receptor activation, as well as the mutations of proline in glycine residues impaired the NGF-induced activation. NMR spectra showed that upon TMD dimerization the eJTM did not fold in transient structures and that cross-linking of two eJTM results in alteration of the transmembrane domain structure.

Collectively, these recent data suggests that the juxtamembrane region can interact directly with the neurotrophin and hence transmit conformational changes to the transmembrane domain⁵¹. This could insert an additional structural element for NT specificity and selectivity, explaining the different binding affinities between Trk isoforms. Indeed, the TrkA splice variant,

containing an 18-bp exon in the eJTM region, showed increased activation by NT3, compared to the TrkA isoform lacking the variable exon¹³, and similarly, alternative splicing of the TrkB transcript leads to a TrkB splice isoform in the eJTM region that confers greater specificity for BDNF binding, compared to NT4 and NT3⁵².

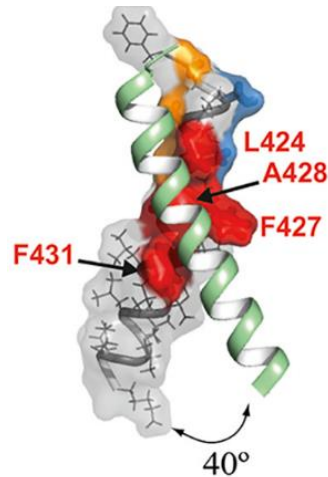


Figure 1.5. Structure of the transmembrane of TrkA receptor. NMR structure of TrkA TMD dimer in detergent micelles. The dimer interface is shown in red and the residues of the dimer motif are labeled in one-letter amino acid code. Image of PDB: 2N90 taken from Franco et al. 2020⁵³.

The transmembrane domain is a single pass α -helix, spanning across the plasma membrane, which structure of TrkA receptor has been characterized in detergent micelles by NMR spectroscopy⁵³. Two transmembrane domains interface forming a cross angle of 40° between the two α -helices through a dimerization sequence motif “LXXFAXFF” (figure 1.5-A), that is conserved across species and in TrkC, but not TrkB receptor. Cysteine mutation scanning, cross-linking and functional studies validated that the identified dimer conformation correspond to the active state, as constitutive dimerization by cross-linking reflected ligand-independent activation of the TrkA receptor *in vitro*. Similarly, insertion of leucine residues between the eJTM and TM domain resulted in rotation of the transmembrane and ligand-independent activation, suggesting that upon ligand binding such rotational movement could take place, re-orienting the intracellular domains and hence triggering the receptor activation⁵³.

The intracellular domains of Trks have a sequence identity of about 70% and contains 10 evolutionarily conserved tyrosine residues, three of which are in the so called “activation” or “autoregulatory loop”. The Trk-ICD presents typical topology of tyrosine protein kinases, consisting of two lobes, an N-lobe of five β -strands and α -helical C-lobe, bridged by a hinge linker⁵⁴ (Figure 1.6).

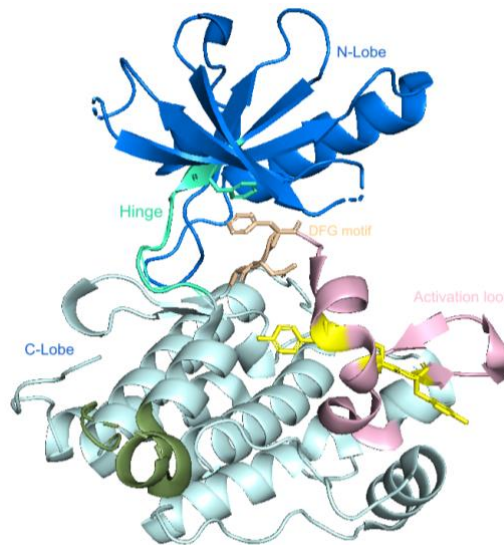


Figure 1.6. Structure of the intracellular domain (ICD) of TrkB. Crystal structure of the TrkB tyrosine kinase domain in inactive state. The scaffold of the N- and C- lobes are shown in blue and cyan respectively, while the functional and regulatory structural elements are shown in different colors. The KID is shown in green, the activation loop in pink with the three tyrosine residues highlighted in yellow, the DFG motif is shown in orange, with the phenylalanyl residues facing the gatekeeper phenylalanine of the hinge linker in water blue. Image of PDB:4F0I created with PyMol Molecular Graphics System, Version 2.0 Schrödinger, LL.

Using adenosine triphosphate (ATP) as donor substrate, the kinase domain catalyzes phosphorylation of the three tyrosine residues within an activation loop, which phosphorylation enhances the catalytic activity and triggers the signaling cascades. The active site is located between the two lobes, where magnesium ion and ATP are coordinated by conserved lysine and glutamate residues of the N-lobe and an aspartate residue of an aspartate-phenylalanine-glycine (DFG) motif⁵⁵. The DFG motif is conserved across the RTK receptors, the glycine residue (lacking the β carbon) is needed to accommodate the activation loop in the active site, while the phenylalanine residue flips between an active (DFG-in) and inactive (DFG-out) conformations, pointing towards or away from the catalytic site and making T-stacking

interactions with another phenylalanine, known as *gatekeeper residue*, preventing the access of ATP in the binding pocket⁵⁶.

Another important structural element is the kinase insert domain (KID), which presents major differences between the Trk receptors in amino acid residues composition and length, a loop that is phosphorylated providing a docking site for adapter signaling proteins⁵⁷.

1.4. Trks activation mechanism

The activation mechanism of Trk receptors upon neurotrophin binding is still not fully clarified and currently different models have been proposed. The first and classic model states a mechanism whereby the ligand binding induces receptor dimerization, bringing the intracellular domains into close proximity and thus enabling the transphosphorylation of tyrosine residues, which requires a precise orientation of the kinase domains, such that the phosphate group can be transferred from ATP to the tyrosine residues of the paired receptor.

In contrast, the second activation model claims that the Trk receptors exist as pre-formed dimers in the lipid bilayer and upon ligand binding conformational changes occur, that spread from the extracellular to the intracellular domains, reorganizing the kinases orientations into a signaling competent orientation. This conformation activation model is supported by the evidence of preformed dimers at the plasma membrane⁵⁸ and by quantitative FRET-based experiments⁵⁹. Indeed, the thermodynamic stability of the unliganded dimers was shown to be higher than Trk monomers and lower than liganded Trk dimers, implying a structurally distinct dimeric state.

Furthermore, FRET analyses revealed that unbound Trk dimers have a different thermodynamic stability, suggesting that increased Trk expression level on the plasma membrane is reflected in a transition from monomeric to dimeric populations, even in the absence of neurotrophins⁵⁹. This suggests a new model of activation, called the "*transition model*", which combines the classical and preformed dimers models⁵³.

1.5. Signaling pathways via Trk receptors

As described in previous sections, neurotrophins play a pivotal role in the development, maintenance and functionality of the central and peripheral nervous system⁶⁰. In the peripheral nervous system, specific population of neurons express specific neurotrophin receptors, that selectively respond to locally and constitutively produced neurotrophins, which activation evokes cell survival and differentiation responses. For instance, TrkA receptor is expressed at the nerve terminals of sympathetic and sensory neurons involved in nociception and temperature sensation, which depend on neurotrophin for survival⁶¹. During embryonic development, many neurons compete to establish connections to target sites, but only those activated by NGF are preserved from cell death by receiving survival, differentiation and axonal growth signals, which are then maintained in adulthood⁶². In absence of neurotrophins, TrkA, as well as TrkC, triggers apoptotic programs behaving as dependence-receptors^{63,64}.

In contrast, in the central nervous system neuronal survival is not dependent on neurotrophin-Trk signaling and there is an overlapping expression of NT-Trk signaling pairs, which pathways modulate synaptic morphogenesis and functionality. Particularly, TrkB-BDNF is the most widely expressed neurotrophin, highly expressed in hippocampus, amygdala, cerebellum, neocortex, thalamic and hypothalamic nuclei⁶⁵⁻⁶⁷, TrkC-NT-3 is expressed during development in hippocampus, cerebellum and amygdala⁶⁶, whereas NGF expression is restricted to striatal and basal forebrain cholinergic neurons⁶⁸.

After development, neurotrophin are involved in remodeling synaptic formations, such as cone growth, axonal arborization, dendritic spine formation, branching pattern, number and location⁶⁹. Synaptic plasticity is fundamental for learning, memory and behavior, and thus preferential modulation of only responsive neurons in an activity-dependent manner is required⁷⁰. This is ensured by activation-dependent expression of neurotrophin and NT receptors, as well as by regulation of NT secretion⁷¹ and upregulation of receptor expression at the plasma membrane in response of Trk activation⁷². Thus, dysregulation of Trk signaling pathways in the CNS correlates with onset of psychiatric and neurodegenerative conditions, such as decreased levels of BDNF with depression and memory decline, increased NGF with anxiety, aggression and stress^{73,74,75}.

Considering all these different functions, a common feature of NT-Trk signaling systems emerges, whereby two modes of signal propagation occur, differing in localization and pattern of activated signaling molecules⁶⁰.

Firstly, a local action at the nerve terminal, where signaling cascades lead to axonal growth and synaptic morphogenesis, and secondly a distance action in the neuronal soma⁷⁶, where NT-Trk pairs are retrogradely transported in endocytosis vesicles along the axon to activate transcription of target genes, such as Trk receptor genes, endosomal effectors, cytoskeletal regulators, promoting secretion of growth factors, inhibition of apoptotic program and maintenance of synapse assembly on dendritic surfaces^{77,78,79} (figure1.7).

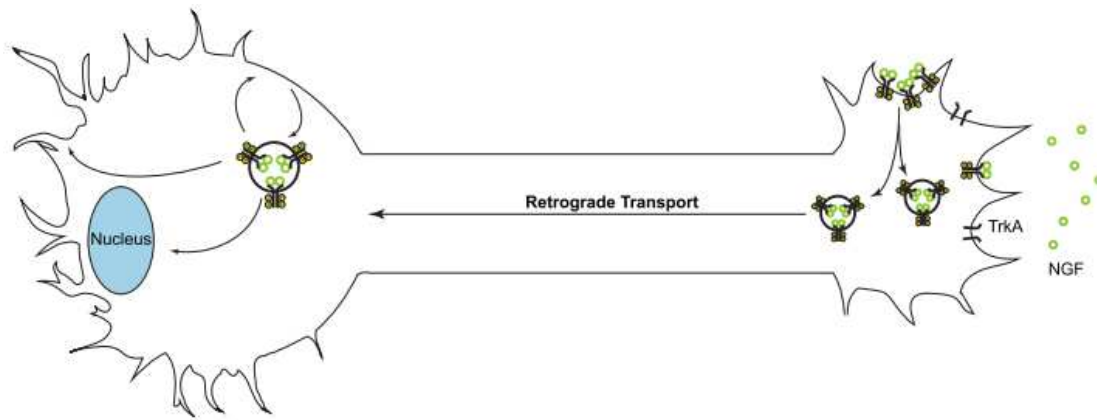


Figure 1.7. Illustration of retrograde transport of TrkA-NGF complex. At the axonal terminal, upon NGF binding TrkA receptor forms active dimers, which are internalized in endosome vesicles and retrogradely transported in the neuronal soma, which could be localized millimeters or meter distant. Here, active endosome signaling complexes activate transcription factors to induce transcription of target genes in cell nucleus, inhibit pro-apoptotic proteins, and localize at the dendritic surface to modulate spine formation and synaptic assembly. Image readapted from Scott-Solomon et al, 2018⁷⁸.

As previously described, upon NT binding the Trk receptors are activated by transphosphorylation of the three tyrosine residues within the activation loop, which enhances the kinase activity, resulting in further phosphorylation of tyrosine residues within the intracellular juxtamembrane region and the disordered tail of the cytoplasmic domain⁷⁴. These phosphotyrosine residues (pY) form docking site for recruitment of adaptor proteins, containing phosphotyrosine-binding (PTB) or Src-homology-2 (SH2) domains, such as Src homology collagen-like (Shc) and phospholipase-C γ (PLC γ), that are in turn phosphorylated providing new pYs scaffolds for other signaling proteins, propagating the phosphorylation cascades that terminates with ERK and MAP kinases (MAPK), phosphoinositide 3-kinase (PI3K)/Akt and PLC γ pathways activation⁸⁰ (figure 1.8).

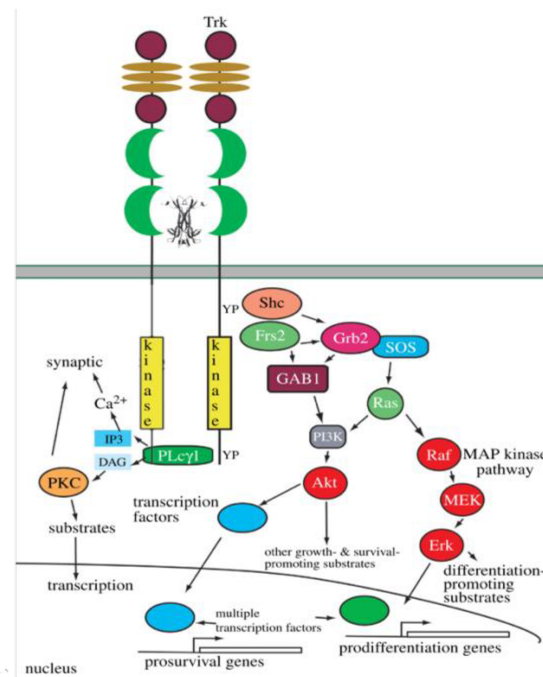


Figure 1.8. Overview of signaling pathways mediated by Trk receptors. Schematic illustration of the signal transduction cascades activated by Trk receptors. Upon binding of NT, conformational changes bring to close proximity the kinase domains, allowing transactivation by phosphorylation of tyrosine residues within the activation loop, which activation initiates MAPK, PI3K/Akt and PLC γ signaling pathways. Phosphorylated tyrosine residues (pY) form Reichardt docking site for the adaptor proteins, Sh2, Frs2, PLC that are in turn phosphorylated and by association and activation of subsequent signaling proteins transmit the signal terminating in transcription of target genes as well activation of target protein involved in synaptic plasticity. Image readapted from Reichardt, 2006⁸¹.

The phosphorylation of the MAPK pathway activates transcriptional factors, such as the cyclic adenosine monophosphate response-element binding protein (CREB), regulating the

expression of gene target for neuronal differentiation and survival. Neurotrophins can trigger two different phases of MAPK activation. First, a transient activation through subsequent activation of Grb2-SOS complex, GTP-Ras, Raf, Erk1/2, Erk5 and MAP kinases, that terminates by activation of phosphatases or intermediates, such as SOS which phosphorylation disrupts Grb2-SOS complex. Second, a prolonged activation through endosome signaling, facilitated by Trk receptors internalization, that consists in the recruitment of adaptor fibroblast receptor substrate-2 (FRS2) and subsequent activation of ARMS, Crk, C3G, GTP-Rap, Raf and terminating with Erk5, but not Erk1/2, and MAP kinases⁸².

Another pathway propagated by Trk receptors is the phosphoinositide 3-kinase (PI3K)/Akt pathway. By SH2 domain engagement, the Shc adaptor is recruited at the pY residues within the Trk intracellular domains, and once phosphorylated, Shc associates with Grb2 and Gab1 activating PI3K and, subsequently, Akt. The final Akt activation results in phosphorylation of substrates that directly inhibit the caspase cascade, as well as the activity of several transcription factors of pro-apoptosis genes⁸³.

Furthermore, PLC γ is docked on pY residues and then activated by Trk-mediated phosphorylation, generating inositol trisphosphate (IP3) and diacylglycerol (DAG) by hydrolysis of phosphatidylinositol 4,5-bisphosphate (PtdIns (4,5)P2). The effects of DAG are mediated by the activation of DAG-regulated protein kinases, such as the different isoforms of protein kinase C (PKC), just as the effects of IP3 are mediated by the mobilization of calcium ions (Ca²⁺) from intracellular storage, which increases the intracellular Ca²⁺ concentration, activating Ca²⁺-regulated protein kinases (CaM kinases) and other CaM-regulated target proteins. In addition, the depletion of PtdIns (4,5)P2 directly affects the activity of membrane proteins that interact with phosphatidylinositides, such as the activation of cation channels.⁸¹

2. Thesis overview and objectives

This research project is part of the EuroNeurotrophin (ENT) consortium, a Horizon2020 research and innovation programme (Marie Skłodowska-Curie grant agreement No765704) which aims to design and develop new small molecules with neurotrophin like effects in order to fill the gap of the existing lack of treatments for neurodegenerative diseases.

Since the neurotrophin and NT receptor axes play a critical role in the development and maintenance of the nervous system, the dysregulation of which is correlated with pathological conditions, neurotrophins and NT receptors have long been considered pharmacological candidates to achieve neuroprotective and neurogenic effects^{84,85}.

However, the use of neurotrophins as therapeutic agents *per se* has been hindered by their poor pharmacokinetic profiles, pleiotropic effects and limited diffusion across the blood-brain barrier (BBB), requiring novel^{86,87} or invasive⁸⁸ procedures for delivery, often associated with adverse effects such as neuropathic pain⁸⁹. For this reason, the development of peptides or small compounds with agonist effects has been the focus of extensive studies aimed at providing new drugs with improved pharmacological profiles^{90,91}.

Recently, the synthetic C-17-spiroepoxy dehydroepiandrosterone derivative, called BNN27, was shown to specifically interact with and activate downstream signaling pathways of TrkA and p75 receptors^{92,93}. Briefly, it was shown that BNN27 induced the auto-phosphorylation of TrkA tyrosine residues (490, 674, 675 and 785) in a dose- and time- dependent manner in CHO cells transfected with TrkA, but not with TrkB and TrkC. Furthermore, anti-apoptotic effects were observed in experiments based on PC12 cells and rat primary sympathetic neurons, as well as axonal growth was observed in mouse dorsal root ganglia sensory neurons, after exposure of BNN27 in combination with low concentration of NGF.

Also, saturation transfer difference (STD) NMR spectroscopy confirmed the binding event between BNN27 and recombinant TrkA-ECD, which was more consistent in presence of NGF. Molecular dynamics and *in silico* modelling identified three potential binding sites, two of which were located at TrkA-NGF interface, suggesting a bridging function of BNN27 in the TrkA and NGF heterodimer.

Within the EuroNeurotrophin network, new molecules with neurotrophin-like effects have been developed and screened *in vitro* and *in vivo* models, from chemical analogues of BNN27,

such as ENT-A010⁹⁴, to pharmacophore based drugs, as well as natural products isolated from marine bacteria.

Given the lack of structural information on ligand – protein complexes, the main objective of the PhD thesis project was to provide the structural and biophysical characterization of the complex between the neurotrophin receptors and the identified small agonists, in order to elucidate the structural features for ligand binding and thus drive the receptor-based drug design. In addition, we attempted to structurally characterize the complex between BDNF and TrkB receptor, whose three-dimensional structure is still missing.

More specifically, we aimed to define the structures of the extracellular domain of the TrkA and TrkB receptor by X-ray crystallography and to integrate the structural data with binding affinity values and kinetic profiles by biophysical methods, such as by Grating Coupled Interferometry (GCI).

Such information is crucial for a better understanding of the molecular mechanisms underlying the ligands binding, just as the structure of BDNF and TrkB receptor complex would shed light on the mechanism of receptor activation, allowing a better interpretation of the structure-function relationship.

To address these, milligram yields of pure recombinant proteins were required, and thus first purpose of this thesis was to develop purification protocols for the TrkA and TrkB ectodomains. Since the d5 domains are the ones involved in the interaction with the neurotrophins, conferring specificity to ligands, efforts were firstly focused on developing expression and purification protocol of TrkA-d5 and TrkB-d5 domains in bacterial expression system, and secondly on the production of the whole TrkA and TrkB ectodomains in mammalian expression system. Finally, crystallization screening and optimization of hit conditions were conducted, as well as preliminary studies for single particle cryo electron microscopy (Cryo-EM), in an attempt to determine the structures of the neurotrophin receptor and ligand complexes.

3. The d5 domain of TrkA and TrkB receptors

Potential binding sites of BNN27 have been identified at the interface between the d5 domain of TrkA and NGF⁹². Consequently, to drive the receptor-based drug design of the new neurotrophin mimetics, the research activities have been focused on milligram-scale production of the d5 domain of TrkA and TrkB ectodomains for structural studies by X-ray crystallography.

The main difficulty to produce the target proteins was the tendency of insoluble production, consisting in incorrectly folded protein that accumulate as inclusion bodies (IBs) when over-expressed in *Escherichia coli*.

To overcome this problem, different strategies have been performed at the Structural biology laboratories at the University of Siena, which methods and results are presented in this chapter. The first section describes methods and results on the expression and purification of the TrkA-d5 domain. The second section sets out the co-expression and purification of TrkB-d5 and BDNF.

3.1. Production of TrkA d5 domain: material and methods

3.1.1. Construct design

The first crystal structures of the d5 domain of TrkA, TrkB and TrkC receptors consisted in no-native and inactive β -strand-swapped dimer, where a β -strand of one monomer switches with the β -strand of the other monomer, occluding the neurotrophin binding site⁹⁵. Shoemark et al. proposed to introduce a disulfide bond that stabilizes the monomer conformation by mutating P285 and F367 residues of TrkA into cysteine residues (figure 3.1). They showed that the cysteine mutations increased the production of functional TrkA-d5 monomers without affecting the NGF interaction⁹⁶.

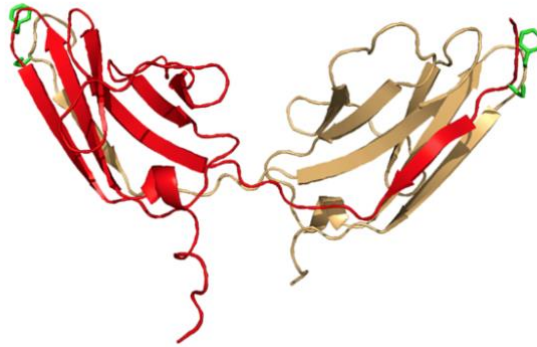


Figure 3.1. Crystal structure of the d5 domain of TrkA (PDB 1WWA). The two TrkA-d5 monomers are shown in red and gold. The TrkA-d5 dimer assumes an inactive conformation, where the β -strand of one monomer switches with the strand of the other, hindering the neurotrophin binding site. In green, the side chains of the residues P285 and F367 are shown, which mutations in cysteines introduce a disulfide bond that stabilizes the native monomer conformation. Image created with PyMol Molecular Graphics System version 2.0 Schrödinger,LLC

Therefore, the P285C and F367C mutations were introduced in the gene sequence encoding the TrkA-d5 domain (283-389), which was cloned into two different vectors: a pET-28a-TEV plasmid, conferring a cleavable hexa-histidine tag at the N-terminus, and a pMAL-c5E plasmid with a cleavable maltose-binding protein (MBP) tag at the N-terminus.

To promote a proper refolding of the TrkA-d5, another construct was designed removing seven terminal residues of “TrkA-d5” construct, predicted to be intrinsically disordered⁹⁷, and adding five aspartate residues at the N-terminus, which negative charge was suggested to help the protein refolding⁹⁶. This second construct, named “NMR TrkA-d5”, was cloned by Gibson assembly into pET-28a(+)-TEV plasmid and pETDuet plasmid. Having two multiple cloning site (MCS), the pETDuet vector allows the co-expression of two interacting molecules, as TrkA-d5 and NGF, cloned in MCS1 and MCS2, respectively. Construct sequences and plasmids used for the expression and purification trials are listed in figure 3.2 on the following page.

Construct	Sequence	vector
TrkA-d5	SFCASVQLHTAVEMHHWCIPFSVDGQPAP	pMAL-c5E
	SLRWLFNGSVLNETSFIFTEFLEPAANETVR HGCLRLNQPTHVNNNGNYTLAANPCGQA SASIMAAFMDNPFEPNED	pET28a-TEV
NMR TrkA-d5	DDDDVVSFCASVQLHTAVEMHHWCIPFS	pET28a-TEV
	VDGQPAPSLRWLFNGSVLNETSFIFTEFLE PAANETVRHGCLRLNQPTHVNNNGNYTL AANPCGQASASIMAAFMDNP	pETDuet-1

Figure 3.2. Table of TrkA-d5 constructs. Two different constructs of TrkA-d5 were designed and used for expression and purification trials. In table, vector name and sequences in one-letter amino acid abbreviation are shown. The cysteine mutations are highlighted in red, the predicted disordered residues in black and the five aspartate residues insertion at the N-terminus of TrkA-d5 are shown in green.

3.1.2. Transformation

Transformation of all constructs was done in the same way. An aliquot of 2 μ l of plasmid (100 ng/ μ L) were added to 100 μ l of competent *Escherichia coli* cells and incubated 40 minutes on ice. A heat shock was performed heating the cells at 42°C for 40 seconds. Cells were let on ice for 5 minutes before adding 400 μ L of warm S.O.C. medium (2% tryptone, 0.5% yeast extract, 10 mM NaCl, 2.5 mM KCl, 10 mM MgCl₂, 10 mM MgSO₄, and 20 mM glucose) and then incubated at 37°C for one hour at 180 rpm. 200 μ L of culture were plated on Luria Bertani (LB) (10 g/L tryptone, 10 g/L NaCl, 5 g/L yeast extract) agar plate containing either 100 μ g/mL ampicillin (amp) or 50 μ g/mL kanamycin (kan), depending on plasmid antibiotic resistance. Plates were incubated at 37°C overnight.

3.1.3. Expression and purification of pMAL-c5E/TrkA d5

To achieve a soluble expression of the TrkA-d5 domain, the recombinant protein was produced using the MBP-tag at the N-terminus. After cell transformation, a single colony was inoculated in 10 mL of LB medium supplemented with 100 µg/mL amp and grew overnight at 37°C and 220 rpm. Thereafter, the overnight culture was diluted in 1 L of growth medium and when the cell density reached an optical density at 600 nm (OD₆₀₀) of 0.6, expression of the recombinant protein was induced using 1 mM of isopropyl β-D-1-thiogalactopyranoside (IPTG) and conducted for 24 hours at 18°C under shaking at 220 rpm. Cells were harvested by centrifuging for 20 minutes at 4000xg and 8°C, and pellet stored at -20°C.

To purify the target protein, cell pellet was thaw on wet ice and suspended in lysis buffer containing 2 mM phenylmethylsulfonyl fluoride (PMSF), 1 mM EDTA, 300 mM NaCl, 40 mM Tris-HCl pH=8.2 and 0.5 mg/mL of lysozyme. Also, higher ionic strength (500 mM NaCl), different salt (250 mM KCl) and low concentration of denaturing agent (2 M Urea) were tested to prevent formation of soluble aggregates during protein purification.

After one hour incubation of enzymatic lysis, cells were mechanically disrupted by sonicating for 20 seconds at 80% amplitude with 20 seconds intervals. Cell lysate was centrifuged at 11000 rcf for 1 hour at 4°C and then supernatant was applied onto MBP-Trap High Performance 5 mL column for affinity chromatography. The column was previously mounted on ÄKTASTART chromatography system (GE Healthcare) and equilibrated in buffer A (1 mM EDTA, 300 mM NaCl, 40 mM Tris-HCl pH=8.2). Protein elution was performed by isocratic elution of 100% buffer B (10 mM maltose, 1 mM EDTA, 300 mM NaCl, 40 mM Tris-HCl pH=8.2s) for 5 column volumes (CVs), detected as absorption at 280 nm and collected in 2 mL fractions. All buffers and protein sample were sterile filtered with 0.22 µm filter. Samples were taken at each purification step for SDS-PAGE evaluation.

From SDS-PAGE analysis, fractions that exhibited a band around 55 kDa were pooled together and concentrated using a 30000 molecular weight cut off (MWCO) centrifugal filter (Pierce™, Thermo Fisher Scientific). To further purify the MBP-TrkA-d5 domain, HiLoad Superdex200 prep grade16/600 (GE Healthcare) column was mounted on ÄKTAPRIME chromatography system (GE Healthcare). The column medium separates globular molecules in the molecular weight range from 10000 to 600000 Da. The column was equilibrated with 2 column volume of buffer A before sample injection. Protein were eluted with an isocratic

gradient for 1.5 column volume and collected in 4 mL fractions. Absorption at 280 nm was used to detect protein. Sample of eluted fractions were taken for sodium dodecyl sulphate – polyacrylamide gel electrophoresis (SDS-PAGE) analysis.

Finally, to estimate incubation time and units of bovine enterokinase (Ek) required for MBP-tag cleavage, aliquots of 50 µg of fusion protein were incubated with 0, 0,1, 0,5 and 1 units of Ek for 1, 3, 5 and 72 hours. Samples were taken for SDS-PAGE evaluation and compared to the proteolytic activity of 1 unit EK on a positive control.

3.1.4. Expression test pET-28a(+)-TEV/TrkA d5

To find the best condition for optimal expression of the histidine-tag TrkA-d5 (His₆-TrkA-d5), in terms of solubility and high yields, multiple aspects were taken in consideration as growth medium, temperature, inductor concentration, harvesting time, additives and *Escherichia coli* strains. Particularly, three different strains were tested for protein over-expression: BL21(DE)3, ArcticExpress (DE)3 and Rosetta-Gami 2(DE)3 cells. Methods for expression trials and the conditions tested for each strain are described below.

I. His₆-TrkA-d5 expression in BL21(DE)3 cells

A single colony of BL21(DE)3 cells transformed with pET-28a(+)-TEV/TrkA-d5 plasmid was inoculated in LB medium supplemented with 50 µg/mL kan, and incubated overnight at 37° C and 220 rpm. An aliquot of the overnight culture was diluted in both LB and Zyp-5052 media added with 50 µg/mL kan and cells were grown at 37°C and 220 rpm. When optical density (OD₆₀₀) reached 0.6, expression in LB cultures was induced by adding 1 mM IPTG and conducted overnight at 18° C and 35° C. To increase the solubility and the final yield of recombinant proteins, low percentages of ethanol (EtOH) were tested by adding 2% and 3% to the culture medium just before induction.

Medium	LB	LB +2%	LB +3%	Zyp-5052	LB	LB +2%	LB +3%	Zyp-5052
IPTG	1 mM	1 mM	1 mM		1 mM	1 mM	1 mM	
Temp.	35°C	35°C	35°C	35°C	18°C	18°C	18°C	18°C

Figure 3.3. Expression tests of His₆-TrkA-d5 in BL21(DE)3 cells. Conditions tested for expression trials are reported in table. Cells were grown overnight at two different temperatures (18°C and 35°C) in two different growth media (LB and Zyp-5052), testing induction with 1 mM of IPTG and low percentages of EtOH (2% and 3%).

The day after, cells were harvested by centrifuging at 4000xg and 8°C for 20 minutes. Using ultrasounds, cells were lysed and lysate was clarified by centrifuging at 13000 rcf for 30 minutes. Samples of soluble and insoluble fractions of each condition (table in figure 3.3) were taken to evaluate the expression level by SDS-PAGE analysis.

II. His₆-TrkA-d5 expression in ArcticExpress (DE)3 cells

A colony of ArcticExpress(DE)3 cells transformed with pET28a-TEV/TrkA-d5 plasmid was inoculated in LB medium added with 50 µg/mL kanamycin and 20 µg/mL gentamicin, and incubated overnight at 37° C and 220 rpm. The day after, an aliquot of the overnight culture was diluted in both LB and Zyp-5052 media and incubated at 30° C and 220 rpm. After 3 hours, 2% and 3% EtOH were added and expression of LB cultures was induced with either 0.1 mM or 1 mM IPTG. After ethanol addition and IPTG induction, temperature was lowered to 12°C and expression was conducted for 48 hours for all condition tested (figure 3.4). Cell pellet was harvested by centrifugation for 20 minutes at 4000 rcf and 8°C, lysed by ultrasounds and lysate was centrifuged at 13000 rcf at 4°C for 30 minutes. Samples of soluble and insoluble fractions were taken for SDS-PAGE and Western Blot analyses (method described in section 3.1.5).

Medium	LB	LB	LB	LB	Zyp-5052	Zyp-5052	Zyp-5052
IPTG	1 mM	1 mM	0.1 mM	0.1 mM			
EtOH		2%		3%		2%	3%

Figure 3.4. Expression tests of His₆-TrkA-d5 in ArcticExpress (DE)3 cells. Conditions tested for expression trials are reported in table. After 3 hours of cells growth at 30°C, 2% and 3% of EtOH were added to the growth media, auto-inducing (Zyo-5052) and IPTG induction with either 0.1 mM and 1 mM were tested.

III. His₆-TrkA-d5 expression in Rosetta-Gami 2(DE)3 cells

A single colony of Rosetta-Gami 2(DE)3 cells transformed with pET28a-TEV /TrkA-d5 plasmid was inoculated in LB medium supplemented with 50 µg/mL kanamycin, 34 µg/mL chloramphenicol and 12.5 µg/mL tetracyclines, and incubated overnight at 37° C and 220 rpm. The overnight culture was diluted in fresh LB, Super Broth (SB) (35 g/L tryptone, 10 g/L NaCl, 5 g/L yeast extract) and Zyp-5052 medium and let grown at 37°C and 220 rpm. When the optical density (OD₆₀₀) reached 0.8, the expression of the recombinant protein was induced adding either 0.1 or 1 mM of IPTG and conducted at 18° C under shaking at 220 rpm. After 24 hours and 48 hours, cells were harvested centrifuging at 4000xg and 8°C for 20 minutes. Pellet was resuspended and lysed by ultrasounds, then clarified by centrifugation for 30 minutes at 13000 rcf and 4°C. Samples of soluble and insoluble fractions were taken for evaluation by SDS-PAGE.

Medium	LB	LB	LB	LB	SB	SB	SB	Zyp-5052	Zyp-5052
IPTG	0.1 mM	0.1 mM	1mM	1mM	0.1 mM	1 mM	0.1 mM		
Harvesting	24h	48h	24h	48h	48h	24h	48h	24h	48h

Figure 3.5. Expression tests of His₆-TrkA-d5 in Rosetta-Gami2(DE)3 cells. Conditions tested for expression trials are reported in table. LB, SB and auto-induction (Zyp-5052) media, as well as IPTG concentrations of 0.1 mM and 1 mM, harvesting time at 24 h and 48 were used.

3.1.5. Expression and purification of His₆-TrkA-d5

To scale up the His₆-TrkA-d5 production, a colony of BL21(DE)3 transformed with pET-28a(+)-TEV/TrkA-d5 plasmid was inoculated in 10 mL LB medium supplemented with 50 µg/mL kanamycin. The overnight culture was then diluted in 500 mL of fresh LB-kan medium and cell growth was conducted at 37°C and under shaking at 220 rpm. When density reached an OD₆₀₀ of 0.6, expression was induced by adding 1 mM IPTG and 3% of EtOH and temperature was lowered at 18°C. After 24 hours, cells were harvested at 4000 rcf for 30 minutes at 8° C and about 5 grams of fresh cell pellet were suspended in lysis buffer (0.2 mM PMSF, 150mM NaCl, 50 mM Tris-HCl pH=8.5 and 0.5 mg/mL lysozyme). After one hour of lysozyme digestion at room temperature, cell lysis was further obtained by sonication (20 seconds on and 20 seconds off cycles).

Lysate was clarified by centrifuging at 11000 rcf for one hour at 4°C. Then, the IB pellet was washed for three times, resuspending the insoluble fraction in different wash buffers and collecting the IB pellet by centrifugation at 11000 rcf for 30 minutes. To solubilize the cell debris, the first wash was conducted suspending the IBs in wash buffer (150mM NaCl, 50 mM Tris-HCl pH=8.5) supplemented with 0.1% Triton-X. Second wash was conducted using wash buffer added with 2 M urea in order to remove possible contaminating proteins.

For the final wash, high ionic strength was used to get rid of nucleic acids (1 M NaCl, 50 mM Tris-HCl pH=8.5). Finally, the inclusion bodies were solubilized in denaturation buffer (8M urea, 2 mM DTT, 0.150 M NaCl, 50 mM Tris-HCl pH=8.5) under stirring at room temperature and overnight. After inclusion bodies denaturation, the denatured solution was centrifuged at 11000 rcf for 30 minutes and target protein was refolded and purified employing three different strategies:

- I. Affinity chromatography in denaturing condition and refolding by dialysis
- II. Dialysis refolding and affinity chromatography in native state
- III. On-column refolding

I. Affinity chromatography in denaturing condition and refolding by dialysis

First strategy was to purify the His₆-TrkA-d5 domain in denaturing condition. For affinity chromatography, HisTrap High Performance (HP) 5 mL column (Cytiva) was mounted on ÄKTASTART chromatographic system and equilibrated with 5 column volumes of binding buffer (8 M urea, 20 mM imidazole, 150 mM NaCl, 40 mM Tris-HCl pH=8.5). The denatured solution was filtered before loading onto the column. Bound proteins were eluted using a gradient from 0% to 60% elution buffer (8 M urea, 500 mM imidazole, 150 mM NaCl, 40 mM Tris-HCl pH=8.2), a 5 CVs step of 60% (300 mM imidazole) and a final step of 100% elution buffer (500 mM imidazole). Elution was detected as absorption at 280 nm (Abs₂₈₀) and 4 mL fractions were collected. Samples of each purification step were taken for SDS-PAGE analysis. From the SDS-PAGE evaluation fractions that corresponded to His₆-TrkA-d5 elution, were pooled together and target protein was refolded by step-wise gradient dialysis, using dialysis tubing of 3000 MWCO. The protein solution was adjusted to 0.1 mg/mL protein concentration and dialyzed against 1:20 refolding buffer (150 mM NaCl, 40 mM Tris-HCl pH=8.5) containing 4 M urea at 4°C.

Second refolding step was conducted dialyzing against 1:20 of refolding buffer supplemented with 2 M urea and a final dialysis step against 1:40 of refolding buffer. Then,

protein solution was centrifuged for 1 hour at 11000 rcf and 4° C. Samples of supernatant and pellet were taken to evaluate the yield of the obtained refolded protein by SDS-PAGE analysis.

II. Dialysis refolding and affinity chromatography in native state

Second strategy was to refold the target protein before to perform the purification by affinity chromatography. Following the process described above, refolding was achieved by step-wise gradient dialysis and then protein solution was centrifuged for 1 hour at 11000 rcf and 8°C. Samples of supernatant and pellet were taken for SDS-PAGE analysis. The refolded supernatant was loaded onto the HisTrap HP affinity column, previously equilibrated with 5 CVs of buffer A (20 mM imidazole, 150 mM NaCl, 40 mM Tris-HCl pH=8.5), bound proteins were eluted using a linear gradient from 0% to 100% of elution buffer (500 mM imidazole, 150 mM NaCl, 40 mM Tris-HCl pH=8.5). Absorbance at 280 nm was detected and eluted protein collected in 4 mL fraction. All buffer and protein solution were filtered using 0.22 µm filter. Samples of flow-through, column wash and eluted fractions were taken for SDS-PAGE evaluation.

III. On-column refolding

Third strategy was to refold the target protein when bound to the stationary phase of the affinity column. The HisTrap HP column was equilibrated with binding buffer (8 M urea, 20 mM imidazole, 150 mM NaCl, 40 mM Tris-HCl pH=8.5). The denatured sample was loaded onto the column using a flow of 0.5 mL/min. Column was washed with 5 CVs before applying a slow linear gradient from 8 M to 0 M urea buffer (20 mM imidazole, 150 mM NaCl, 40 mM Tris-HCl pH=8.5). Then, using a gradient from 0 to 100% of elution buffer, elution of refolded protein was performed. Absorbance at 280 nm was monitored for protein elution. Samples of all purification steps were taken and analysed by SDS-PAGE.

Finally, to further purify the His₆-TrkA-d5 domain and to estimate the quality of the refolded proteins a size exclusion chromatography was performed. HiLoad Superdex 75 prep grade 16/600 (GE Healthcare) column was mounted on the ÄKTAprime chromatography system and equilibrated with 2 column volumes of buffer (150 mM NaCl, 40 mM Tris-HCl pH=8.5). The column medium separates globular molecules between 3000 and 70000 Da. From the SDS-PAGE analysis of refolding strategies, eluted fractions corresponding to TrkA-d5 domain were concentrated up to 2 mL, using 3000 MWCO centrifugal filter (Pierce™, Thermo Scientific) just

before injection. Protein were eluted with an isocratic gradient for 1.5 column volume and collected in 4 mL fractions. Absorption at 280 nm was used to detect protein elution. Sample of eluted fractions were taken for SDS-PAGE and Western blot analyses.

For Western Blot (WB), once separated by the electrophoresis run, proteins were transferred from the polyacrylamide gel to nitrocellulose membrane by iBlot 2 Dry Blotting System (Thermo Scientific). After blotting, the membrane was washed several time with Milli-Q water and PBS buffer added with 0.2% Tween-20 (PBS-T). Thereafter membrane was blocked for one hour in 5% bovine serum albumin dissolved in PBS-T buffer and then washed three times for 5 minutes in PBS-T buffer at room temperature under gentle shaking. The membrane was incubated for two hours in antibody solution (anti-His6tag – HRP conjugated monoclonal antibodies, Sigma Aldrich) under gentle agitation. Finally, the membrane was washed three times for 5 minutes in PBS-T buffer and visualized using the chromogenic 1-Step™ Ultra TMB-Blotting Solution (ThermoFisher scientific).

3.1.6. Expression and purification of NMR-TrkA-d5 construct

To improve the solubility, the NMR-TrkA-d5 construct was cloned into the pETDuet vector for co-expression with NGF (section 3.1.1) and expression was tested in Rosetta-Gami 2(DE)3 cells, screening different expression conditions (Figure 3.6).

Medium	LB	LB	LB	LB	SB	SB	SB	Zyp-5052	Zyp-5052
IPTG	0.1 mM	0.1 mM	1mM	1mM	0.1 mM	1 mM	0.1 mM		
Harvesting	24h	48h	24h	48h	48h	24h	48h	24h	48h

Figure 3.5. Expression test of His₆-TrkA-d5 in Rosetta-Gami2(DE)3 cells. Conditions tested for expression trials are reported in table. LB, SB and auto-induction (Zyp-5052) media, as well as IPTG concentrations of 0.1 mM and 1 mM, harvesting time at 24 h and 48 were used.

A single colony transformed with pETDuet/NMR-TrkA-d5 plasmid was inoculated in LB medium supplemented with 50 µg/mL kan, 34 µg/mL chloramphenicol and 12.5 µg/mL tetracyclines, and incubated overnight at 37°C and 220 rpm. The overnight culture was diluted at 1:100 ratio in fresh LB, SB and Zyp-5052 media and let grown at 37°C and 220 rpm. When the optical density (OD₆₀₀) reached 0.6, the expression of recombinant protein was induced adding either 0.1 or 1 mM of IPTG and conducted at 18°C under shaking at 220 rpm. Two harvesting time were tested, centrifuging the cell culture at 4000xg and 8°C for 20 minutes after 24 hours and 48 hours. Pellet was resuspended in buffer and lysed by ultrasounds, then lysate was clarified by centrifugation for 30 minutes at 13000 rcf and 4°C. Samples of soluble and insoluble fractions were taken for evaluation by SDS-PAGE.

Because neither the co-expression with NGF either the oxidative cytoplasm of the Rosetta-Gami cells helped to achieve a soluble expression of the target protein, the NMR-TrkA-d5 construct was cloned in pET28a-TEV plasmid and used to improve protein the refolding protocol.

Expression and inclusion bodies isolation were performed as described in section 3.1.5. After solubilization in 8M urea, the solubilized sample was refolded by oxidative refolding, dialysis against buffer containing 1M Arginine, 5 mM reduced L-glutathione (GSH) and 1 mM oxidized L-glutathione (GSSG), 150 mM NaCl and 40 mM Tris-HCl pH 8.5. After dialysis refolding, the protein was centrifuged for 1h at 11000 rcf and 4°C.

Taking advantage of the His₆-tag metal chelation, affinity chromatography was conducted using HisTrap High Performance column, previously equilibrated with 5 CVs of buffer A. Elution

was performed by step gradient of 10%, 30 % and 100% elution buffer (500 mM imidazole, 150 mM NaCl, 40 mM Tris-HCl pH=8.5). Absorbance at 280 nm was detected and eluted protein collected in 4 mL fractions. Using a Slide-A-Lyzer™ cassette (ThermoFisher Scientific), fractions corresponding to eluted NMR-TrkA-d5 were concentrated by dialysis against 20000 poly-ethylene glycol (PEG) concentrating solution.

Once concentrated to 2 mL, sample was loaded on the HiLoad Superdex75 prep grade column for size exclusion chromatography. Absorbance at 280 nm was detected and eluted protein collected in 2 mL fractions. Samples were taken at each purification step for SDS-PAGE analysis.

3.1.7. Circular dichroism spectroscopy

After size exclusion chromatography, fractions corresponding to the His₆-TrkA-d5 elution volume were pooled together, buffer was exchanged by dialysis against CD buffer (10 mM Tris-HCl pH=8.5). Then, protein concentration was adjusted to 20 μM for circular dichroism (CD) spectroscopy. The far-UV CD spectra of TrkA-d5 was recorded on a Jasco J-815 spectropolarimeter in a 0.1 cm Quartz cuvette. The spectra were recorded in the wavelength range from 190 nm to 250 nm, using a scanning speed of 200 nm/min, 0.5 data pitch and 3 spectra were accumulated. Buffer spectrum was recorded and subtracted from protein spectrum, CD data were plotted and analysed using CAPITO web server-based tool.⁹⁸

3.2. Production of TrkA D5 domain: results

To achieve milligram scale productions of the TrkA-d5 for structural studies, the first experimental plan was to improve the solubility of the recombinant protein in *E. coli* cells, then second plan was to optimize the existing protocols of protein refolding from inclusion bodies^{47,48,99}.

For this purpose several strategies were adopted, such as the use of a solubility tag, expression trials by testing different *E. coli* strains and expression conditions and finally performing different refolding methods. All results obtained are described in this section.

3.2.1. Expression and purification of MBP-TrkA-d5 construct

First strategy to achieve a soluble expression was to clone the gene sequence of the TrkA-d5 domain (283-389) as fusion protein with the maltose-binding protein (MBP) (see section 3.1.1). The MBP-tag is a well-studied tag that have been reported to bring solubility and to facilitate target purification by binding to amylose resin. The TrkA-d5 gene was cloned inside the pMAL-cE5 vector conferring the MBP-tag at the N-terminus and a cleavage recognition site for bovine enterokinase (Ek).

The fusion protein over-expression was obtained by induction with 1 mM IPTG in LB growth medium at 18°C and 220 rpm. After 24 hours, cells were harvested, suspended in lysis buffer and lysed by enzymatic lysis and ultrasounds sonication. Then, lysate was clarified by centrifugation and the MBP-TrkA-d5 was purified by affinity chromatography on MBPTrap HP column.

From the chromatogram in figure 6.7, only one sharp elution peak was obtained. As shown in the SDS-PAGE analysis (figure 6.7), the eluted fraction consisted in a clear band around 60 kDa. This was in accordance with the theoretical molecular weight of 55 kDa of MBP-TrkA-d5, calculated by ProtParam of ExPaSy server¹⁰⁰.

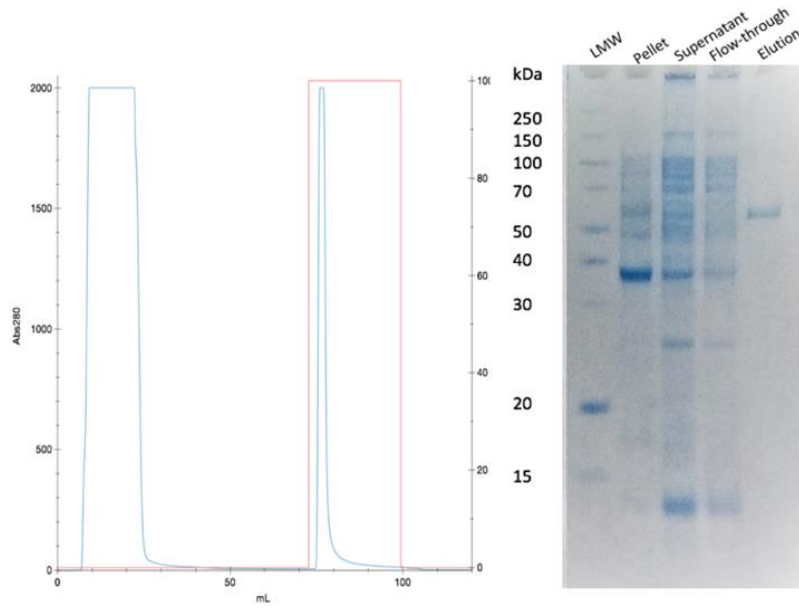
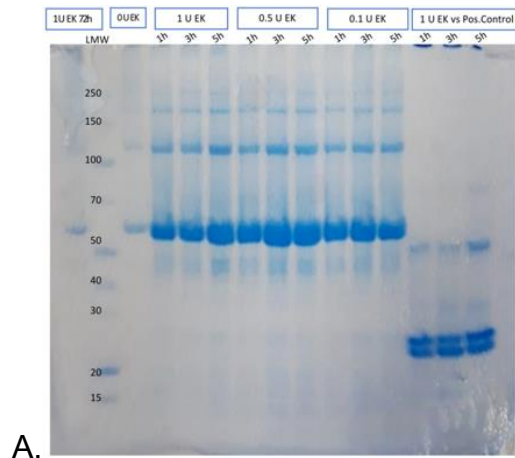
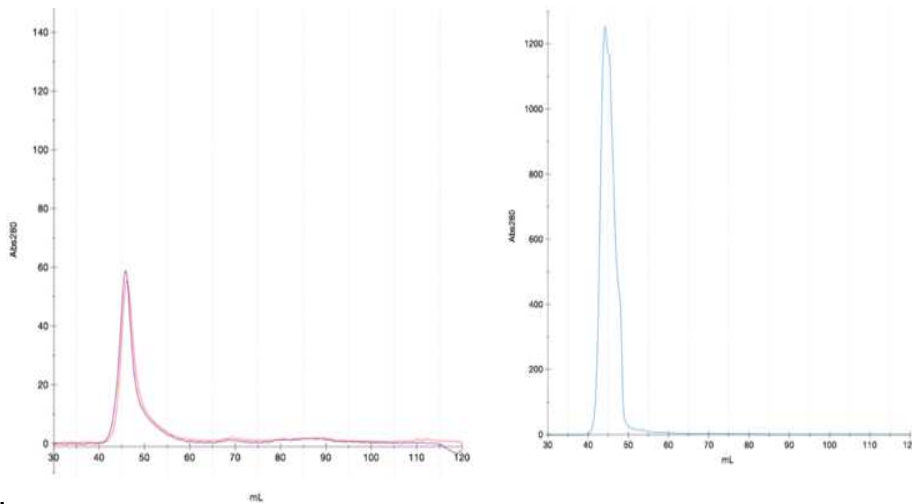


Figure 3.7. MBP-TrkA-d5 purification. On the left, the chromatogram of MBP-TrkA-d5 affinity chromatography is shown. Protein elution was detected as absorbance at 280 nm (Abs280) and shown as a blue curve. On the x-axis, the elution volume is given in mL, on the left y-axis the absorbance units, while on the right y-axis the percentage of elution buffer (10 mM maltose, 1 mM EDTA, 300 mM NaCl, 40 mM Tris pH 8.2). On the right panel, samples of pellet, supernatant, flow-through and eluted fraction (“Elution”) were analysed by SDS-PAGE. Molecular weight of standard protein (LMW) is shown in kDa.

To remove the MBP-tag, different incubation times and enterokinase concentrations were tested. As shown in figure 3.8-A, a band around 55 kDa was visible in all conditions tested, meaning that the cleavage of the MBP-tag did not occur. The proteolytic activity of Ek was checked by a positive control and cleavage was visible at each incubation time. Thus, it was supposed that either the cleavage sequence was hidden inside the overall fusion-protein folding or by intramolecular aggregation.



A.



B.

Figure 3.8. MBP-tag cleavage test by enterokinase and size exclusion chromatography of MBP-tag. A) The proteolytic activity of enterokinase was evaluated by SDS-PAGE analysis. Samples were taken after 1, 3 and 5 hours incubation at 37°C with 0.1 U, 0.5 U and 1 U Ek per 50 µg of fusion protein. As negative control, no protease was added. Also, 1U of Ek was tested for 72 hours and against a positive control. Molecular weight of standard protein (LMW) is shown in kDa. **B)** Chromatograms of MBP-TrkA-d5 gel filtration on HiLoad Superdex200 pg 16/600. On the x-axis, the elution volume is given in mL, while protein elution was monitored as absorbance at 280nm (Abs280 on y-axis). The red curve shows the elution profile of TrkA-d5 buffered with 250 mM KCl, the purple curved is the elution profile of the sample in presence of 2 M urea and the blue curve in high ionic strength (0.5 M NaCl).

To check the quality of the produced protein, size exclusion chromatography was run on the Superdex200 16/600 pg column. As shown on the chromatogram in figure 3.7 B, the MBP-TrkA-d5 eluted as a single peak in the void volume at 45 mL. This suggested the production of soluble aggregates, where the MBP-tag brought in solution misfolded and aggregated target protein. In the attempt to dissolve such aggregation, protein sample was purified using high ionic strength (0.5 M NaCl), low concentration of denaturing agent (2 M urea) and to buffer the protein sample using a different salt (0.25 M KCl)¹⁰¹. However, chromatograms of all gel filtrations showed the MBP-TrkA-d5 elution in the void volume (figure 3.7-B).

3.2.2. His₆-TrkA-d5 expression tests

Second strategy to improve the TrkA-d5 solubility was to test expression conditions that allow the protein over-production in the soluble fraction. As shown in the illustration in figure 3.9, different aspects of the workflow for protein production in *E. coli* expression system were manipulated to this scope.

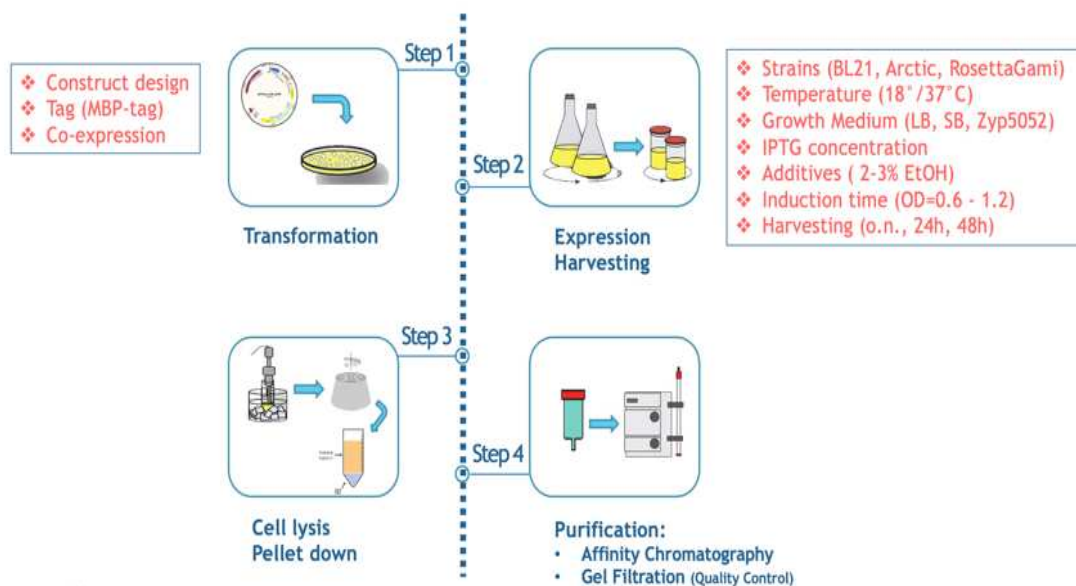


Figure 3.9. Workflow of recombinant protein production in *E. coli* expression system. The illustration summarizes the steps for the production of recombinant proteins. In the boxes, the different aspects that were manipulated and tested to achieve a soluble expression of TrkA-d5 are highlighted in red.

As described in section 3.1.4, expression of the His₆-TrkA-d5 tests were conducted using three different strains of *E. coli*.

First of all, production of the target protein was tested in BL21(DE)3 cells comparing the expression level between LB and Zyp-5052 auto-inducing¹⁰² media at 18°C and 35°C. Moreover, because it was shown that low percentage of ethanol enhances protein yield and solubility¹⁰³, the effect of 2% and 3% ethanol was evaluated. As shown in the SDS-PAGE analyses (figure 3.10), a clear band around 15 kDa was visible in pellet samples of all conditions tested.

Since the molecular weight of His₆-TrkA-d5 was calculated to be 14.38 kDa, it was expected that the bands corresponded to the His₆-TrkA-d5, indicating accumulation in the insoluble fractions as inclusion bodies. In addition, a thicker 15 kDa band was visible in the lane corresponding to the pellet of expression in LB+3% EtOH at 18°C (figure 3.10-B), suggesting that the ethanol increased the target protein yield in the insoluble fraction.

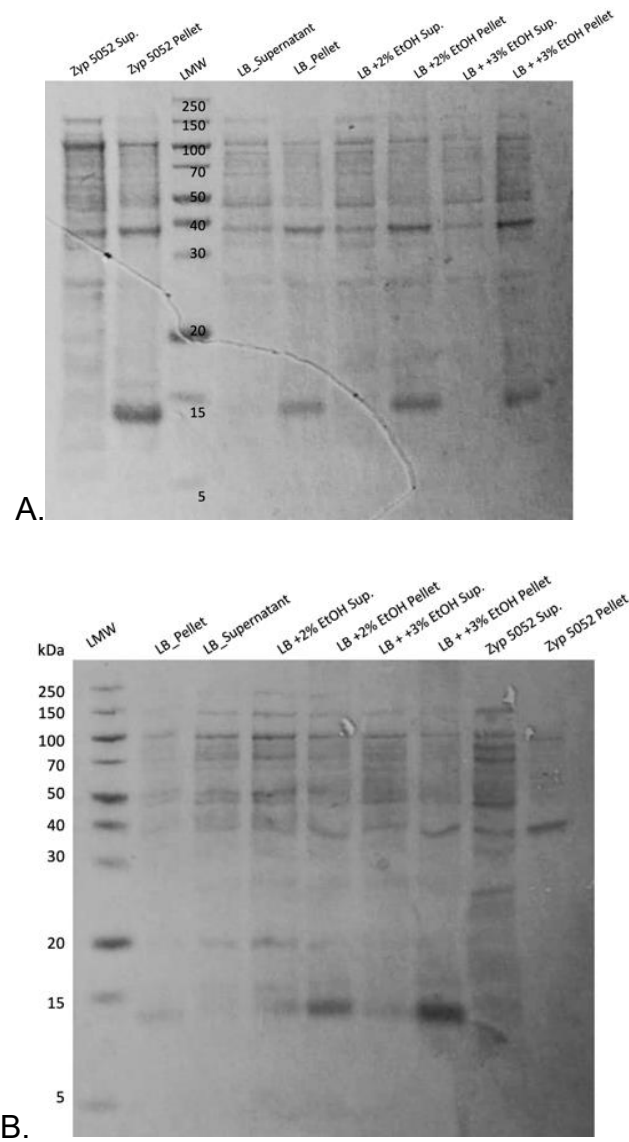


Figure 3.10. SDS-PAGE analysis of His₆-TrkA-d5 expression test in BL21(DE)3 strain. A) SDS-PAGE analysis of expression test conducted at 35°C and **B)** at 18°C. Samples from soluble fractions (Sup.) and insoluble fraction (Pellet) were analysed. At the top of each lane, growth medium and EtOH percentage are indicated. Molecular weights of the LMW markers are shown in kDa.

Second of all, the expression of His₆-TrkA-d5 was carried out in ArcticExpress(DE)3 cells. This engineered strain of *E. coli* constitutively expresses cold-adapted chaperonins Cpn10 and Cpn60 of *Oleispira antarctica*, that showed high refolding activities at 12°C¹⁰⁴. Such low temperature potentially allows the heterologous proteins to properly fold, and hence to increase the final yield of active and soluble protein. The expression was tested in both LB and Zyp-5052 media supplemented without and with 2% or 3% ethanol. From the SDS-PAGE analysis in figure 3.11, a band around 15 kDa was visible in pellet of all conditions tested, but also a light one in the supernatants of the Zyp-5052 medium expression. Thus, using anti-His₆ antibodies Western blot analysis was performed to clearly detect the soluble expression of His₆-TrkA-d5.

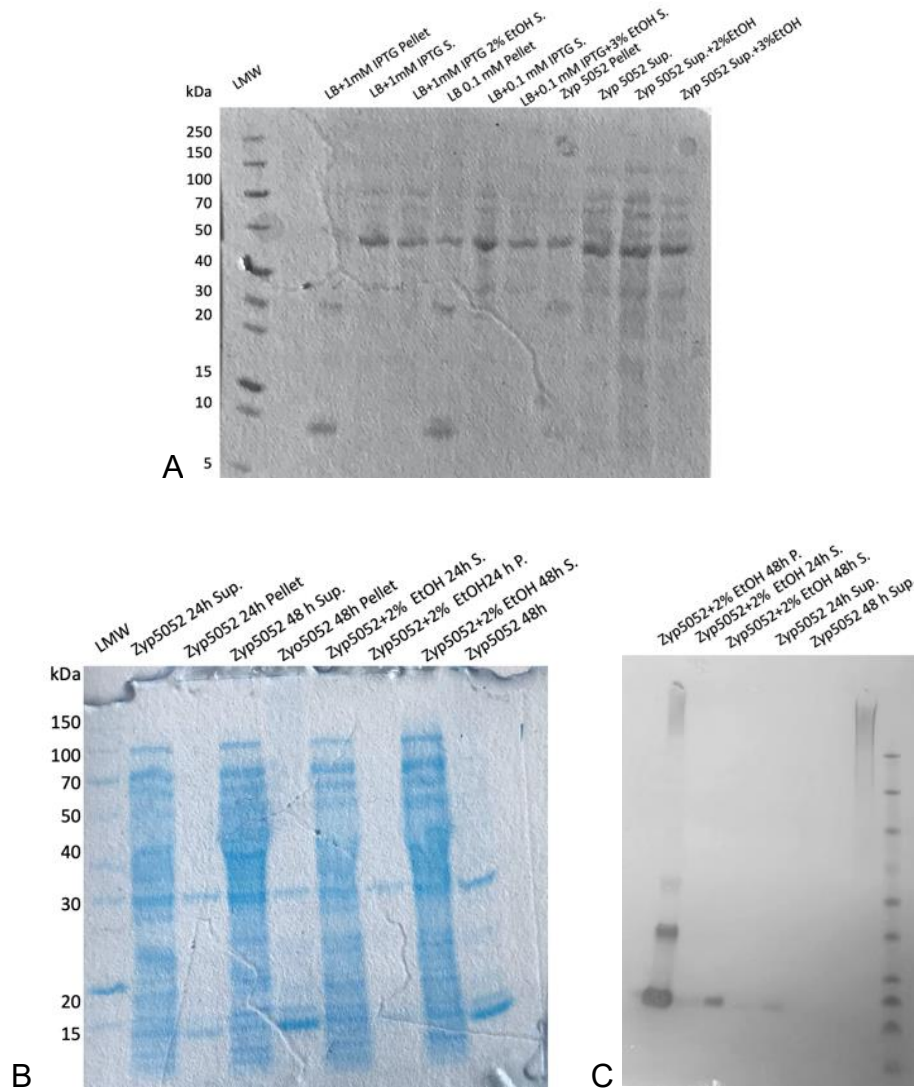


Figure 3.11. SDS-PAGE and Western blot analyses of His₆-TrkA-d5 expression test in ArcticExpress (DE)3 strain. A) SDS-PAGE analysis of the expression tests conducted for 48 hours in LB medium testing 0,1 mM and

1 mM IPTG concentration and the addition of 2% and 3% ethanol, and **B)** Test in Zyp5052 medium after 24 and 48 hours without and with 2% ethanol. Samples from the soluble fractions (sup.) and insoluble fraction (pellet) have been analysed. At the top of each lane, growth medium, IPTG concentration and EtOH percentage are indicated. Molecular weight of the LMW markers is shown in kDa. **C)** Western Blot analysis of soluble fractions of His₆-TrkA-d5 expression in Zyp5052 with 2% and without ethanol after 24 and 48 hours.

As shown in figure 3.11-C, a thick band was visible around 15 kDa and 30 kDa in pellet lane, indicating His₆-TrkA-d5 accumulation in inclusion bodies either as monomer and dimer state. Light bands around 15 kDa were visible in supernatant lanes, a thicker one after 48h of expression in medium supplemented with 2% ethanol, appearing to confirm the ethanol effect on protein solubility and yield. Therefore, the protein production was scaled up to 1L cell culture and protein purification was conducted by affinity chromatography using the HisTrap HP 5 mL column (section 3.1.5). However, the soluble fraction of His₆-TrkA-d5 was not enough concentrated to be detected during elution from the column (chromatogram not shown). Overall, the expression at low temperature and the effect of ethanol on protein solubility did not significantly affect the protein yield needed for structural studies.

Last attempt to improve the soluble production of His₆-TrkA-d5 was to avoid formation of nonnative disulfide bonds during protein synthesis and folding in *E. coli* expression.

Owing thioredoxin and glutathione reductase mutations, Rosetta-Gami 2(DE)₃ cells produce an oxidative cytoplasm that enhance the native disulfide bond formation. Expression tests were conducted in fresh LB, SB and Zyp-5052 media, inducing with either 0.1 or 1 mM of IPTG and performed at 18°C for 24 and 48 hours.

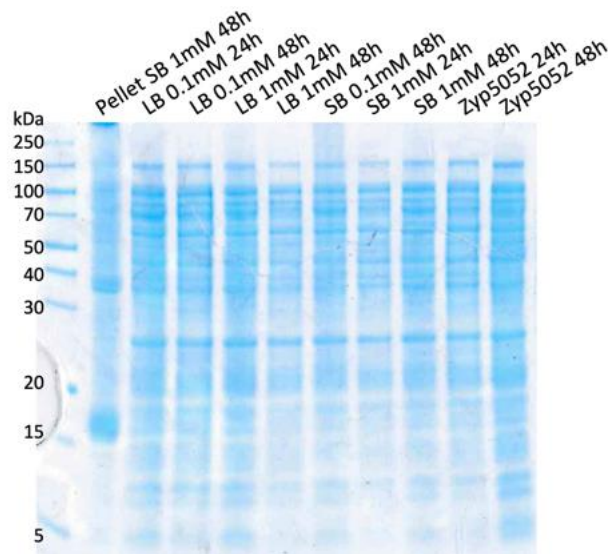


Figure 3.12. SDS-PAGE analysis of His₆-TrkA-d5 expression test in Rosetta-Gami 2(DE)3 strain. Protein expression was conducted for 24 and 48 hours in LB and SB media and induced by either 0.1 mM and 1 mM IPTG, as well as in autoinducing Zyp5052 medium. At the top of each lane, cell growth medium, IPTG concentration and harvest time are indicated. Molecular weight of the LMW markers is shown in kDa.

As indicated by the SDS-PAGE analysis in figure 3.12, the expression of His₆-TrkA-d5 in Rosetta-Gami cells consisted mainly in inclusion bodies formation as a major band at 15 kDa was detected only in the pellet lane.

Based on these results, it was not possible to boost the solubility of TrkA-d5 in *E. coli* expression system and thus the experimental activities moved on the optimization of protein purification from the inclusion bodies.

3.2.3. His₆-TrkA-d5 purification

To recover the His₆-TrkA-d5 from the inclusion bodies, the production was scaled up to 0.5 L of LB medium supplemented with 50 µg/mL kanamycin. Adding 1 mM IPTG and 3% ethanol in cell growth medium, expression was induced and conducted overnight at 18°C and 220 rpm. Thereafter cells were harvested and fresh cell pellet was promptly suspended in lysis buffer and lysed by lysozyme digestion and ultrasounds sonication. Lysate was clarified by centrifugation and the inclusion body pellet was isolated by three consecutive washes. To reduce the amount of DNA, membrane vesicles and cell debris that may co-sediment during centrifugation, low concentrations of denaturing agent (2 M urea), high concentration of NaCl (1M) and 0.1% Triton X-100 were added to washing buffers. Finally, the inclusion bodies were solubilized in denaturation buffer containing 8M urea and 2 mM DTT overnight. Samples of supernatant and pellet after each washing step were taken and analysed by SDS-PAGE. The SDS-PAGE analysis is shown in figure 3.13. The band indicating the His₆-TrkA-d5 domain at 15 kDa was visible in the insoluble fraction after each washing step and in the solubilized sample.

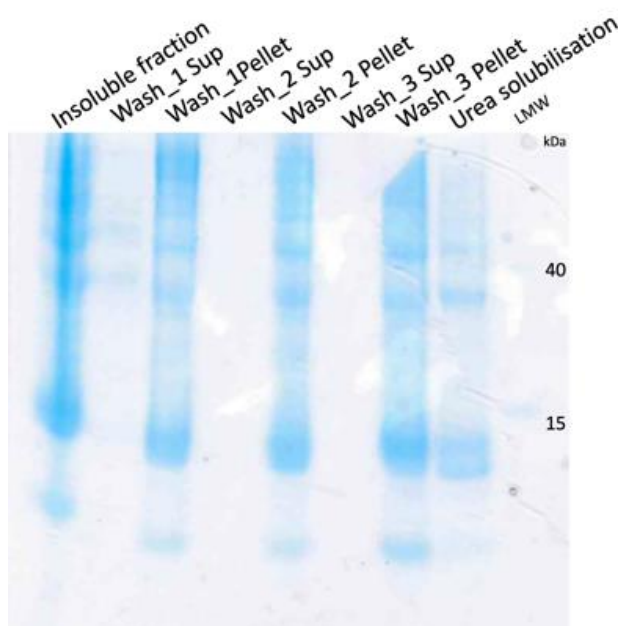


Figure 3.13. SDS-PAGE analysis of His₆-TrkA-d5 inclusion bodies isolation. SDS-PAGE analysis of the target protein recovery from the inclusion bodies. Supernatant and pellet was analysed after each washing step (Wash_1, Wash_2 and Wash_3), as well as the sample after solubilization in 8 M urea. Molecular weight of the LMW markers is shown in kDa.

The denatured solution was centrifuged at 10000 rcf for one hour and samples of supernatant and pellet were analysed by SDS-PAGE. As shown in figure 3.14, the soluble fraction analysed in “supernatant” lane consisted of the His₆-TrkA-d5 (15 kDa band), as well as contaminating proteins, therefore further purification was needed. To search the best strategy for protein refolding in the active monomer conformation (see section 3.1.1), three different methods were performed:

- I. Affinity chromatography in denaturing condition and refolding by dialysis
- II. Dialysis refolding and affinity chromatography in native state.
- III. On-column refolding

First strategy was to purify the His₆-TrkA-d5 in denaturing condition. The advantage of this method is to obtain a pure sample and hence to avoid unwanted interactions with contaminating proteins during refolding.

As shown in the chromatogram (figure 3.14-A), a major peak was visible around 45 mL of elution volume (20% B), which analysis by SDS-PAGE confirmed to be the 15 kDa target protein (figure 3.14-B).

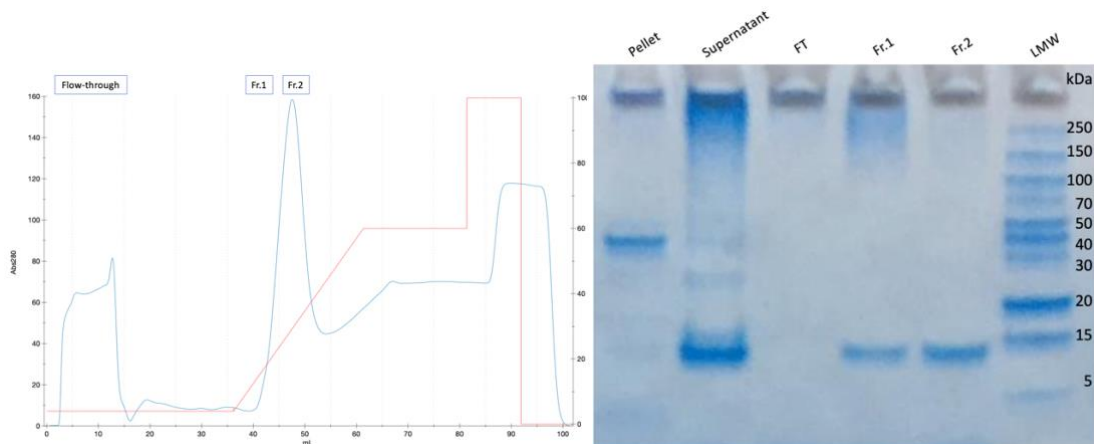


Figure 3.14. Affinity chromatography in denaturing condition. A) Chromatogram of the affinity chromatography. The blue curve is the absorbance at 280 nm and the red line the percentage of elution buffer used. On x-axis, the elution volume is given in mL **B)** SDS-PAGE analysis of pellet and supernatant after urea denaturation, flow-through (FT) and fractions eluted from the column. Molecular weight of the LMW markers is shown in kDa.

The eluted fractions were pooled together and protein concentration was adjusted to 0.1 mg/mL before refolding by step-wise gradient dialysis. According to this refolding method, the urea is gradually removed from the buffer. In the first step, the buffer was supplemented with 4 M urea, second step with 2 M urea and finally dialysis was conducted against refolding buffer without urea.

In the second strategy, the denatured protein was first refolded and then purified by affinity chromatography. As described before, refolding was achieved by step-wise dialysis and thereafter protein solution was centrifuged and loaded onto the column. As shown in figure 3.15-B, the 15 kDa band was visible in both supernatant and pellet after centrifugation, indicating that part of the denatured protein did not refold correctly and precipitated.

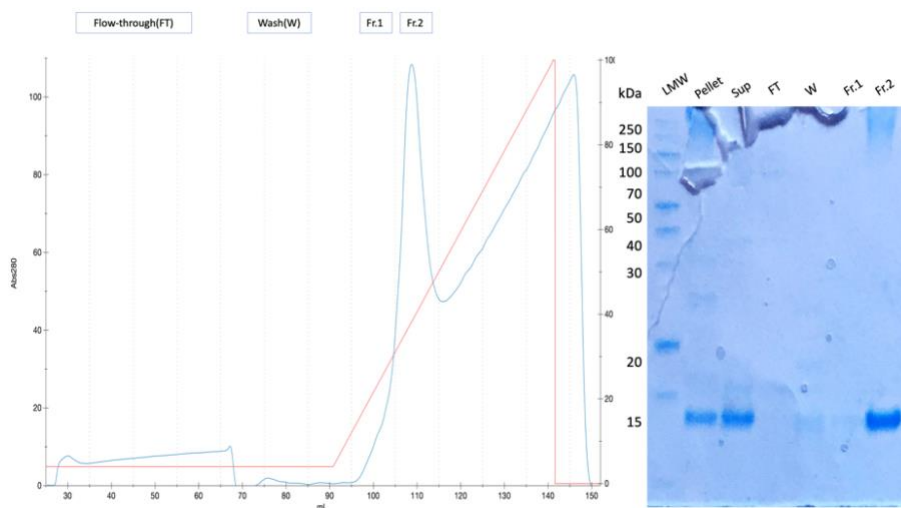


Figure 3.15. Affinity chromatography after refolding. A) Chromatogram of the affinity chromatography. The blue curve is the absorbance at 280 nm and the red line the percentage of elution buffer used. On x-axis, the elution volume given in mL. **B)** SDS-PAGE analysis of pellet and supernatant after refolding, flow-through (FT), wash (W) and fractions eluted from the column (Fr.1 and Fr.2). Molecular weight of the LMW markers is shown in kDa.

Elution was conducted using a linear gradient from 0% to 100% of elution buffer. From the chromatogram (figure 3.15-A), only a sharp peak eluted at 105-110 mL of elution volume (30-40 % B), consisting in pure refolded His₆-TrkAd5 as evaluated by SDS-PAGE analysis (figure 3.15-B).

Third strategy was to refold the target protein directly on column. This method allows to keep the denatured proteins bound to the column matrix during refolding, avoiding intermolecular interactions that may lead to protein misfolding.

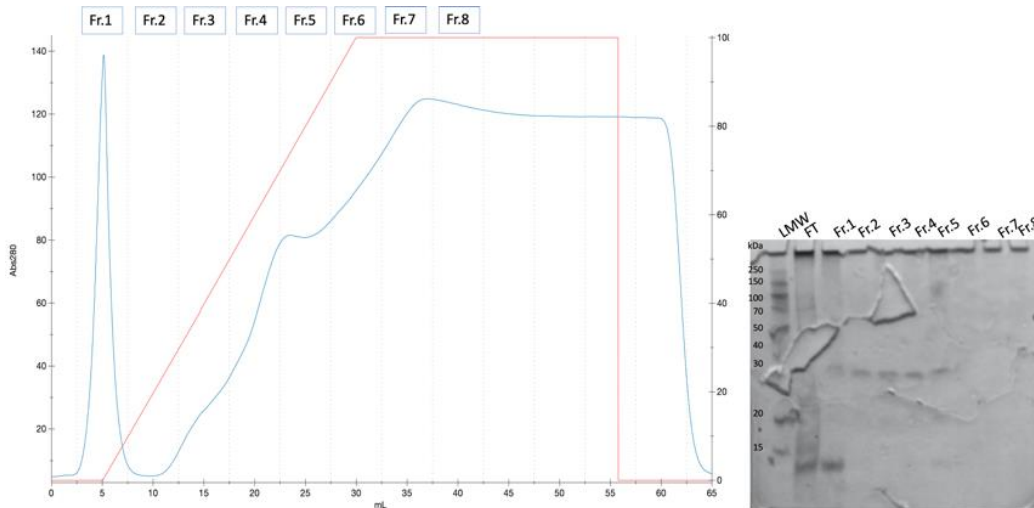


Figure 3.16. Hi_6 -TrkA-d5 on-column refolding. A) Chromatogram of the elution profile of Hi_6 -TrkA-d5 refolded on-column. The blue curve is the absorbance at 280 nm and the red line the percentage of elution buffer used. On x-axis, the eluted volume is given in mL **B)** SDS-PAGE analysis of flow-through (FT) and fractions eluted from the column (Fr.1 to Fr.8). Molecular weight of the LMW markers is shown in kDa.

As shown in the SDS-PAGE (figure 3.16-B), a clear band around 15 kDa was visible in the first fraction at 5 mL of elution volume (Fr.1), proving elution of refolded Hi_6 -TrkA-d5 in the first peak of the chromatogram (figure 3.16-A). Bands around 30 kDa were seen in the other eluted fractions (from Fr2 to Fr6), suggesting elution of Hi_6 -TrkA-d5 refolded in dimeric conformation. In addition, a marked band was visible in the unbound fraction (FT), demonstrating that a portion of the denatured protein flew through the column and was not refolded, thus decreasing the final yield of refolded protein.

Finally, size exclusion chromatography was performed to check the quality of the refolded protein. In the chromatogram (figure 3.17), the elution profiles of the His₆-TrkA-d5 refolded by the three different methods were overlaid.

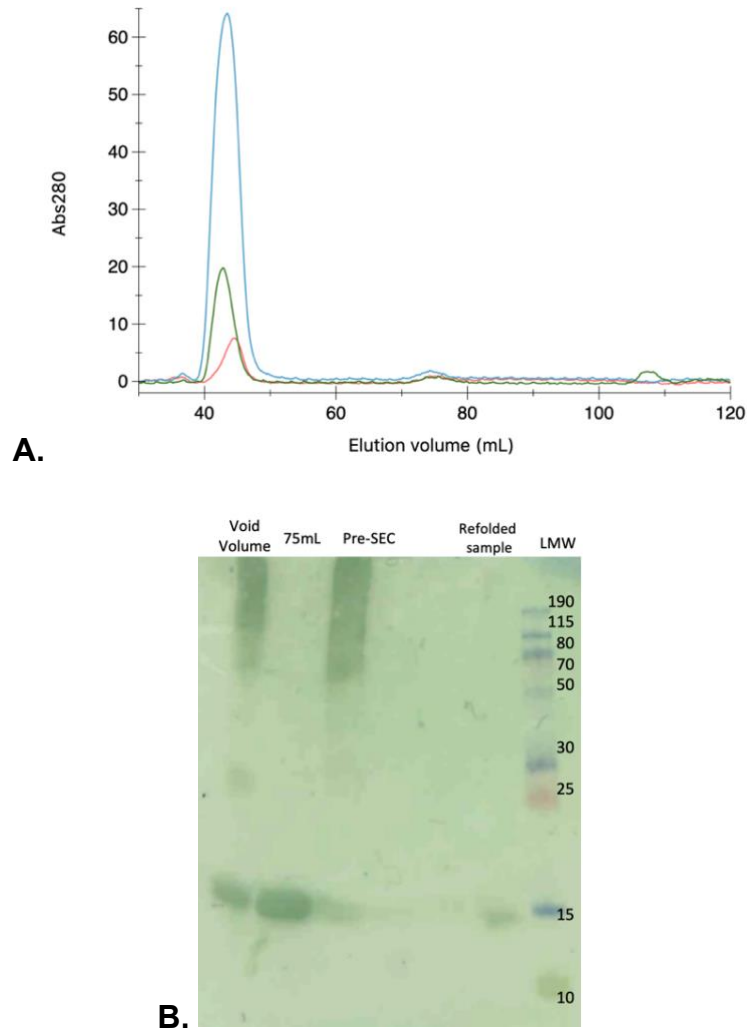


Figure 3.17. Size exclusion chromatography of refolded His₆-TrkA-d5. **A)** Overlay of the elution profiles of the His₆-TrkA-d5 refolded by three different refolding strategy. Samples of refolded protein by (I) affinity in 8M urea and step gradient refolding (green curve), (II) step-gradient dialysis before affinity chromatography (blue curve) and (III) on-column refolding (red curve) were applied on the HiLoad Superdex75 pg 16/600 for size exclusion chromatography. **B)** Western blot analysis of refolded sample (strategy II), concentrated sample before injection (“pre-SEC” lane), concentrated sample eluted at 75 mL and void volume (45mL).

The three curves were characterized by a major peak eluted around 45 mL, corresponding to the column void volume, and a slight shoulder around 75 mL, corresponding to the expected

elution volume of 15 kDa proteins. Because fractions were not enough concentrated for analysis by SDS-PAGE, no bands were visible (data no shown).

So, using antibodies against the poly-histidine tag, Western blot analysis was conducted to detect His₆-TrkA-d5 elution. As shown from the nitrocellulose membrane (figure 3.17), the void volume consisted in the target protein, visible as a band around 15 kDa and a slight band around 30 kDa, indicating that the refolding by the three different strategies did not produce natively folded protein but resulted in soluble aggregates of His₆-TrkA-d5.

In addition, the fraction at 75 mL was concentrated and analysed by Western Blot, which blotting confirmed to be the His₆-TrkA-d5 monomer.

The folding state of the purified His₆-TrkA-d5 monomer was validated by circular dichroism (CD) spectroscopy. As described in section 3.1.17, using CAPITO web server-based tool the far-UV spectrum (top panel) and a double wavelength plot¹⁰⁵ (222 nm versus 200 nm) (bottom panel) were plotted.

As shown in figure 3.18, the spectrum profile exhibited a positive ellipticity at 200 nm and a global minimum at 217 nm, in accordance with a β -strand spectrum characterized by a less intensive positive band at 197 nm and a negative band at 217 nm.

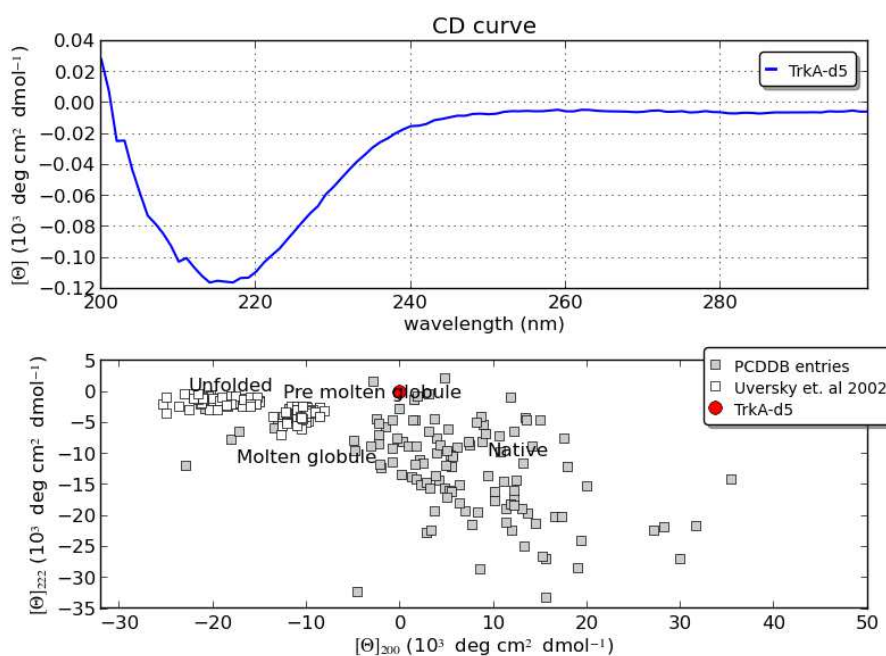


Figure 3.18. Far-UV CD spectra of His-TrkA-d5 monomer. On top, the Far-UV CD spectrum of 20 μ M His-TrkA-d5 recorded at 25°C in 10 mM Tris pH 8.5. On the x-axis, the wavelength in nm and on the y-axis the molar ellipticity in 10^3 degrees $\text{cm}^2 \text{dmol}^{-1}$ are given. Bottom figure, the plot of the molar ellipticity at 200 nm versus 222 nm. Region of folded protein in native, molten globule and pre-molten globule as well as unfolded protein are illustrated. The red spot indicates the 200/222 value of His-TrkA-d5.

From the double wavelength plot, where the spectral values at 200 versus 222 are plotted to evaluate unfolded or pre-molten globule state¹⁰⁵, the his-TrkA-d5 monomer (red spot) was fit in the native region, meaning that the target protein was correctly refolded. However, the final yield of refolded TrkA-d5 monomer was 100 μ g per liter of cell culture, not sufficient for structural studies by X-ray crystallography.

3.2.4. Expression and purification of NMR-TrkA-d5 construct

Second construct used to optimize the production of the TrkA d5 domain, consisted in the encoding gene sequence from 283 to 382 residues, designed by Shoemark et al.⁹⁶ for the NMR spectroscopy studies. As described in section 3.1.1, two point mutations (P and C) were introduced to promote the formation of a stabilizing disulfide bond, as well as five aspartate residues were designed at the N-terminus of the target protein to facilitate protein refolding. This construct, named NMR-TrkA-d5, was cloned as fusion protein with N-terminal hexahistidine tag in both pET28a and pETDuet plasmid.

In an attempt that the introduced mutations along with the NGF co-expression through pETDuet vector could lead to TrkA-d5 soluble production, expression tests were conducted in Rosetta-Gami(DE)3 cells. As shown from the SDS-PAGE analysis (figure 3.19), the bands around 15 kDa corresponding to NMR-TrkA-d5 (14.3 kDa) and NGF (13.2 kDa) were visible only in the insoluble fraction as inclusion bodies.

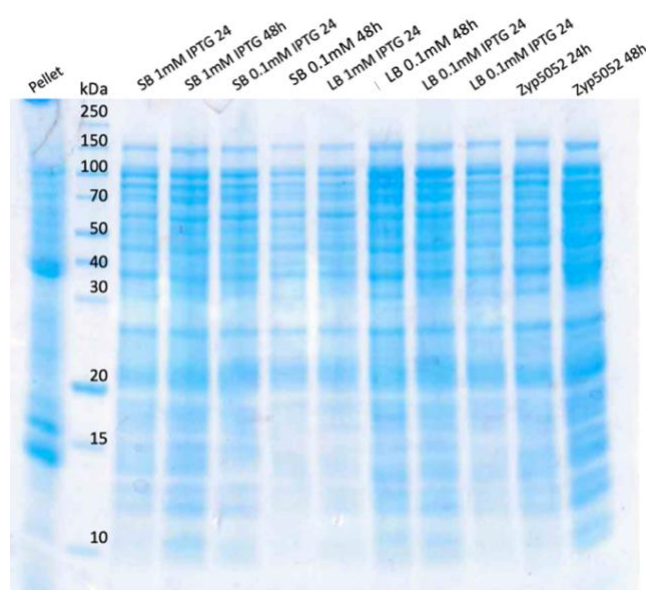


Figure 3.19 Expression tests of NMR-TrkA-d5 in Rosetta-Gami2(DE)3 cells. Conditions tested for expression are reported at the top of each lane. LB, SB and auto-induction (Zyp-5052) media, as well as IPTG concentrations of 0.1 mM and 1 mM and harvesting time at 24 h and 48 were tested. Samples of soluble and insoluble fractions were taken and evaluated. Molecular weight of standards protein is indicated in kDa.

Because the concerted effects along with the oxidizing cytoplasm of Rosetta-gami cells could not help to enhance the protein solubility, the purification protocol of Shoemark et al. was tested.

The only difference consisted in the affinity chromatography by Ni²⁺-metal chelation instead of anion exchange chromatography. They suggested that the concentration step by centrifugal concentrators was critical for protein aggregation, and thus protein concentration was achieved by hygroscopic effect, removing water by dialysis in a concentrating solution of PEG 20000. However, during gel filtration the target protein was eluted in the void volume as soluble aggregates. This protocol was performed several times leading to the same results, concluding that it was not reproducible.

Taking in consideration that the disulfide bond formation in eukaryotic cells is a complex process that involves disulfide isomerase and the more oxidizing environment of the endoplasmic reticulum¹⁰⁶, where disulfide bonds are reduced and rearranged¹⁰⁷, oxidative refolding using GSSG/GSH couple was performed.

Besides, because the suppressive effect of high concentration of arginine on protein aggregation is well established¹⁰⁸⁻¹¹⁰, 1 M of L-arginine was included in the oxidative refolding buffer. After refolding, the NMR-TrkA-d5 was purified by affinity chromatography and thereafter gel filtration was conducted to assess the quality of the refolded sample. As shown in the chromatogram (figure 3.20-A), the target protein was purified by affinity chromatography and eluted at 10% and 30% of buffer B from the HisTrap HP column. Sample was dialyzed to remove the imidazole and then dialyzed against concentrating solution of PEG 20000. From the chromatogram of the gel filtration (figure 3.20-B), the majority of refolded protein eluted in the void volume and a small aliquot at the expected elution volume of 75 mL.

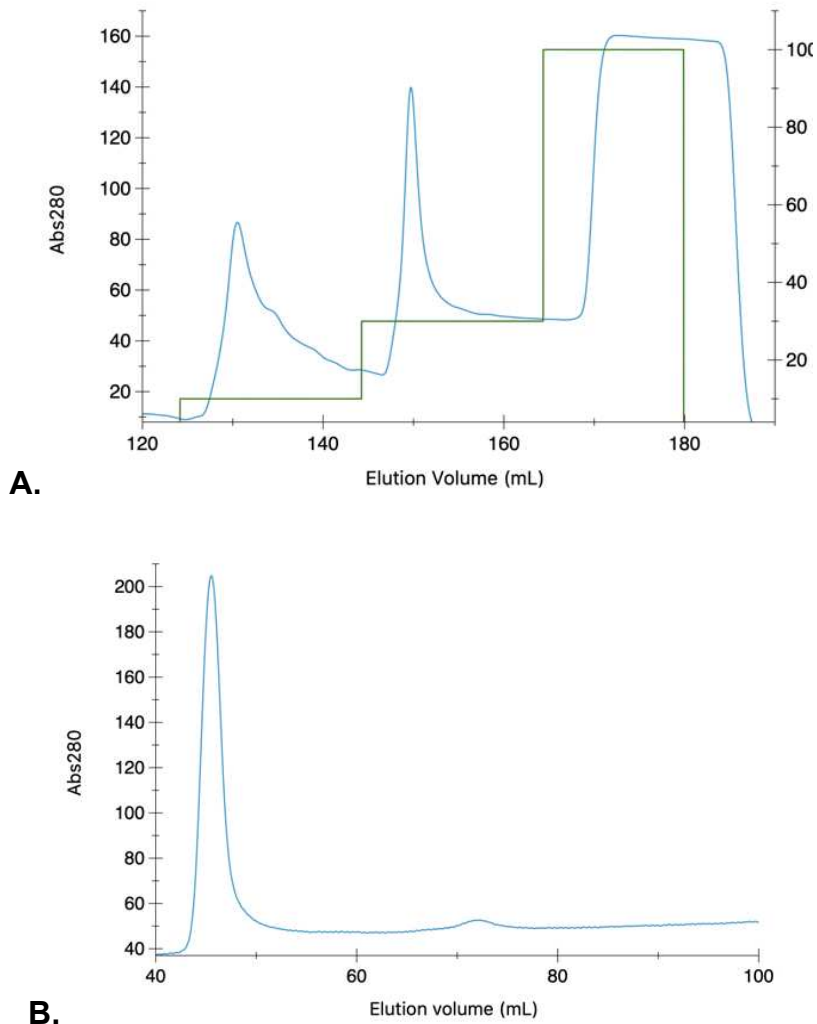


Figure 3.20. Purification of refolded NMR-TrkA-d5 construct. **A)** Affinity chromatography on HisTrap column of the refolded NMR-TrkA-d5 and **B)** size exclusion chromatography of the purified protein. On the x-axis the elution volume is given in mL and on the y-axis the absorbance at 280 nm.

Collectively, the observations based on the SDS-PAGE analyses of the expression tests, as well as the outcome of elution in the void volume of the refolded protein, indicated that the TrkA-d5 domain production yielded mainly inclusion bodies from which protein recovery was not possible. Therefore, research activities moved on to the production of the whole extracellular domain of TrkA in mammalian expression system.

3.3. Production of TrkB d5 domain: material and methods

3.3.1. Construct design

To overcome the insolubility of the TrkB-d5 domain in *E. coli* expression system, the target protein was cloned in pETDuet vector (Novagen) for co-expression together with BDNF. As described in section 3.1.1, containing two multiple cloning sites (MCS1 and MCS2), the pETDuet vector allows the co-expression of two interacting proteins, which may lead to the correct folding during protein synthesis and hence to soluble over-production. The gene sequence of TrkB-d5 (284-395) was cloned in MCS1 with a hexa-histidine tag and a TEV cleavage site at the N-terminus, while the sequence encoding the mature form of BDNF (128-247) was cloned in MCS2. Codon usage of both sequences was optimized for efficient translation and mRNA half-life in *E. coli*, by GenScript service.

3.3.2. TrkB-d5 and BDNF co-expression tests

For the co-expression of TrkB-d5 and BDNF in *E. coli* cells, different media and variables as induction temperature, harvesting time and IPTG concentration were evaluated. A single colony of BL21(DE)3 cells transformed with pETDuet/TrkBd5-BDNF plasmid was inoculated in LB medium added with 100 µg/mL of ampicillin and grown overnight at 37°C and 220 rpm. The overnight culture was diluted in a 1:100 ratio in fresh LB, SB and auto-induction Zyp-5052 media. When cell density reached an OD₆₀₀ of 0.6, temperature was lowered to 18°C and expression in LB and SB cultures was induced by adding either 0.1 mM or 1 mM IPTG. After 24 hours and 48 hours, cells were harvested by centrifugation at 4000xg for 20 minutes at 8°C. Using ultrasounds, cells were lysed on ice and lysate was clarified by centrifuging for one hour at 11000 rcf and 4°C. Samples of soluble and insoluble fractions of all conditions tested (table in figure 3.21 on the following page) were taken and evaluated by SDS-PAGE and Western blot analyses, as described in section 3.1.5.

Medium	LB	LB	LB	LB	SB	SB	SB	SB	Zyp-5052
IPTG	1 mM	1 mM	0.1 mM	0.1 mM	1 mM	1 mM	0.1 mM	0.1 mM	
Harvesting	24h	48h	24h	48h	24h	24h	48h	24h	48h

Figure 3.21. Expression test of pETDuet/TrkB-d5 – BDNF vector in BL21(DE)3 cells. Conditions tested for expression trials are reported in table. The co-expression of TrkB-d5 and BDNF was tested in three different growth media (LB, SB and Zyp-5052), using either 0.1 mM or 1 mM concentrations of IPTG and conducted at 18°C for 24 and 48 hours.

3.3.3. Expression and purification of TrkB-d5 and BDNF

To scale up the production, cells were grown in 1 L of SB medium supplemented with 100 µg/mL ampicillin at 37° C and under shaking at 220 rpm. When optical density reached an OD₆₀₀ of 0.6, over-expression of the recombinant proteins was induced adding 1 mM IPTG and conducted for 48 hours at 18°C. Moreover, to further increase the yield of soluble target protein, a late induction at OD₆₀₀ of 1.2 was performed.

To pellet down the cells, cell culture was centrifuged for 30 minutes at 4000xg and 8°C. Cell pellet was suspended in lysis buffer (0.2 mM PMSF, 150 mM NaCl, 50 mM Tris-HCl pH=7.5) and lysed on ice by ultrasounds, using 75% amplitude and cycle of 20 seconds on and 20 seconds off. To separate the soluble from the insoluble fractions, lysate was clarified by centrifuging for 1 hour at 11000 rcf at 8°C. To purify the target proteins, affinity chromatography was conducted using HisTrap FastFlow 5 mL (GE Healthcare) column, mounted on ÄKTASTART system. Clear lysate was loaded onto the column, previously equilibrated in binding buffer (20 mM imidazole, 150 NaCl, 50 mM Tris-HCl pH=7.5). Flow-through was collected and elution of bound proteins was achieved by step gradient elution, using 8%, 30%, 100% of elution buffer (500 mM imidazole, 150 NaCl, 40 mM Tris-HCl pH= 7.5) and collecting 4 mL fractions. All buffer and protein solution were sterilized filtered using 0.22 µm filter before use. Protein elution was followed as absorption at 280 nm (mAbs₂₈₀) and fractions containing the target protein were identified by SDS-PAGE and Western blot analyses. From the analyses, fractions corresponding to the His₆-TrkB-d5 were pooled together and concentrated using 3000 MWCO centrifugal filter (Pierce™, Thermo Scientific). To further purify the target proteins, concentrated sample was loaded onto the HiLoad 16/600 Superdex75 prep grade column, previously equilibrated in gel filtration buffer (150 NaCl, 50 mM Tris-HCl pH=7.5). Using a flow of 1 mL min⁻¹, isocratic elution was performed for 1.5 column volume collecting 5 mL fractions. Absorption at 280 nm was used to detect protein elution. Samples of eluted fractions were taken for SDS-PAGE and Western Blot analyses.

3.3.4. Mass spectrometry and circular dichroism analysis

To confirm the molecular weight of the eluted protein from the HiLoad 16/600 Superdex75 pg column, and thus to identify the monomer and dimer conformation of the target protein, as well as the identity of co-eluted proteins, mass spectrometry analysis were performed on service (Toscana Life Science, Mass Spectrometry facility). For peptide mass fingerprinting, protein sample was run on SDS-PAGE and each band was treated by trypsin digestion before analysis. Regarding electrospray ionization - mass spectrometry (ESI-MS), protein samples were prepared in 150 μL of water with a final concentration of 3 μM and analysed using LTQ Orbitrap mass spectrometer equipped with ESI source interfaced to UPLC Easy LC 1000.

In addition, the purified sample was characterized by Far-UV circular dichroism (CD) spectroscopy as described in section 3.1.7 and CD spectra were plotted and analysed by CAPITO web server-based tool⁹⁸.

3.3.5. Crystallization screen of TrkB-d5

The purified monomer of TrkB-d5 domain was concentrated and quantified by UV/visible spectra using the extinction coefficient ($\epsilon=25565 \text{ M}^{-1} \text{ cm}^{-1}$), computed by ProtParam tool of ExPasy server¹⁰⁰.

Crystallization screens of Jena Bioscience Screen (Basic 1-4 and Classic 6), as well as Crystal Screen 1 and 2 (Hampton research) were manually set up using the sitting drop method. Drops consisted in 2 μL of protein solution at final concentration of either 5 mg/mL and 7.5 mg/mL and 2 μL of reservoir, equilibrated over 200 μL reservoir. All screen plates were stored at room temperature. To date, no crystals have been observed in the condition tested for crystal growth.

3.4. Production of TrkB D5 domain: results

Because of the known insolubility of the TrkB-d5 domain in *E. coli* expression system^{48,84,111}, the gene encoding the d5 domain was cloned into the multiple cloning site 1 of pETDuet vector for co-expression together with the encoding sequence of the mature form of BDNF, cloned in the multiple cloning site 2. The idea was to enhance the protein solubility by providing the native interacting partner and hence improving protein folding.

Firstly, the growth conditions were established by expression tests, secondly the production was scaled up for protein purification and lastly the purified protein was characterized by mass spectrometry and circular dichroism spectroscopy before to set up crystallization screening. The results achieved are described in the sections below.

3.4.1. TrkB-d5 and BDNF co-expression tests

As described in section 3.3.2, the co-expression of TrkB-d5 and BDNF was conducted in three different media at 18° C, testing the induction with either 1 mM and 0.1 mM IPTG and the effect of autoinduction for 24 and 48 hours. After harvesting and sonication of the cells, samples of the soluble and insoluble fractions were analysed by SDS-PAGE (figure 3.22-A).

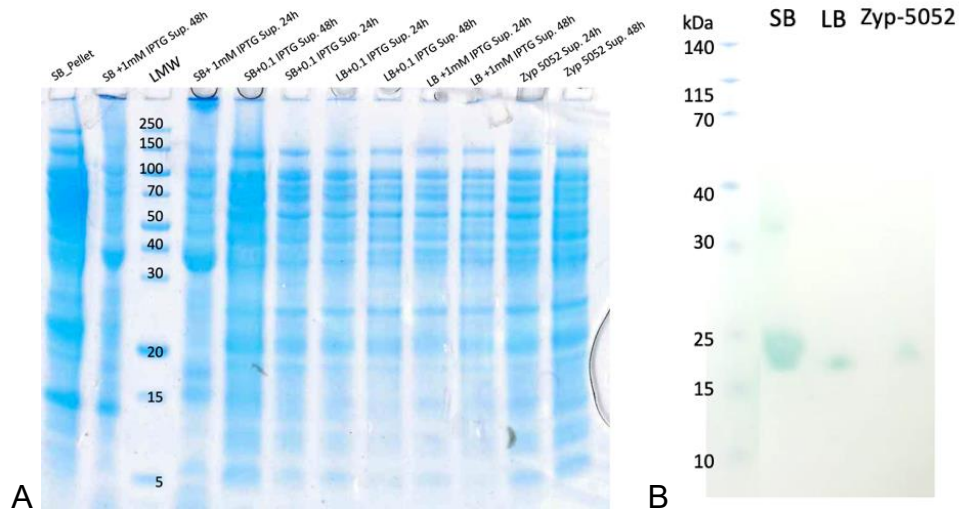


Figure 3.22. SDS-PAGE and Western Blot analyses of pETDuet/TrkB-d5 – BDNF vector expression test. A) Conditions tested are reported at the top of each lane. The co-expression was tested in LB, SB and Zyp-5052 growth media, using either 0.1 mM or 1 mM concentrations of IPTG and conducted at 18°C for 24 and 48 hours. The molecular weight of standard protein is indicated in kDa in the “LMW” lane. **B)** Western blot analysis of the supernatant after 48 hours of induction by 1 mM IPTG and co-expression in LB, SB and Zyp5052 medium.

Here, a band around 15 kDa was visible in both pellet and supernatant lanes of the expression conducted in SB medium for 48h, which was not visible or faint in the other lanes indicating that the expression of a protein with a molecular mass of approximately 15 kDa was induced. Because TrkB-d5 was calculated to have a molecular mass of 14,9 kDa and BDNF a molecular mass of 13,5, it was expected that the overexpressed protein was TrkB-d5. To further verify the expression of TrkB-d5 domain and compare the expression level between the different growth media, the supernatant of cells induced by 1 mM IPTG in SB, LB and auto-inducing Zyp5052 media were blotted and analysed by Western Blot (figure 3.22-B). Using anti poly-histidine tag HRP- conjugated monoclonals, TrkB-d5 was detected in all soluble fractions (“SB”, “LB” and “Zyp-5052” lanes), showing a thicker band in the “SB” lane. Thus, this expression condition was chosen for scaling up the production.

3.4.2. Expression and purification of TrkB-d5 and BDNF

E. coli cells were transformed with pETDuet plasmid encoding TrkB-d5 and BDNF, grown until the optical density OD_{600} reached approximately 0.6-0.8 and induced with 1 mM IPTG for 48 hours at 18°C. To increase the protein yield, expression protocol was further optimized by late induction at OD_{600} 1.2.

After harvesting and cell lysis, supernatant was loaded on the HisTrap HP 5 mL column. The unbound proteins were collected (the flow-through, "FT" lane), the column was washed and the bound proteins were eluted by step gradient elution. Samples at the different purification stages were taken and analysed by SDS-PAGE (figure 3.23).

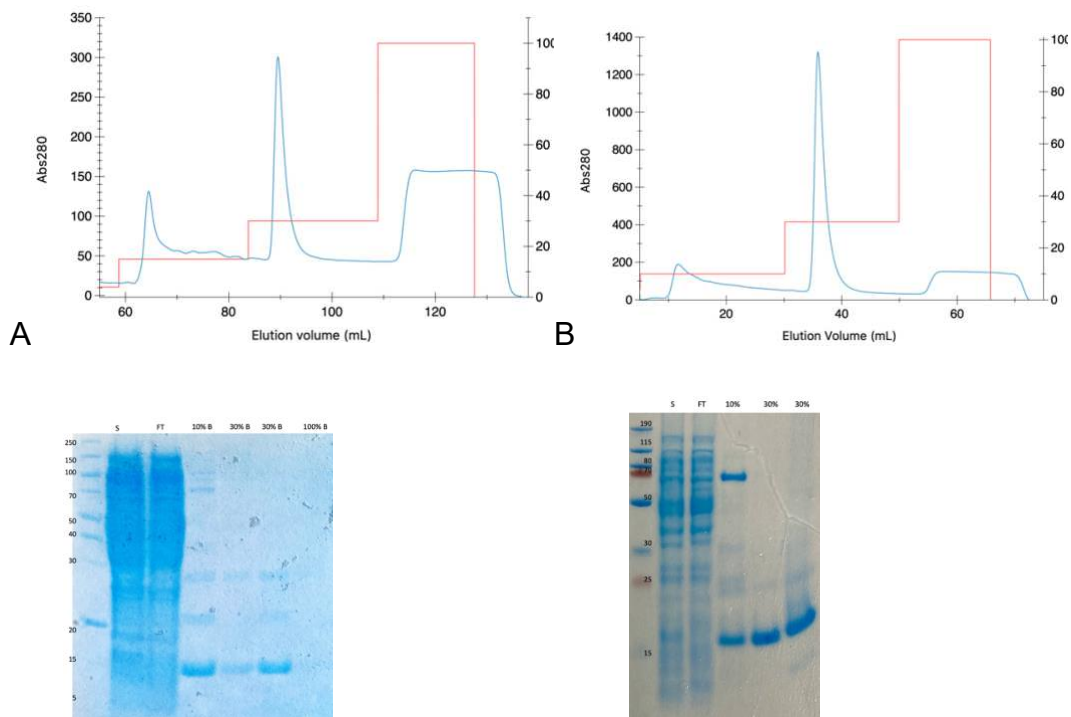


Figure 3.23. Purification of TrkB-d5 and BDNF by affinity chromatography. A) On top, chromatogram of the purification of TrkB-d5 and BDNF co-expression induced at OD_{600} 0.6 and **B)** chromatogram of the purification of TrkB-d5 and BDNF late induction. The blue line is the absorbance at 280 nm and the red line the percentage of elution buffer. On the x-axis the elution volume is given in mL and on the y-axis the absorbance at 280 nm. On bottom, the SDS-PAGE analyses of the supernatant (S), flow through (FT) and fractions eluted at 10%, 30% and 100% of elution buffer.

As shown in figure 3.23, the elution profile of the supernatant of expression induced at OD₆₀₀ 0.6 (figure 3.23-A) and the elution profile of induced cells at OD₆₀₀ 1.2 (figure 3.23-B) consisted in one peak eluted at 10% of elution buffer (50 mM imidazole) and another major peak at 30% elution buffer (150mM imidazole). From the SDS-PAGE analysis, multiple bands were observed in the “10%” elution lane, one of which at 15 kDa, indicating that TrkB-d5 eluted with contaminants. In “30%” elution lane, three bands were visible, one at 15 kDa corresponding at TrkB-d5, one at 25 kDa and another at 30 kDa, probably corresponding to TrkB-d5 dimer.

Two main differences were observed between the purification of the late induction and the induction at OD₆₀₀ 0.6. Firstly, the observation that the peak at 30% elution of the late induction was 4 fold higher, indicating that induction at OD₆₀₀ 1.2 increased protein yield. Secondly, an additional faint band was visible below 15 kDa in the SDS-PAGE analysis, probably corresponding to BDNF.

Thereafter the fractions corresponding to the 30% elution were pooled together, concentrated and loaded onto the gel filtration column. The chromatogram of the purified sample from the co-expression induced at 0.6 is shown in figure 3.24-A, while the elution profile of the late induction purification is shown in figure 3.26-A.

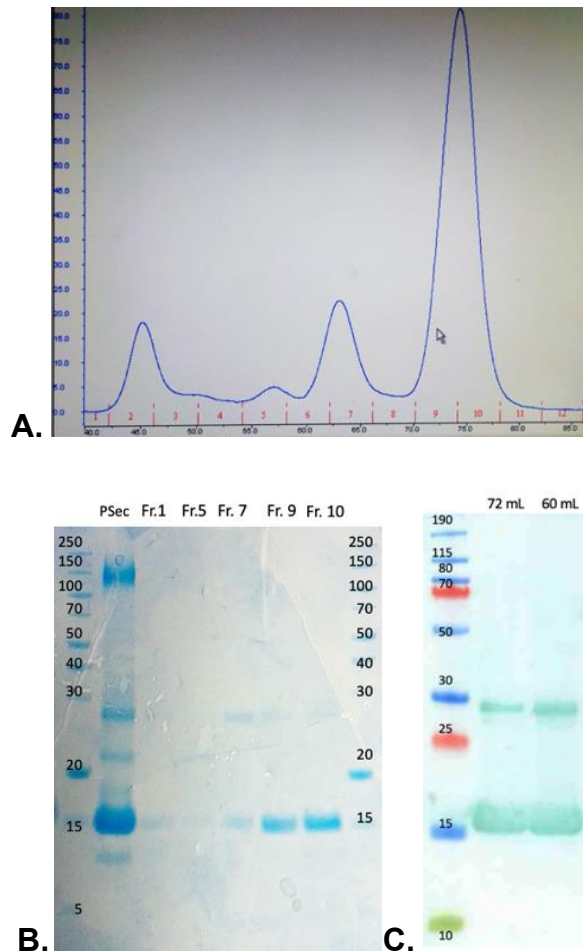


Figure 3.24. Purification of TrkB-d5 and BDNF co-expression by size exclusion chromatography. A) Elution profile of the TrkB-d5 and BDNF co-expression at OD₆₀₀ 0.6. On the x-axis the elution volume is given in mL and on the y-axis the absorbance at 280 nm. **B)** SDS-PAGE analyses of the supernatant (S), flow through (FT) and fractions eluted at 10%, 30% and 100% of elution buffer.

Starting from the first chromatogram, four peaks were eluted and the corresponding fractions were analysed by SDS-PAGE (figure 3.24-B). Sample before injection was analysed in “P_{Sec}” lane, where multiple bands were visible, among these the 15 kDa band corresponding to the TrkB-d5 and a slight band under 15 kDa presumably corresponding to BDNF. The first peak consisted in the void volume (“Fr.1” lane), the second peak eluted around 57 mL was analysed in “Fr5” lane and two faint band at 15 kDa and above 20 kDa were visible. The third peak eluted at 62.5 mL showed two bands, one at 15 kDa and the other at 30 kDa (“Fr7” lane), and the final peak was analysed in “Fr9” and “Fr10” lanes, showing a more intense band at 15 kDa.

The eluted fractions were concentrated and blotted for Western Blot analysis using anti histidine tag antibodies. As shown in figure 3.24-C, two bands were lighted up, suggesting that

the 15 kDa band consisted in TrkB-d5 domain in monomer conformation and the band around 30 kDa to the dimer conformation.

Besides the mentioned observations made from the SDS-PAGE and Western Blot analyses, mass spectrometry was used to indicate the exact mass and thus to identify the eluted proteins. Using electron-spray ionization mass spectrometry (ESI-MS), the mass in native state of the eluted fractions at 60 mL and 72 mL was analysed. As shown in figure 3.25-A, only one peak at 14989 Da was observed confirming that the eluted protein at 72 mL corresponded to the TrkB-d5 purified in monomer conformation.

On the other hand, the analysis of the elution at 60 mL resulted in a peak at 29978 Da (3.25-B), exactly twice the mass of elution at 72 mL, confirming the dimer conformation of TrkB-d5.

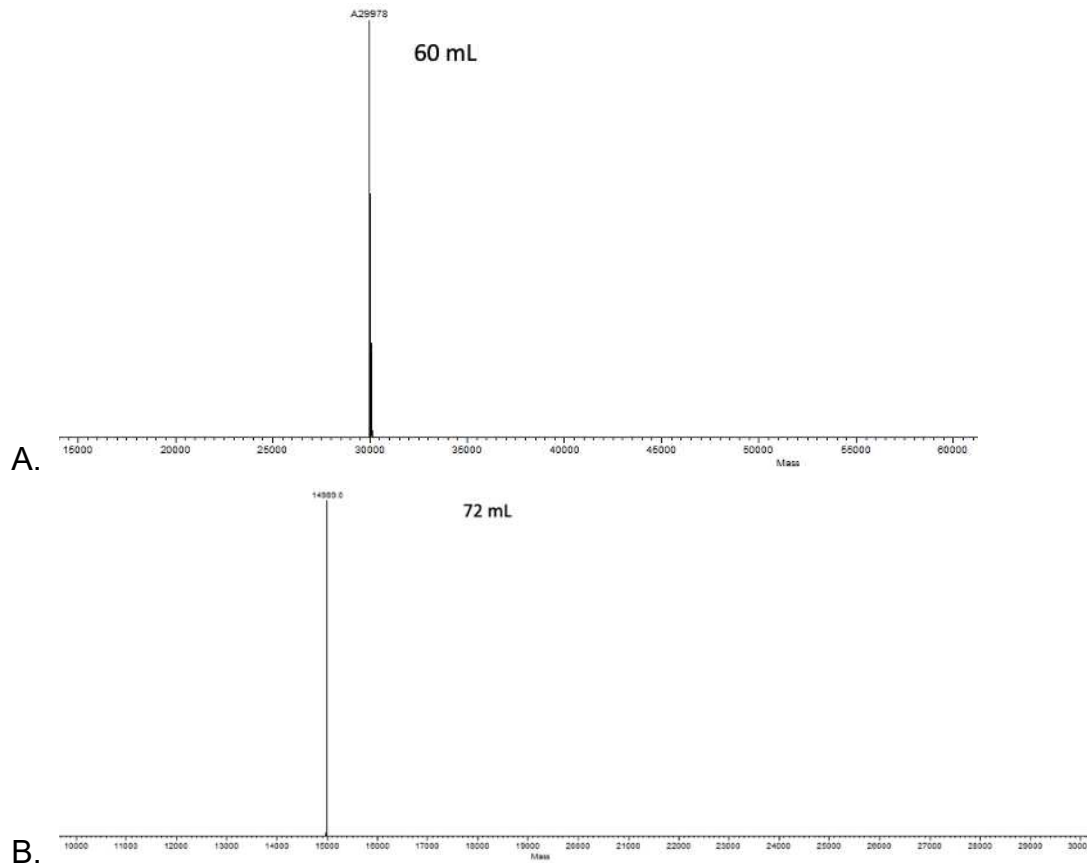
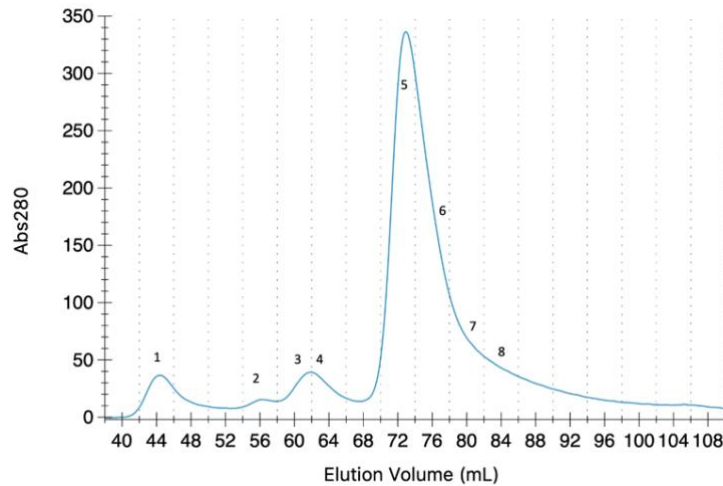
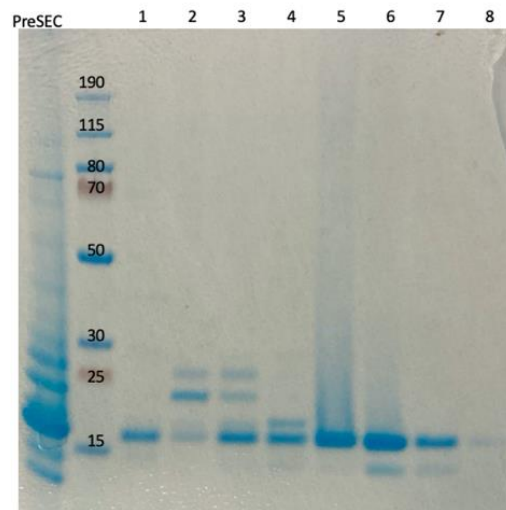


Figure 3.25. ESI-MS Orbitrap spectrum in native state **A)** Spectrum of the eluted fraction at 72 mL and **B)** of the fraction eluted at 60 mL of the HiLoad Superdex 200 pg 16/60 column. On the x-axis the mass is given in Dalton (Da) and on the y-axis the relative abundance. Theoretical molecular weight of TrkB-d5 is 14911,54 Da, determined molecular weight 14989 Da.

Analyzing the chromatogram of the late induction (figure 3.26 A-B) important differences were observed. Besides the higher elution peak at 72 mL, corresponding to the TrkB-d5 monomer elution, a faint band under 15 kDa was visible in the tail of the peak analysed from lane 6 to 8, presumably corresponding to BDNF (13.5 kDa). Moreover, it was speculated that the band around 25 kDa visible in the fractions analysed in lane 2 and 3, and visible in “Fr5” lane of figure 3.22-B, corresponded to the BDNF dimer.



A.



B.

Figure 3.26. Size exclusion chromatography of TrkB-d5 and BDNF co-expression at late induction. A) Chromatogram of the TrkB-d5 and BDNF purification. The elution curve is highlighted in blue together with the number of each fraction analysed by SDS-PAGE. On the x-axis the elution volume is given in mL and on the y-axis the absorbance at 280 nm. **B)** SDS-PAGE analysis of the eluted fractions. At the top of each lane, the number of the fraction analysed is given.

To verify the identity of the bands in lane 2, peptide mass fingerprinting analysis were conducted on service at Toscana Life Science. As shown in figure 3.27-A, after trypsin digestion of the band at 25 kDa 15 peaks were identified covering the 82.5% of the BDNF sequence (figure 3.27 A-B). The digestion of the band at 15 kDa covered 78.9% of TrkB-d5 domain and 40% of BDNF and the band at about 13 kDa 51.1% TrkB-d5 and 40% BDNF (figure 3.27-A). The ambiguous identification of both TrkB-d5 and BDNF at 15 kDa and around 13 kDa was probably due to the proximity of the two bands, not sufficiently separated by the electrophoretic run.

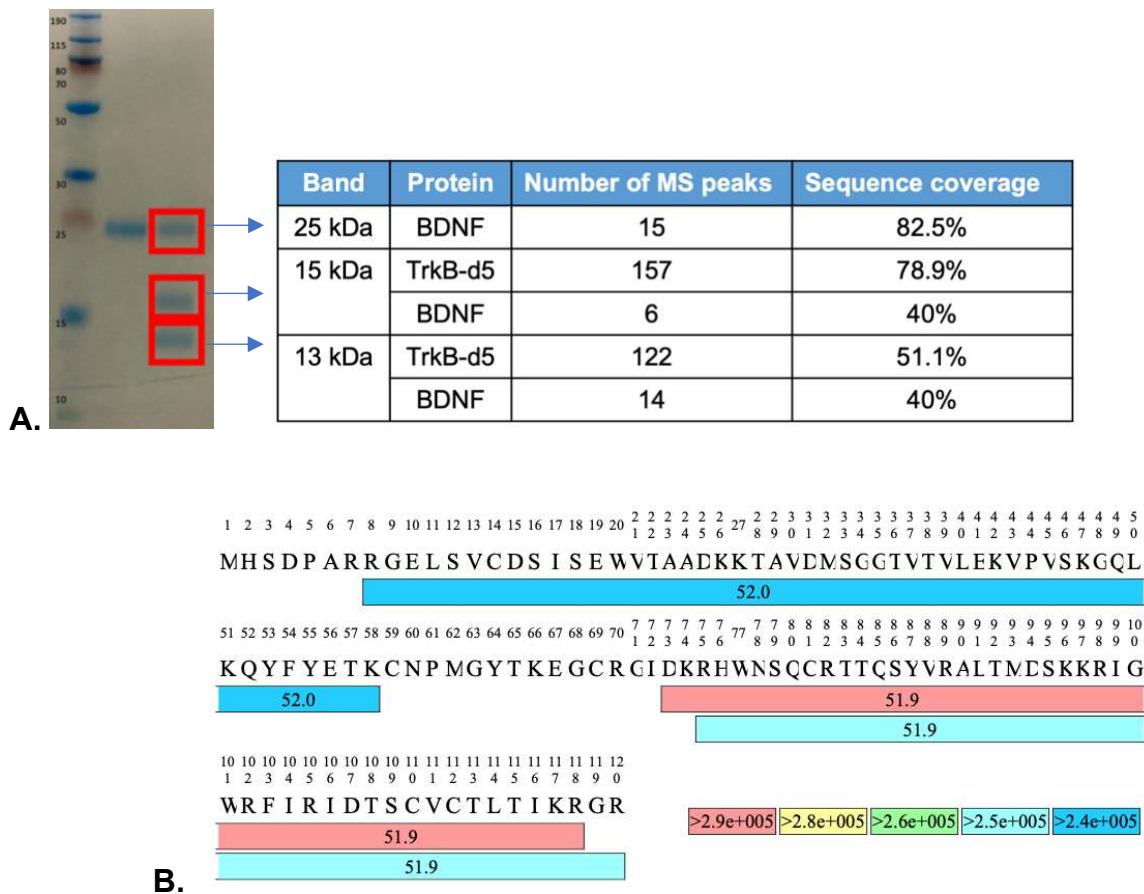


Figure 3.27. Peptide mass fingerprint from SDS-PAGE analysis. A) SDS-PAGE analysis of elution peak at 57 mL (lane 2) from HiLoad Superdex200 16/600 pg. On the right, the table shows the identified peaks after trypsin digestion of each band and the sequence coverage of the target proteins. **B)** Illustration of the identified peptides by mass fingerprinting of the band at 25 kDa and corresponding coverage of BDNF sequence. The color legend for signal intensity is shown.

Based on these results, it was speculated that the peak at 57 mL corresponded to the elution of TrkB-d5 and BDNF complex. Besides, it was possible to conclude that the co-expression strategy of TrkB-d5 and BDNF allowed the soluble expression of TrkB-d5 monomer, the expression of BDNF at lower yield respect to TrkB-d5 but not the purification of TrkB-d5 and BDNF as a complex.

Next, secondary structure and folding of the purified TrkB-d5 monomer was verified by circular dichroism (CD) spectroscopy. Briefly, far-UV CD records the unequal absorption of right-handed and left-handed circularly polarized light by a chiral chromophore, i.e. the peptide bonds of protein backbone. The final spectrum of a given protein will provide an estimate of the secondary structure composition, with secondary element with highest propensity having the largest impact on the spectrum profile.

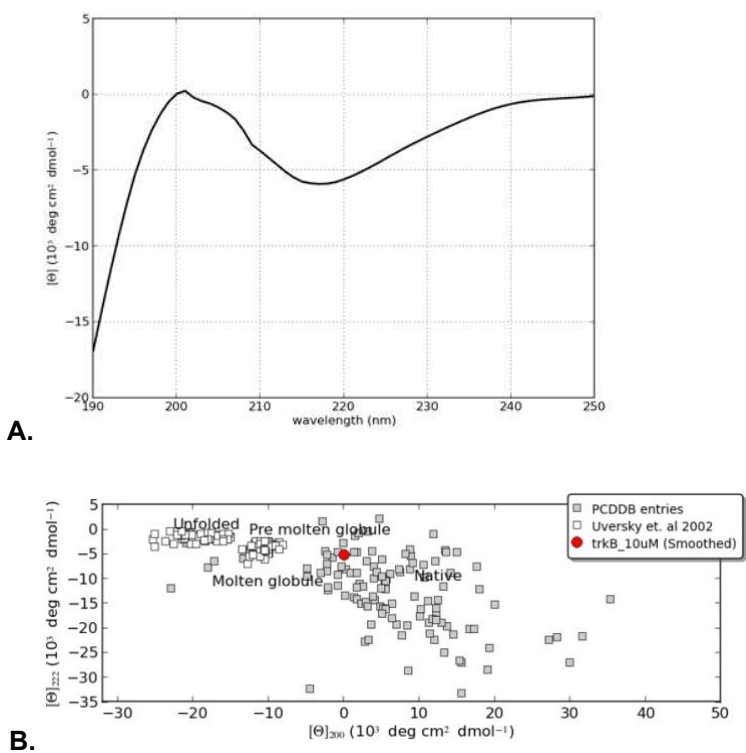


Figure 3.28. Far-UV CD spectra of TrkB-d5 monomer. A) Far-UV CD spectrum of 10 μM TrkB-d5 recorded at 25°C in 10 mM Tris pH 7.5. On the x-axis, the wavelength in nm and on the y-axis the molar ellipticity in 10^3 degrees $\text{cm}^2 \text{dmol}^{-1}$ are given. **B)** Plot of the molar ellipticity at 200 nm versus 222 nm. Region of folded protein in native and molten globule, as well as pre-molten globule and unfolded protein are illustrated. The red spot indicates the 200/222 value of TrkB-d5.

The far-UV CD spectrum of 10 μ M TrkB-d5 was recorded and data plotted by CAPITO server (figure 3.28). Here, the overall profile was deficient in positive molar ellipticity and showed a spectral minimum in the 210 to 220 nm range. This was in accordance with a β -strand basis spectrum, characterized by a less intensive positive band at 197 nm and a negative band at 217 nm. In addition, the spectral values at 200 versus 222 were plotted by CAPITO to estimate the protein folding state¹⁰⁵ (figure 3.28-B), indicating folding of the Trkb-d5 monomer (red spot) in the native region.

Collectively, the data presented in this chapter showed that the production of TrkB-d5 in monomer and native conformation was achieved by late induction of *E. coli* cells and co-expression together with BDNF, obtaining a final yield of 5 mg/mL.

4. The extracellular domain of TrkA and TrkB receptors

This chapter is divided into four main sections, which describe the methods utilized and the results achieved for studies on TrkA and TrkB ectodomains. The first section outlines the experimental procedures for the production of TrkA and TrkB extracellular domains in mammalian expression system and the results of their expression and purification. The second section focuses on crystallization screening and optimization for structural characterization by X-ray crystallography, while third section describes preliminary studies for the structural characterization by Single Particle Cryo Electron Microscopy. The fourth section will present the biophysical characterization of the interaction between the purified target proteins and the neurotrophin mimetics developed within the EuroNeurotrophin consortium.

4.1. Production of TrkA and TrkB ectodomains: material and methods

4.1.1. Gibson Cloning

The encoding sequences of human TrkA and TrkB receptors were purchased at Source BioScience as cDNA I.M.A.G.E. clones¹¹². The sequences corresponding to the ectodomains (TrkA-ECD 33-416, TrkB-ECD 32-430 residues) were extracted by polymerase chain reaction (PCR) and inserted into p α -HBiP mammalian expression vector by Gibson Assembly, providing a translocation signal at the N-terminus and an octa-histidine tag at the C-terminus.

To perform the Gibson Assembly, the p α -HBiP vector (4627 bp) was open by enzymatic digestion using BamHI and EcoRI (Anza™, Invitrogen) for 15 minutes at 37° C in thermocycler (SimpliAmp™, ThermoFisher Scientific) according to manufacturer's protocol. PCR products encoding TrkA-ECD (1155 bp) and TrkB-ECD (1192 bp) were amplified from cDNAs (I.M.A.G.E. clone 5200930 and clone 4941763, respectively), using Platinum SuperFi™ II PCR Master Mix (Invitrogen), forward and reverse primers as described in figure 4.1.

Fwd TrkA-ECD
GCTCAGCGCGGCGGGCCGGATCCGCCGACCCCTGCCCCGAT

Rev TrkB-ECD
GGTGATGATGGTGGTGATGGAATCCCAAAGGTGTTTCGTCCTTC

Fwd TrkB-ECD
CTGCTGCTCAGCGCGGCGGGCCGTGCCACGTCCTGCAAATG

Rev TrkB-ECD
GCTCGAGTCAATGATGGTGATGATGGTGATGTTCCCGACCGGTTTTTA

PCR Reaction Protocol		
Step	Temperature	Time
Initial denaturation	98°C	30''
35 cycles	Denature	98°C
	Anneal	62.2 °C
	Extend	72°C
Final extension	72°C	5'

Figure 4.1. Primers design and PCR protocol. On the left panel, forward (Fwd) and reverse (Rev) primers used for PCR reactions are shown. In red, annealing bases to the TrkA-ECD and TrkB-ECD encoding sequences for PCR amplification, in blue the complementary bases to vector backbone for Gibson Assembly. On the right panel, an overview of PCR protocol reporting steps, temperature and time adopted for the reactions.

The reaction mixes were loaded on 1% agarose gel and electrophoresis was run in tris-acetate EDTA (TAE) buffer for 40 minutes at 100 V. The agarose gel was dyed for 20 minutes using Syber™ safe DNA gel stain (Invitrogen), digestion and PCR products were visualized by UV light and purified using the E.Z.N.A. gel extraction kit (Omega Bio-Tec). To clone p α -HBiP/TrkA-ECD and p α -HBiP/TrkB-ECD plasmids, 100 ng of linearized p α -HBiP vector and 2-fold molar excess of either TrkA-ECD or TrkB-ECD PCR products were assembled by incubating for 15 minutes at 50° C in thermocycler. Following incubation, 2 μ L of each reaction were transformed in DH5- α competent cells following standard protocol and cells were plated on LB agar plate containing 50 μ g/mL ampicillin for plasmid selection. After transformation, single colonies were inoculated in 10 mL of LB supplemented with 50 μ g/mL ampicillin and grew overnight at 37° C. Then, DNA of each clone was extracted according to manufacturer's instructions (E.Z.N.A. Mini Prep kit, Omega Bio-Tec), digested by restriction enzymes and analysed by agarose gel electrophoresis. To validate the cloned genes, 400 ng of extracted p α -HBiP/TrkA-ECD and p α -HBiP/TrkB-ECD plasmid DNA were sent for Sanger sequencing (Eurofins genomic, Ebersberg, Germany).

Finally, chloramphenicol amplification was performed to produce milligram-scale quantities of the p α -HBiP/TrkA-ECD and p α -HBiP/TrkB-ECD expression vector, required for mammalian transfection. DH5- α cells transformed either with p α -HBiP/TrkA-ECD or p α -HBiP/TrkB-ECD were inoculated in 200 mL of LB medium added with 50 μ g/mL Amp and grown overnight at 37° C. When optical density OD₆₀₀ reached 2.0, 20 μ g/mL of chloramphenicol were added to reduce proteins synthesis and to allow higher yield and purity of plasmid DNA¹¹³. After five

hours, cells were harvested and target plasmids were purified using E.Z.N.A. Maxi Prep kit (Omega Bio-Tec) following the manufacturer's protocol.

4.1.2. *Transient transfection of TrkA and TrkB in mammalian cells*

Human embryonic kidney 293 (Hek293) (Thermo Fischer Scientific Freestyle™-F) cells were maintained in FreeStyle293™ expression medium (Gibco, Thermo Fisher Scientific) supplemented with 1% of fetal bovine serum (FBS) in a humidified 5% CO₂ incubator at 37° C and 110 rpm. When cell density reached about 2×10^6 cells/mL and cell viability was above 98%, the p α -HBiP/TrkA-ECD and p α -H BiP/TrkB-ECD expression vectors were transiently transfected using polyethylenimine (PEI).

PEI and plasmid DNAs were separately diluted in serum-free Opti-MEM™ (Thermo Fisher Scientific) at 5% of the total production volume in a ratio of 1 μ g DNA to 4 μ g PEI per mL cell culture. After 10 minutes incubation at room temperature, the two mixtures were pooled together and incubated for an additional 15 minutes to allow the formation of DNA-PEI complexes before adding to cell suspension.

First of all, using small scale productions of transfected cells and un-transfected cells, expression test of p α -HBiP/TrkA-ECD was conducted. To evaluate the protein expression, samples of elution from Ni-NTA resin were taken for SDS-PAGE and Western Blot analyses. Then, the productions of both TrkA-ECD and TrkB-ECD were scaled up to 500 mL of cell suspension. Moreover, to lower the glycosylation complexity and heterogeneity of the produced recombinant proteins, cells were supplemented with 1 mg/L of glycosidase inhibitor kifunensine (Bio-Techne) just before transfection, previously resuspended in Opti-MEM™ and filtered with 0.22 μ m filter.

After five days, cells were harvested by centrifugation at 700 rpm for 15 minutes and supernatant was further clarified centrifuging at 2000 rpm for 20 minutes.

4.1.3. Purification of TrkA and TrkB ectodomains

Taking advantage of the affinity between immobilized nickel of the Ni-NTA resin (Qiagen) and C-terminal histidine tag of both TrkA-ECD and TrkB-ECD, the two ectodomains were purified from the clarified growth media as described below. Supernatant was equilibrated in buffer A (20 mM Hepes pH=7.5 and 150 mM NaCl), filtered with 0.44 μ M filter and incubated overnight at 4°C and under stirring with 500 μ L Ni-NTA resin, previously equilibrated in buffer A. The day after, sample and resin were transferred into a gravity column, flow-through was collected and Ni-NTA resin was washed with 5 CVs of buffer A. Target protein was eluted using 3 CVs of buffer A supplemented with 250 mM of imidazole and a final wash was conducted using 3 CVs of 1M imidazole buffer. All purification steps were performed at 4° C. Finally, to get rid of imidazole, buffer was exchanged using PD-10 desalting column (Cytiva), protein target was eluted in 3 mL of buffer A and concentrated using Amicon concentrators (Merck Millipore) with 30000 Da molecular weight cut off (MWCO). Samples of 10 μ L were taken at each purification step for SDS-PAGE evaluation.

4.1.4. In vitro deglycosylation

To remove completely the glycans chains from the target proteins, and hence optimize sample quality for crystallization screenings, endoglycosidases from *Elizabethkingia miricola* (NDEGLY kit, Sigma Aldrich) were used for *in vitro* deglycosylation under native condition. To test the activity of EndoF1 and EndoF2 endoglycosidases, 200 μ g of TrkA-ECD, produced in presence and absence of kifunensine, were incubated for 1 hour at 37°C as described in manufacturer's protocol and glycan's cleavage was evaluated by SDS-PAGE analysis. Reaction protocol that yielded the most homogeneous sample was then scaled up for both TrkA-ECD and TrkB-ECD. Using size exclusion chromatography, de-glycosylated proteins were purified from the endoglycosidases and trimmed glycan chains as described below.

4.1.5. Size exclusion chromatography

To further purify the target proteins, size exclusion chromatography was performed using Superdex200 increase 10/300 column (GE Healthcare), which media separates globular proteins with molecular weight between 10000 and 600000 Da. The column was mounted on Azura Knauer HPLC chromatography system and equilibrated with 2 CVs of buffer A, before sample loading. All buffers and sample were sterile filtered. Protein was eluted with an isocratic gradient for 1.5 column volume and manually collected. Absorption at 280 nm was used to detect protein elution. Fractions were analyzed by SDS-PAGE and concentrated with 30000 MWCO centrifugal filter. Quantity of purified proteins were estimated by UV/visible spectra using theoretical extinction coefficients reported in table (figure 4.2).

Extinction coefficient at 280nm ($\epsilon_{280\text{nm}}$)	
TrkA-ECD	44230 M ⁻¹ cm ⁻¹
TrkB-ECD	50140 M ⁻¹ cm ⁻¹
TrkA-ECD – NGF complex	62085 M ⁻¹ cm ⁻¹
TrkB-ECD – BDNF complex	72975 M ⁻¹ cm ⁻¹

Figure 4.2. Extinction coefficient of TrkA and TrkB ectodomains and neurotrophin – Trk complexes. In table, the theoretical extinction coefficients at 280 nm, computed using ProtParam of ExPaSy¹⁰⁰ server, are listed.

4.1.6. Neurotrophin and Trk receptors complexes purification

To form the complexes between neurotrophin and tyrosine kinase receptors, TrkA-ECD and TrkB-ECD, before and after *in vitro* deglycosylation, were incubated for one hour at 4° C in a 1 to 2 stoichiometry with NGF and BDNF, respectively. The formed complexes between TrkA-ECD and NGF and TrkB-ECD and BDNF were then purified from unbound proteins by size exclusion chromatography and eluted fractions were analysed by SDS-PAGE.

4.2. Production of TrkA and TrkB ectodomains: results

The ability of TrkA and TrkB to transmit downstream signaling in response to NGF and BDNF, relies on specific and high affinity interactions via binding to the extracellular domains. Nowadays, only two crystal structures of TrkA-ECD and NGF complex has been solved by X-ray crystallography, one at low resolution⁴⁶ (3.4 Å) and very recently one at high resolution⁴⁹ (1.8 Å), while no structures of TrkB ectodomain, as well as the structure of the BDNF-TrkB complex, are available and functional and structural characterization is still missing. Therefore, the production of the TrkA and TrkB ectodomains is of major interest to investigate such structures and interactions.

In this chapter, the results achieved for the production of the TrkA and TrkB ectodomains are presented. All data have been acquired at the laboratory of Prof. Beatrice Vallone at Sapienza University of Rome, under the supervision of Dr Linda Celeste Montemiglio.

4.2.1. Gibson Cloning

For mammalian expression of the TrkA and TrkB ectodomains, the genes encoding the human TrkA (33-416 residues) and the human TrkB (32-430 residues) ectodomains were cloned in p α -HBiP expression vector¹¹⁴. As illustrated in figure 4.3, the p α -HBiP vector encloses at the 5' of the encoding sequence the hydrophobic leader peptide from baculovirus protein gp67 (BiP) for extracellular translocation and at the 3' an octa-histidine tag, allowing protein purification from the culture medium by affinity chromatography.

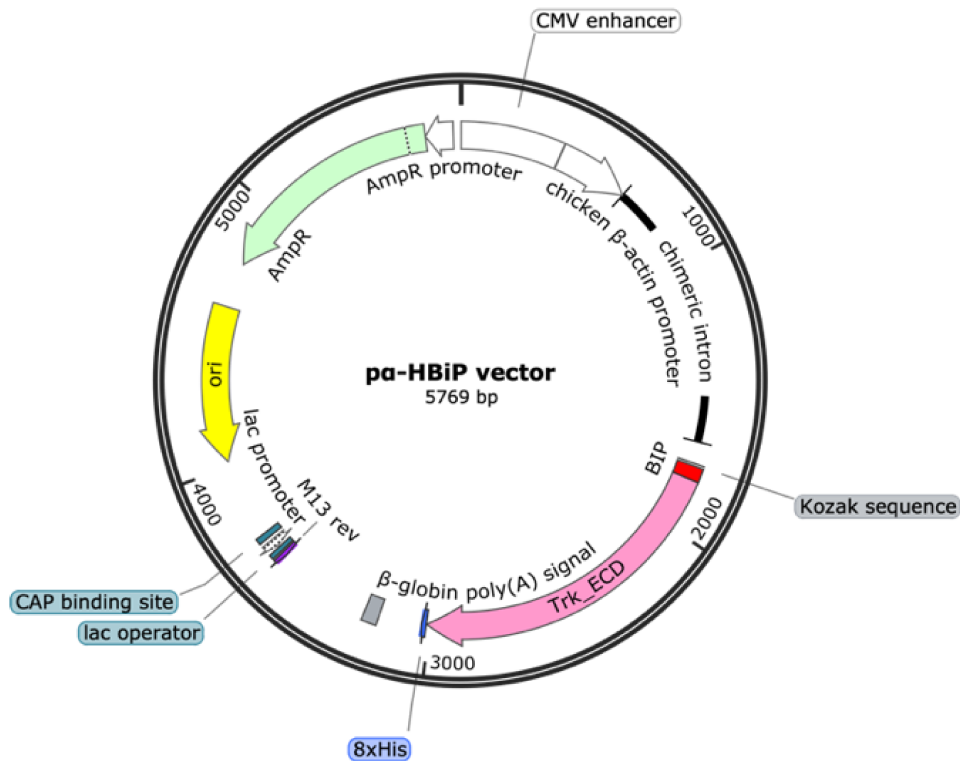


Figure 4.3. Map of p α -HBiP vector. Features of the p α -HBiP vector are illustrated. Particularly, starting from the 5' of the multiple cloning site, the BiP signal in red, the Trk ectodomain encoding sequence in pink and the octahistidine tag in blue. The map was created using SnapGene.

To clone the target genes into the p α -HBiP vector, Gibson Assembly was performed as described in section 4.1.1. The p α -HBiP vector (4627 bp) was linearized by enzymatic digestion using EcoRI and BamHI restriction enzymes, while the TrkA-ECD and TrkB-ECD encoding sequences were amplified by PCR. The digestion and PCR products were analysed by agarose gel electrophoresis and visualized by UV light. From agarose gel analysis (figure 4.4), a band between 4000 and 5000 base pairs was visible, corresponding to the linearized empty vector, and a band above 1000 base pairs was visible in both left and right gels, corresponding to TrkA-ECD (1155 bp) and TrkB-ECD (1192 bp) PCR amplicons, respectively.

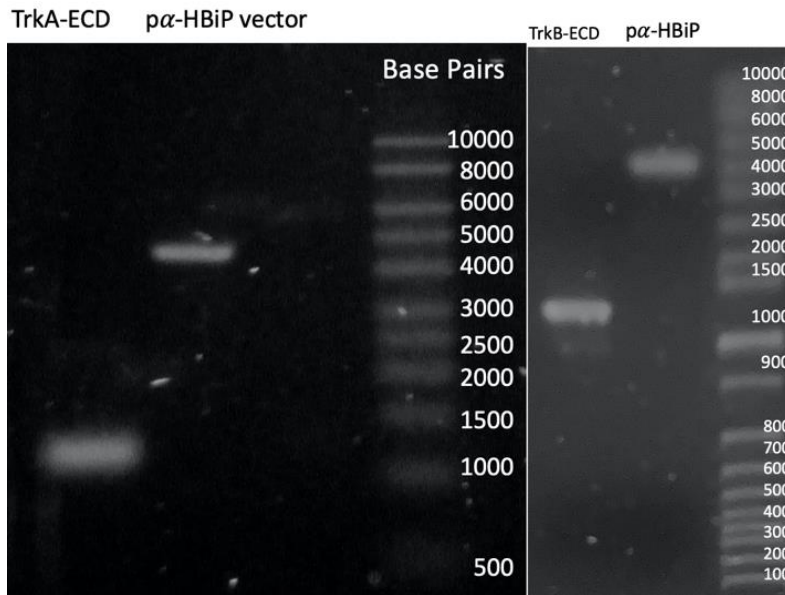


Figure 4.4. Agarose gel analysis of PCR and digestion products. On the left gel, PCR product of TrkA-ECD (1155 bp) and the p α -HBiP vector (4627 bp) digested by BamHI and EcoRI, on the right gel, TrkB-ECD PCR product (1192 bp) and the p α -HBiP vector (4627 bp) digested by BamHI and EcoRI are shown. To the right of each gel, DNA ladder for reference bands is shown.

After gel purification, 24 ng/ μ L of linearized empty vector, 15 ng/ μ L of TrkA-ECD and 17 ng/ μ L of TrkB-ECD amplicons were obtained. The empty p α -HBiP vector was incubated with 2-fold molar excess of either TrkA-ECD and TrkB-ECD PCR products for Gibson cloning and each reaction was transformed in DH5- α competent cells. As shown in figure 4.5, more than 100 colonies grew overnight on selection plates, of which 10 were picked for overnight growth and DNA extraction.

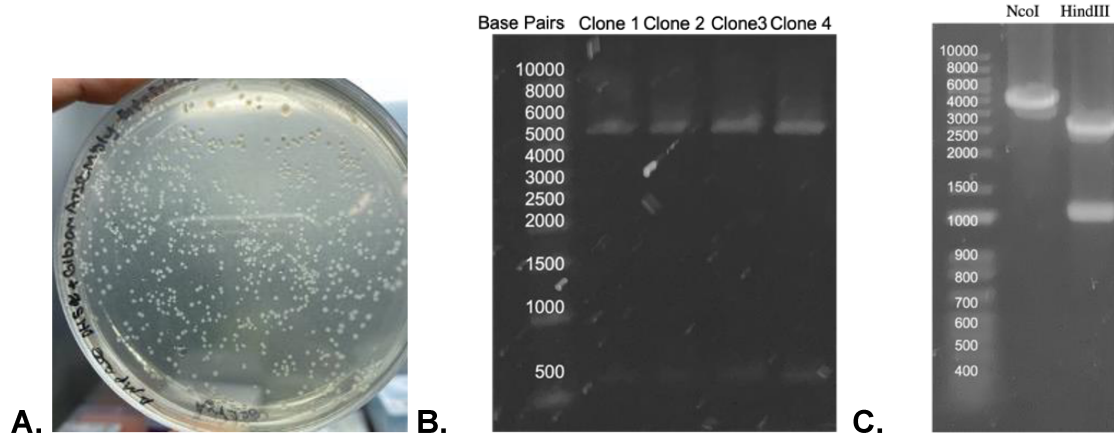


Figure 4.5. DH5- α transformation and DNA analysis after Gibson Assembly. A) On the left, LB selection plate of transformed colonies after Gibson Assembly of TrkA-ECD PCR product and p α -HBiP vector. On the right, agarose gel electrophoresis analysis of plasmid DNAs extracted after Gibson Assembly are shown. **B)** Four clones of p α -HBiP/TrkA-ECD vector were analysed after BamHI digestion, which cleavage produced two fragments, one of 500 bp and one of 5300 bp. **C)** The p α -HBiP/TrkB-ECD vector assembly was analysed by NcoI digestion, used as unique cutter for vector linearization (5800 bp), and by HindIII digestion, which produced two fragments, one of 1200 bp and one of 4600 bp. To the left of each gel, GeneRuler (ThermoFisher) DNA ladder for reference bands is shown.

To verify the insertion of the PCR products into the p α -HBiP vector, the extracted plasmid DNAs were digested and analysed by agarose gel electrophoresis. The p α -HBiP/TrkA-ECD plasmid contains two BamHI restriction sites, as well as the p α -HBiP/TrkB-ECD plasmid contains two HindIII sites, of which one within the encoding sequence. The digestion of p α -HBiP/TrkA-ECD plasmid by BamHI produced two DNA fragments, one of 500 bp and one of 5300 bp, visible in the agarose gel analysis of four different clones (figure 4.5 B). From the agarose gel analysis of the p α -HBiP/TrkB-ECD plasmid assembly (figure 4.5 C), HindIII digestion produced one fragment of 1200 bp and another of 4000 bp. In addition, NcoI was used as unique cutter to linearize the expression vector, visible as a 5000 bp band in the gel (figure 4.5 C). Besides the agarose gel analysis, the sequences of the cloned genes were validated by Sanger sequencing.

Having a low-copy pBR322 origin¹¹³, chloramphenicol amplification was performed to produce milligram yields and higher purity of plasmid DNA for mammalian cells transfection. DNA quantity and quality (260/280 and 260/230 ratios) were estimated by UV/visible spectra, of which values are shown in table (figure 4.6). The final yield obtained was 1.14 mg of p α -HbIP/TrkA-ECD vector and 1.2 mg of p α -HbIP/TrkB-ECD vector.

vector	Abs 260nm	Conc.	260/280	260/230
p α -HbIP/TrkA-ECD	11.415	570 μ g/mL	1.603	2.157
p α -HbIP/TrkB-ECD	12.024	600 μ g/mL	1.600	1.994

Figure 4.6. Table of p α -HbIP/TrkA-ECD and p α -HbIP/TrkB-ECD plasmids. Absorbance at 260 nm, plasmid quantity (concentration) and purity as 260/280 and 260/230 ratios (protein and organic contaminants) after chloramphenicol amplification and MaxiPrep extractions are reported.

4.2.2. Expression and purification of TrkA-ECD and TrkB-ECD

The mammalian expression system allows to express natively folded recombinant proteins that require post-translational modifications, such as glycosylation, disulfide bond formation or enzymatic cleavage¹¹⁵. The absence of these modifications in *E. coli* expression system leads recombinant proteins to accumulate in inclusion bodies¹¹⁶. Therefore, the ectodomains of TrkA (33-416 residues) and TrkB (32-430 residues) receptors were produced by transient transfection of suspension-grown Hek293 cells. When cells grew to density of 2×10^6 cells/mL and the cell viability was above 98%, the plasmid DNA was transfected using PEI in a 1:4 $\mu\text{gDNA}/\mu\text{g PEI}$ ratio. After five days, cells were harvested by centrifugation and the secreted target protein was purified by affinity chromatography from the supernatant, i.e. the growth medium. Through metal chelation, the Ni^{2+} -charged agarose matrix of Ni-NTA resin retains proteins with poly-histidine tag. After overnight incubation, the supernatant and Ni-NTA resin were loaded on gravity column, unbound proteins were collected in the flow-through and matrix was washed to remove unspecific or weakly bound proteins (figure 4.7). Then, target protein was eluted using 250 mM imidazole buffer and a last wash was conducted using high imidazole concentration ($\text{E}_{1\text{M}}$) buffer.



Figure 4.7. Set up for TrkA-ECD and TrkB-ECD purification. After centrifugation, the supernatant was incubated overnight with Ni-NTA resin. Through a peristaltic pump, the supernatant was loaded into the gravity column and flow-through was collected. All purification was conducted at 4° C.

In order to evaluate the protein expression level, two small-scale productions were conducted, one using un-transfected Hek293 cells and the other using p α -HBiP/TrkA-ECD transfected cells. Samples were taken at elution step and analysed by SDS-PAGE and Western Blot.

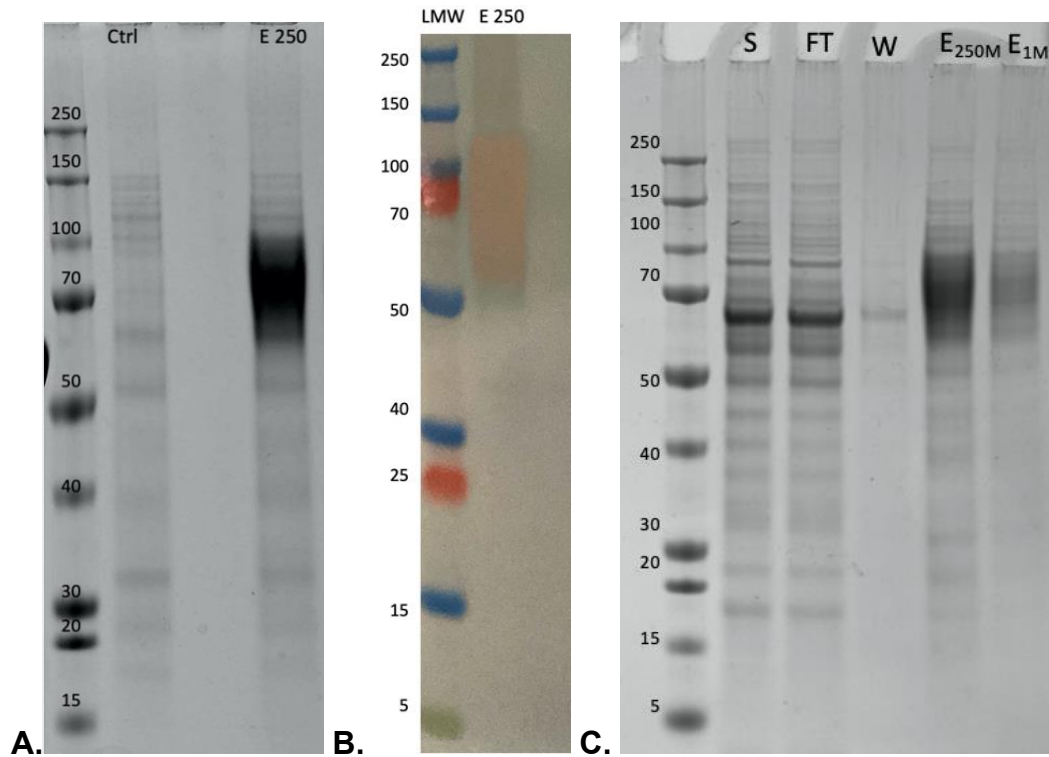


Figure 4.8. SDS-PAGE and Western Blot analyses of TrkA-ECD expression and purification. A) Analysis of the TrkA-ECD expression in Hek293-F cells. The elution of un-transfected cells (Ctrl lane) and the elution of p α -HBiP/TrkA-ECD transfected cells (E₂₅₀ lane) is compared. **B)** Western blot analysis of TrkA-ECD elution with 250 mM imidazole buffer. **C)** Analysis of TrkA-ECD purification. Sample of supernatant (S), flow-through (FT), wash (W), elution (E_{250mM}) and final wash (E_{1M}) were taken and analysed. On the left side of each gel, molecular weight of standard proteins (LMW) is indicated in kDa.

Comparing the purification of un-transfected cells (Ctrl lane) and p α -HBiP/TrkA-ECD transfected cells (“E₂₅₀” lane) after five days (figure 4.8-A), a thick and smear band around 80 kDa was visible in “E₂₅₀” lane, suggesting the overexpression of the target TrkA-ECD in transfected cells. This was further validated by Western Blot analysis using anti-histidine tag monoclonals. As shown in figure 4.8-B, a smeared band from about 50 kDa to 120 kDa lighted up when chromogenic solution was added, confirming the elution of the histidine tagged protein.

From the SDS-PAGE analysis of all purification steps (figure 4.8 C), the band corresponding to the TrkA-ECD was visible in elution lane (“E_{250mM}”) and also in final-wash lane (“E_{1M}”), together with some contaminating proteins. However, not more intense band around 70 kDa were visible in supernatant (“S” lane) and flow-through (“FT” lane), indicating that the target protein was not heavily overexpressed and that all expressed protein bound the Ni-NTA matrix. Moreover, although the theoretical molecular weight of TrkA-ECD is 42 kDa, the shift at higher molecular weights and the smear band in the SDS-PAGE and Western blot analyses were justified by the N-glycosylation of the extracellular domain.

On the one hand, the presence of post-translational modifications are pivotal for protein folding and structural integrity, on the other hand, such glycoproteins produced in mammalian cells have complex and heterogeneous carbohydrates moieties, that hinder the formation of well-ordered crystal lattices¹¹⁷. Therefore, to obtain proteins amenable to crystallize, with less complexity and heterogeneity, the inhibitor of α -mannosidase I kifunensine was added to cell suspensions¹¹⁸. The effect of kifunensine inhibition is the production of glycoproteins with oligomannose chains and hybrid chains, without affecting the overall yield of protein production¹¹⁹.

As shown in figure 4.9, the kifunensine addition in growth media resulted in a more compact band around 70 kDa, visible in elution lane (“E_{250M}” lane) of both TrkA-ECD and TrkB-ECD purification, suggesting less heterogeneity of the samples.

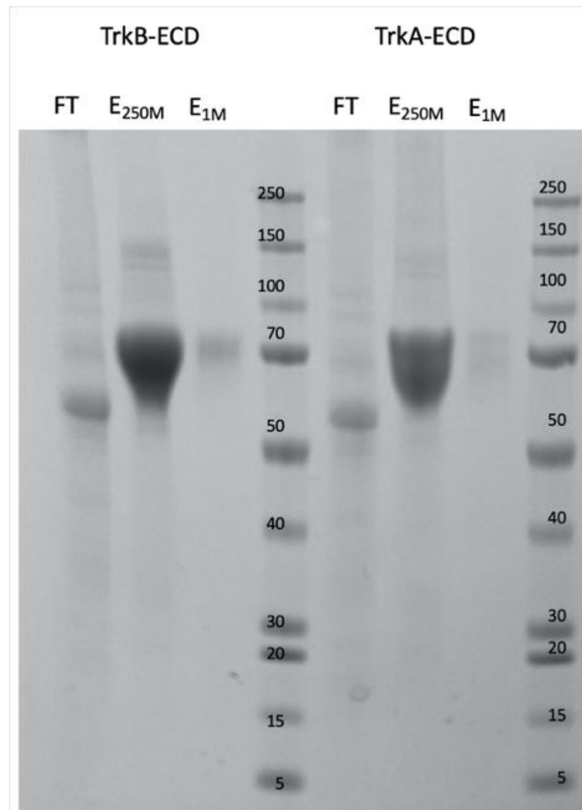


Figure 4.9. SDS-PAGE analysis of TrkA-ECD and TrkB-ECD purification. Analysis of the recombinant proteins expressed in Hek293-F cells in presence of kifunensine inhibitor. On the left side, flow-through (FT), elution (E_{250mM}) and final wash (E_{1M}) samples of TrkB-ECD purification, while on the right side the TrkA-ECD flow-through (FT), elution (E_{250mM}) and final wash (E_{1M}) samples were analysed. To the right, the molecular weight of standard proteins is indicated in kDa.

The TrkA and TrkB ectodomains were further purified by size exclusion chromatography as described in section 4.1.4. As shown in figure 4.10, the elution profile showed a major and sharp peak at 12,2 mL corresponding to TrkA-ECD (left panel) and a sharp peak at 12,3 mL corresponding to TrkB-ECD elution (right panel). Then, collected fractions were concentrated and used for co-crystallization (section 4.3, 4.4) and grating coupled interferometry (GCI) studies (section 4.6).

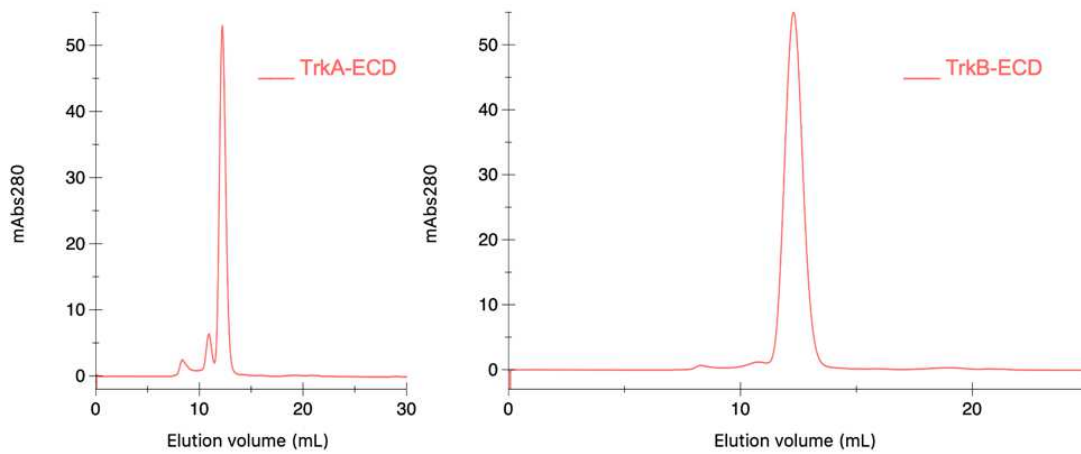


Figure 4.10. Size exclusion chromatography of TrkA-ECD and TrkB-ECD. On the left, chromatogram of TrkA-ECD gel filtration and on the right chromatogram of TrkB-ECD gel filtration are shown. On y-axis, absorbance at 280 nm in milli absorbance unit (mAbs280), on x-axis the elution volume given in mL.

4.2.3. In vitro deglycosylation

The most homogeneous glycans chains obtained through glycosidase inhibition can be further trimmed by endoglycosidases of *Elizabethkingia miricola* under native conditions¹²⁰. As illustrated in figure 4.11, EndoF1 cleaves oligomannose and hybrid oligosaccharides, but not complex chains, between two N-acetylglucosamine residues, generating a truncated moiety with one N-acetylglucosamine residue remaining on asparagine, while EndoF2 cleaves oligomannose at 20-fold reduced rate and biantennary complex glycans, but not hybrid structures¹²¹.

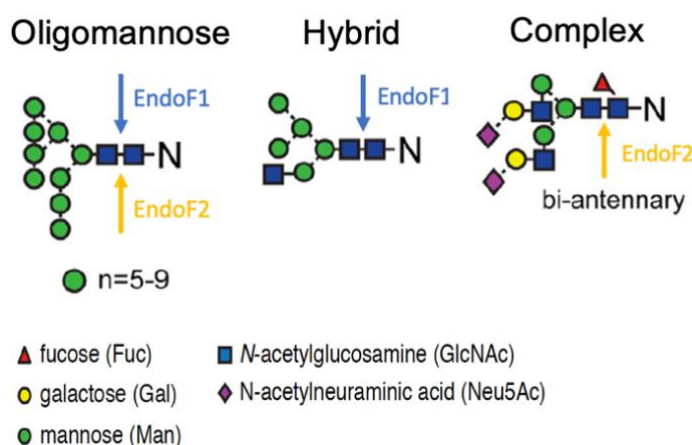


Figure 4.11. Illustration of N-glycosylation and EndoF1 and EndoF2 cleavage sites. Oligomannose, hybrid and bi-antennary complex structures of N-glycosylation are illustrated. The arrows points the cleavage site of the EndoF1 and EndoF2 between two N-acetylglucosamine residues, highlighting the substrate specificity. Figure readapted from Struwe & Robinson, 2019¹²².

To evaluate the glycosylation cleavage, aliquots of TrkA-ECD produced in presence and in absence of kifunensine were incubated with EndoF1 and EndoF2 and cleavage was monitored by SDS-PAGE analysis. As shown in figure 4.12-A, no major changes were visible in the smeared bands of TrkA-ECD in “EndoF1” and “EndoF2” lanes, meaning that in absence of glycosidase inhibitor neither EndoF1 nor EndoF2 were efficient in removing the glycans chains. This suggested that without α -mannosidase I inhibition, Hek293-F cells produce highly complex glycoproteins, which composition could be elucidated by mass spectrometry, but such characterization is outside the scope of this thesis.

Conversely, as shown in figure 4.12-A., after glycosidase inhibition with kifunensine, the TrkA-ECD band was shifted at 50 kDa in “EndoF1” lane but not in “EndoF2” lane, indicating

that only EndoF1 was able to remove the oligomannose moieties of TrkA-ECD. This suggested that the oligomannose chains consisted in hybrid structures that could not be trimmed by EndoF2.

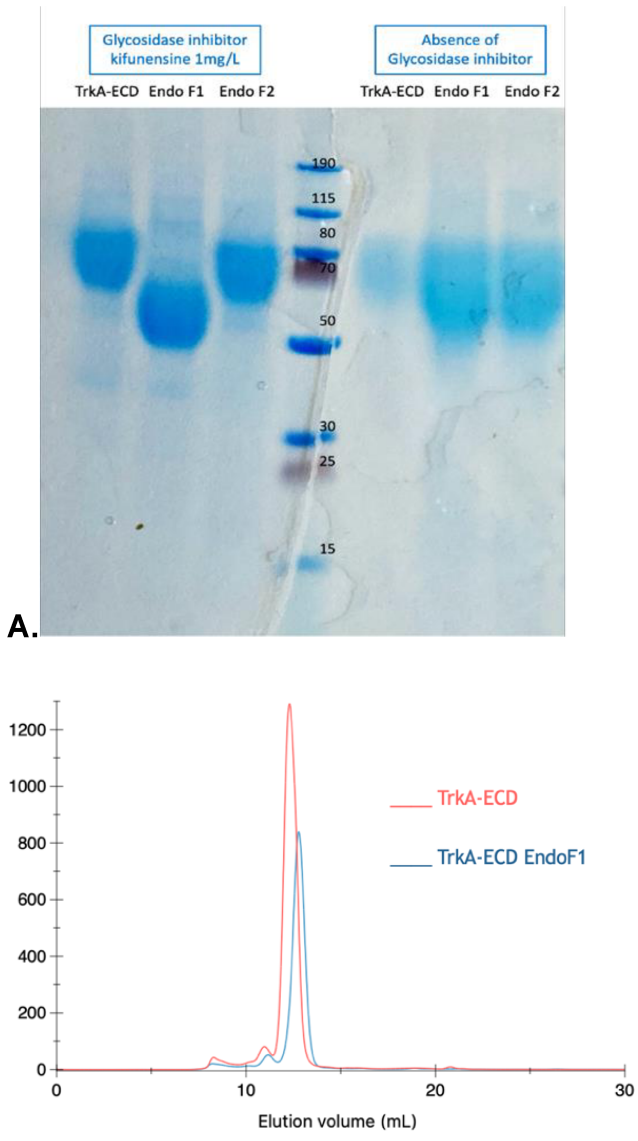
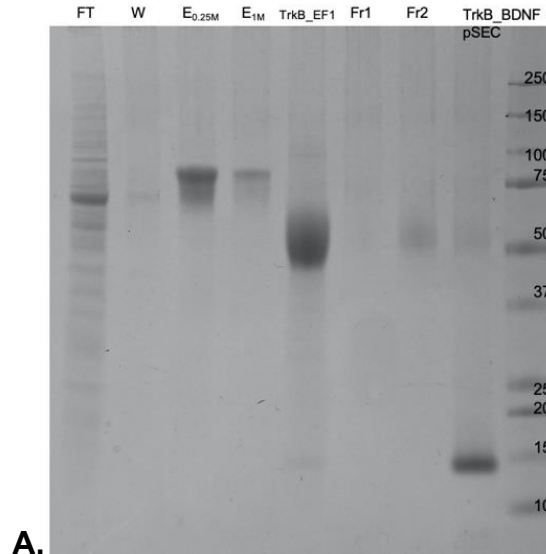


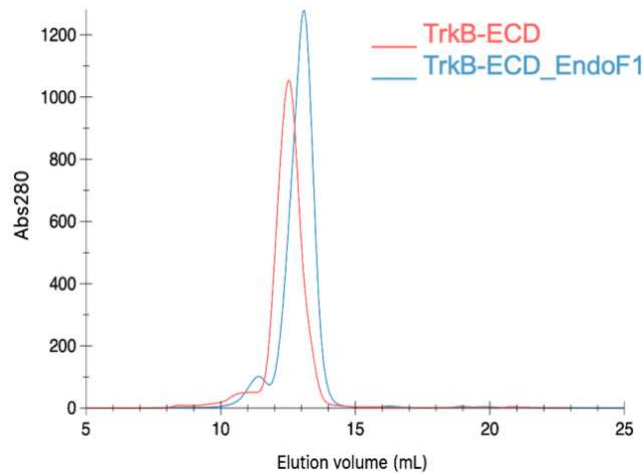
Figure 4.12. Evaluation of the TrkA-ECD *in vitro* deglycosylation. A) SDS-PAGE analysis of TrkA-ECD deglycosylation with and without glycosidase inhibition. On the left side, the target protein was produced in presence of kifunensine (“TrkA-ECD” lane) and the deglycosylation after EndoF1 and EndoF2 treatments are compared (“EndoF1” and “EndoF2” lanes). On the right side, the protein was produced in absence of kifunensine and the deglycosylation treatments of EndoF1 and EndoF2 are shown. Molecular weight of standard proteins is indicated in kDa. **B)** Chromatograms of the size exclusion chromatography of TrkA-ECD with (blue line) and without (red line) EndoF1 treatment. On y-axis, absorbance at 280 nm in milli absorbance unit (mAbs280), on x-axis the elution volume given in mL

The shift at lower molecular weight of TrkA-ECD resulted after EndoF1 treatment was further confirmed by size exclusion chromatography. In the chromatogram (figure 4.12-B), the curves of TrkA-ECD elution before and after EndoF1 treatment were compared. The major peaks corresponded to the elution of the target protein: an elution volume at 12,2 mL of TrkA-ECD without enzymatic deglycosylation (red line) and an elution volume at 13 mL of TrkA-ECD after EndoF1 treatment (blue line). By extrapolation from the calibration curve of the Superdex200 10/300 column, the elution volume of 12,2 mL corresponded to a molecular weight of 127 kDa and the elution volume of 12,7 mL corresponded to 94 kDa protein, a difference of 33 kDa similar to the SDS-PAGE analysis.

Similarly, the TrkB ectodomain was digested by EndoF1 to remove the oligomannose moieties. As shown in figure 4.13-A, samples of TrkB-ECD purification were taken after the affinity chromatography, after EndoF1 treatment and gel filtration. From the SDS-PAGE analysis, a thick band around 75 kDa was visible in both “E_{0.25M}” and “E_{1M}” lanes highlighting the elution of the target protein. The two fractions were pooled together, using a PD-10 desalting column the imidazole was removed and the target protein was incubated with EndoF1. As shown in “TrkB_EF1” lane, after EndoF1 treatment the molecular weight of the TrkB-ECD band shifted at 50 kDa, suggesting the cleavage of the glycans chains. Then, the trimmed TrkB-ECD was further purified by gel filtration. As shown in the overlaid chromatograms of TrkB-ECD gel filtrations (figure 4.13-B), after EndoF1 treatment the elution volume of the TrkB-ECD (blue curve) was delayed at 13 mL from the 12.2 mL without deglycosylation (red curve). By extrapolation from the calibration curve of the column, the elution volume of TrkB-ECD_EndoF1 corresponded to a globular proteins of 80.2 KDa, meaning a shift in molecular weight of about 43 kDa, comparable to the observed shift in the SDS-PAGE analysis, and similar to TrkA-ECD deglycosylation.



A.



B.

Figure 4.13. TrkB-ECD *in vitro* deglycosylation by EndoF1. **A)** SDS-PAGE analysis of TrkB-ECD purification by affinity chromatography and gel filtration after EndoF1 treatment. The target protein was produced in presence of kifunensine and purified by Ni-NTA resin. The flow-through, wash, elution by 250 mM imidazole and final wash with 1 M imidazole were analysed in “FT”, “W”, “E0.25M” and “E1M” lanes. Then, TrkB-ECD was incubated with EndoF1 for one hour at 37°C (“TrkB_EF1” lane) and purified by gel filtration, “Fr1” and Fr2” lanes, corresponding to the first and second peak in the blue chromatogram. Molecular weight of standard proteins is indicated in kDa. **B)** Chromatograms of the size exclusion chromatography of TrkB-ECD before (red line) and after (blue line) EndoF1 treatment. On y-axis, absorbance at 280 nm in absorbance unit (Abs280), on x-axis the elution volume given in mL.

4.2.4. Neurotrophin and Trk receptors complexes purification

To obtain the complex between neurotrophin and cognate receptor for structural studies, TrkA and TrkB ectodomains were incubated with NGF and BDNF, respectively. A size exclusion chromatography was performed to isolate the formed complexes from the unbound proteins. The TrkA and TrkB ectodomains, as well as the NGF and BDNF neurotrophins, were analysed before and after complexes formation and purification by SDS-PAGE analysis. As shown in figure 4.14-A, a thick band at 70 kDa was visible in “TrkA-ECD” and “TrkB-ECD” lanes corresponding to the purified ectodomains, while two bands were visible at 15 kDa and 30 kDa in both “NGF” and “BDNF” lanes, indicating monomer and dimer form, respectively. After incubation, complex formation was evaluated in “TrkA-NGF preSEC” and “TrkB-BDNFpreSEC” lanes, where all three bands were visible.

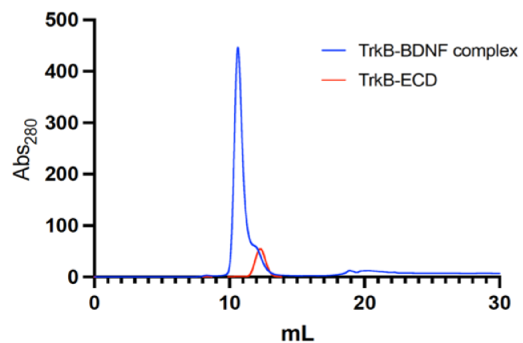
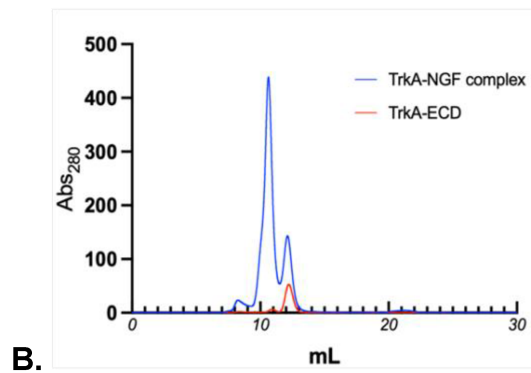
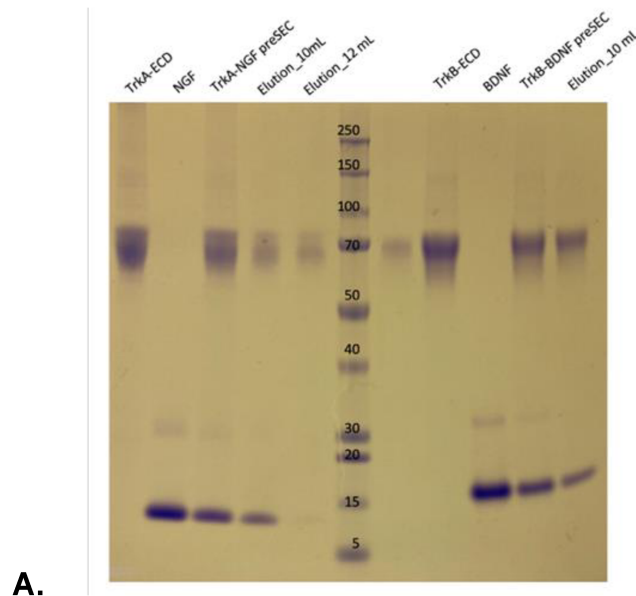


Figure 4.14. Purification of TrkA-NGF and TrkB-BDNF complexes. **A)** SDS-PAGE analysis of target proteins before and after incubation and analysis of eluted fractions from gel filtrations. Molecular weight of standard proteins is shown in kDa. **B)** Chromatograms of the TrkA and NGF complex (top panel) and of the TrkB and BDNF complex (bottom panel) purification by size exclusion chromatography. In blue, the elution profile of the complex

purification and in red the elution profile of the unbound TrkA and TrkB ectodomains are shown. On y-axis, absorbance at 280 nm in absorbance unit (Abs_{280}), on x-axis the elution volume given in mL.

In the bottom panel of figure 4.14-B, the chromatogram of TrkB-BDNF complex purification is shown. One sharp peak eluted at 10 mL of elution volume and a small shoulder eluted around 12 mL. From the SDS-PAGE analysis (figure 4.14-A), the “Elution_10 mL” lane showed two bands at 70 kDa and 15 kDa, suggesting elution of the TrkB-ECD and BDNF complex. The shoulder at 12 mL of elution volume was collected as separated fraction and loaded on the SDS-PAGE, but due to low protein concentration no bands were visible. However, overlapping the elution curves of the TrkB-ECD purification (red line) and TrkB-BDNF complex purification (blue line), it was possible to assume that the 12 mL elution volume corresponded to unbound TrkB-ECD. Extrapolating the apparent molecular weight from the calibration curve, the molecular weight of TrkA-NGF complex resulted 322 kDa and the molecular weight of TrkB-BDNF complex corresponded to 319 kDa. Fraction of the purified complexes were concentrated and used for the preliminary studies by X-ray crystallography and single particle cryo-EM.

Because the oligomannose and hybrid glycosylation of the TrkA and TrkB ectodomains could still compromise protein crystallization, as well as crystal diffraction at high resolution, both TrkA and TrkB ectodomains were treated with the EndoF1 to remove the oligosaccharide chains as described in paragraph 4.1.3. After EndoF1 treatment and purification by size exclusion chromatography, the trimmed TrkA-ECD and TrkB-ECD were incubated with NGF and BDNF respectively, and formed complexes were purified by gel filtration.

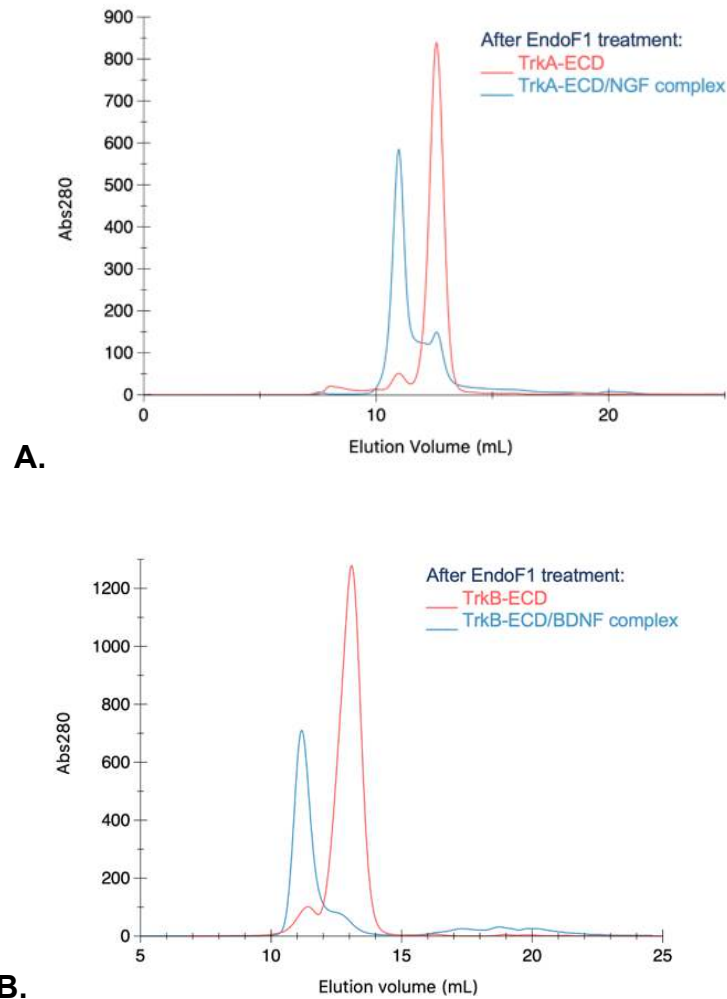


Figure 4.15. Purification of TrkA-NGF and TrkB-BDNF complexes after EndoF1 treatment. **A)** Chromatogram of the TrkA and NGF complex and **B)** of the TrkB and BDNF complex purification by size exclusion chromatography. In blue, the elution profile of the complex purification and in red the elution profile of the unbound TrkA and TrkB ectodomains are shown. On y-axis, absorbance at 280 nm in absorbance unit (Abs₂₈₀), on x-axis the elution volume given in mL.

As shown in figure 4.15-A, the elution profile of the TrkA-NGF complex (blue line) after EndoF1 treatment presented two peaks: a major peak eluted at 11 mL of elution volume and a second peak eluted at 13 mL. Overlapping the elution profile of the TrkA-ECD after EndoF1 treatment, the first peak corresponded to complex elution and the second peak to unbound TrkA-ECD.

Similarly, the TrkB-BDNF complex after EndoF1 treatment was purified by gel filtration and the chromatogram is shown in figure 4.15-B. Here, the elution profile presented a major peak with a small shoulder on the right, corresponding to complex and un-bound TrkB-ECD elution respectively.

The collected fractions of purified complexes were concentrated at different final concentrations for crystallization screening.

4.3. Crystallography

4.3.1. TrkA-NGF and TrkB-BDNF complexes crystallization screening

Right after size exclusion chromatography, peak fractions corresponding to TrkA-NGF complex elution and TrkB-BDNF complex elution were concentrated using 30000 MWCO centrifugal filter and quantified by UV/visible spectra.

As initial crystallization screening, Hampton Research Crystal Screen HT was used for both TrkA-NGF and TrkB-BDNF complex at final concentration of 5 mg/mL. Crystallization screens were set up in sitting drop vapor diffusion method using automated robot and drops of 0.4 μ L, consisting in 1:1 mix of reservoir and protein solution. Due to the low concentrations adopted, no crystal formation was observed. Moreover, the oligomannose moieties of the extracellular domains could insert a degree of flexibility that could hinder the complex crystallogenesis¹²³. Thus, protein concentration was increased and sample quality was improved by EndoF1 deglycosylation of TrkA-ECD and TrkB-ECD, as described in sections 4.1.4 and 4.2.4.

New crystallization screenings were carried out manually for TrkA-NFG complex (7 mg/mL) and TrkB-BDNF complex (10.5 mg/mL) using selected precipitating conditions from Protein Complex Suite (Qiagen) and Index (Hampton research) in hanging drop vapor diffusion method with drops of 1:1 protein-reservoir ratio equilibrated over 500 μ L reservoir. Although the higher concentration used, no crystal formation was observed from the TrkB-BDNF complex set up, but only clear drops or light precipitants, while several precipitating conditions from the TrkA-NGF complex set up resulted in needles, plate-like and single crystals, which precipitant compositions are listed in table (4.16 A-F).

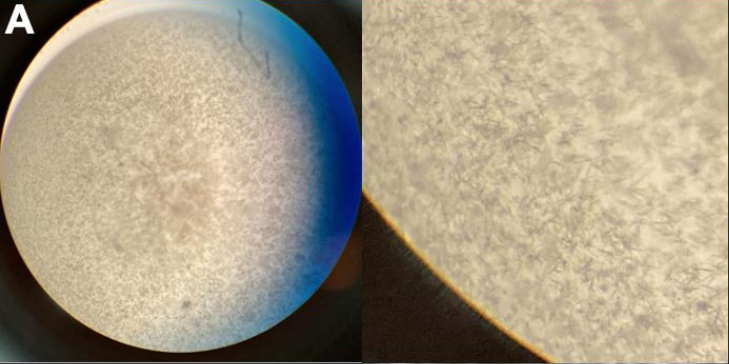
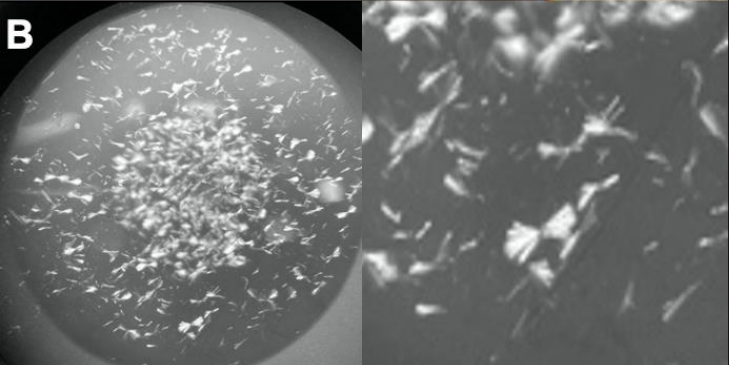
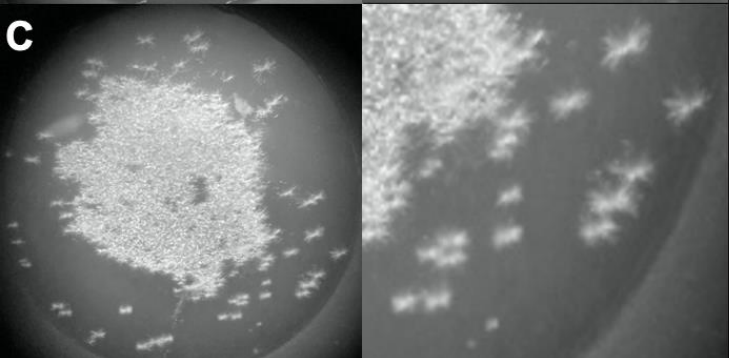
TrkA-NGF complex 7 mg/mL <i>Hanging drop method</i>	
A 	0.1 M Tris pH 8 0.2 M Li-Chloride 20% PEG 8000
B 	0.1 M MOPS pH 7.5 0.1 M Mg-Acetate 12% PEG 8000
C 	0.1 M HEPES pH 7 8% PEG 8000

Figure 4.16 A-C). Crystals, needles and plate-like crystals of TrkA-NGF complex obtained by hanging drop vapor diffusion. In table, pictures of crystal formations, relative zoom-in precipitant solutions composition are shown (A-C and D-F in following page). The hanging drops consisted in 2 μ L of TrkA-NGF complex concentrated at 7 mg/mL in 0.1 M HEPES pH 7.4 and 0.15 M NaCl and 2 μ L of precipitant solution of Protein Complex Suite (Qiagen). Plates were manually set up and stored at room temperature.

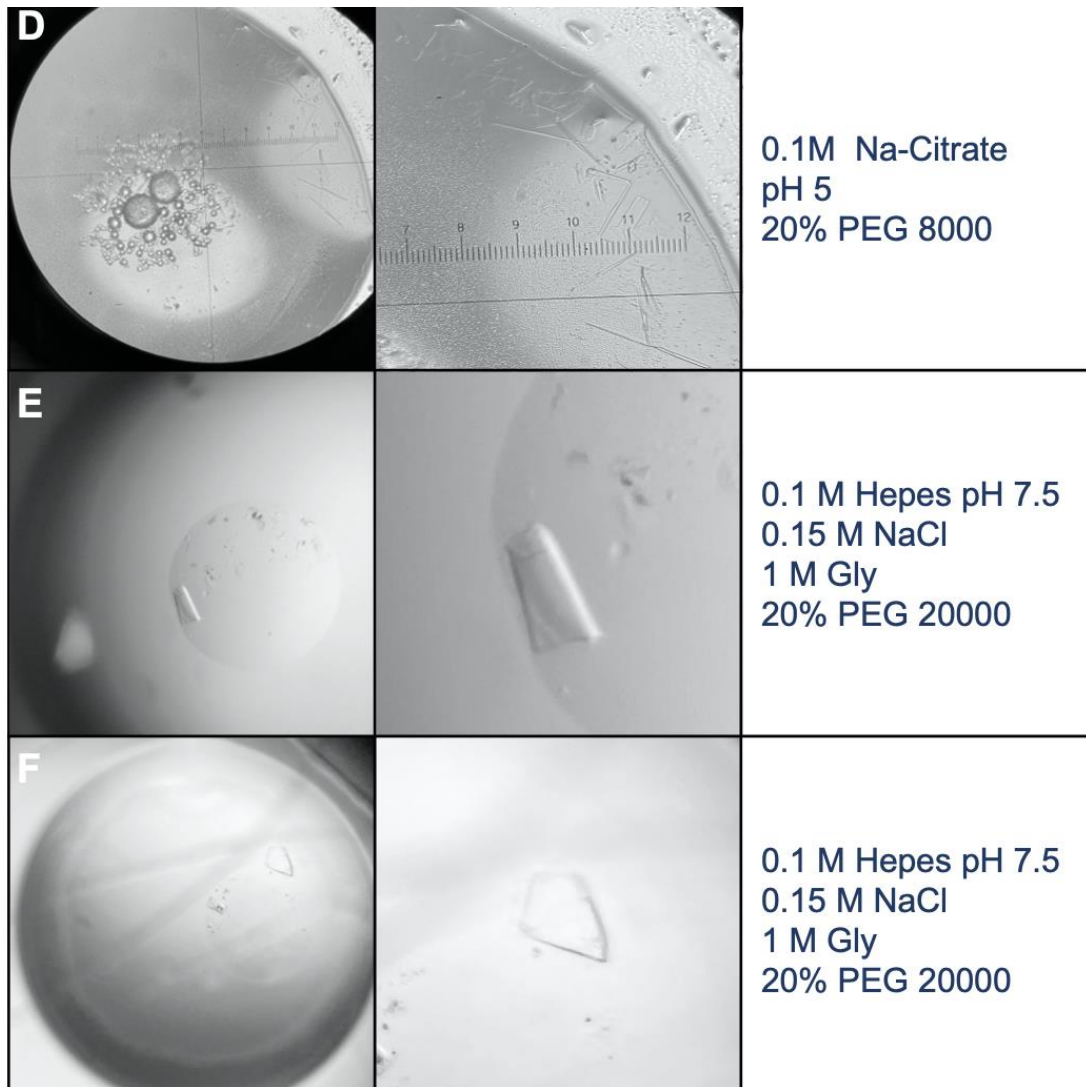


Figure 4.16 E-F). Crystals, needles and plate-like crystals of TrkA-NGF complex obtained by hanging drop vapor diffusion. In table, pictures of crystal formations, relative zoom-in precipitant solutions composition are shown. The hanging drops consisted in 2 μ L of TrkA-NGF complex concentrated at 7 mg/mL in 0.1 M Hepes pH 7.4 and 0.15 M NaCl and 2 μ L of precipitant solution of Protein Complex Suite (Qiagen). Plates were manually set up and stored at room temperature.

As shown in figure 4.16-D, crystals of TrkA-NGF complex were observed as rectangular plates between the oily drops and at the edge of the crystallization drop in precipitant solution of 0.1 M sodium citrate pH=5 and % PEG 8000. Also, three dimensional crystals were observed in precipitant solution of 0.1 M Hepes pH=7.5, 0.15 M sodium chloride, 1M glycine and 20% PEG 20000 (figure 4.16 E-F).

Prior to data collection, crystals were harvested by 0.1-0.2 loops and flash-frozen in liquid nitrogen. Plate-like crystals were cryoprotected by washing in either 25% PEG200 or 25%PEG 8000 just before freezing. Data collection was conducted at Electra synchrotron XRD2 beamline. However, the diffraction images showed very low resolution with diffraction spots at 8 Å, together with concentric rings in addition to the ice ring, pattern ascribed to polycrystalline material.

To optimize crystal formation, microseeding matrix screening technique (MMS) was performed. Briefly, seeds are obtained by crushing crystals and used to promote crystal growth in metastable conditions, where crystal nucleation does not take place spontaneously, and hence to increase the number of crystallization hits.

Needle in a bow-like shape of TrkA-NGF complex grown in 0.1 M magnesium acetate, 0.1 M MOPS pH 7.5 and 12% PEG 8000 (figure 4.16-B) were harvested and crushed by vortex for 2 minutes in a seed-bead tube, kept on ice and used immediately for MMS. Automatic high-throughput screening was performed using Oryx4 robot and Protein Complex Suite (Qiagen). All crystallization screens were set up in sitting drop vapor diffusion method, using drops of 0.20 μ L protein solution, 0.06 μ L seeding stock and 0.14 μ L precipitant solution. Plates were stored at 20° C. After one month, from the MMS plate of TrkB-BDNF complex, sea urchin like crystals grew in 0.1 M MES pH 6, 0.1 M calcium acetate and 15% PEG 400 (figure 4.18-A), as well as rods formation was observed in 0.1 M Hepes pH 7.5 and 25% PEG 2000 MME.

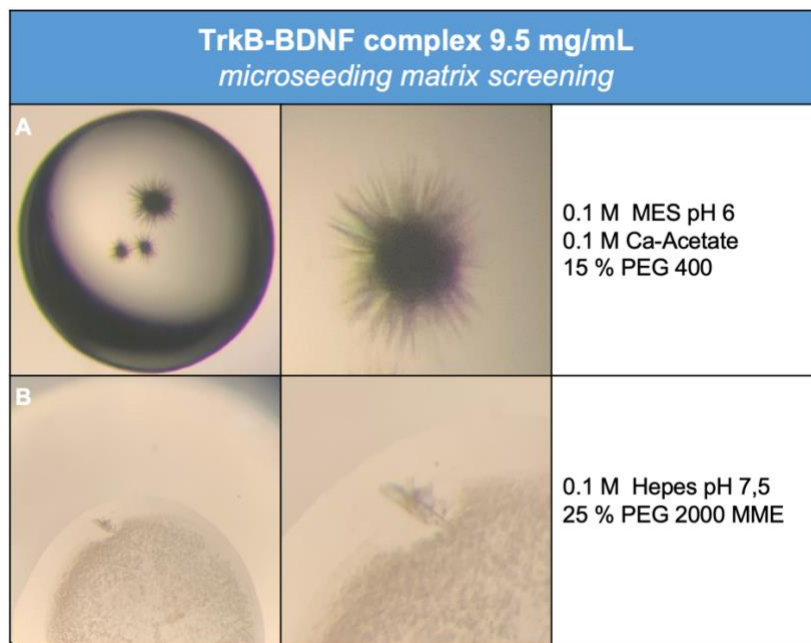


Figure 4.18. Crystal formations of TrkB-BDNF complex obtained by microseeding matrix screening. A) Sea-urchin like crystal and **B)** rods formation pictures of TrkB-BDNF complex, relative zoom-in and precipitant solutions composition are shown in table. The sitting drops consisted in 0.2 μ L of TrkB-BDNF complex concentrated at 9.5 mg/mL in 0.1 M HEPES pH 7.4 and 0.15 M NaCl, 0.14 μ L of precipitant solution of Protein Complex Suite (Qiagen) and 0.06 μ L seed-stock obtained from TrkA-NGF complex needles. Plates were stored at 20° C.

4.3.2. Co-crystallization screening

Before crystallization, TrkA-ECD was mixed with ENT-A010 compound in a 1:2 molar ratio, as well as TrkB-ECD mixed with ENT-C117 compound in 1:2 molar ratio, and incubated one hour at room temperature. Automatic high-throughput screening was performed using Crystal Screen HT (Hampton Research) and the sitting drop vapor diffusion method. Crystallization drops consisted of 0.3 μ L reservoir solution and 0.4 μ L protein-ligand solution at a final concentration of 8 mg/mL. No crystal formation was observed under all condition tested.

To optimize the crystal growth conditions, protein concentration was increased to 10 mg/mL and 15 mg/mL and 24-well plates were set up manually, using AmSO4 Suite (Qiagen) and Index (Hampton Research) screens in hanging drop diffusion method with drops containing protein-ligand and precipitant solution in 1:1 ratio. All screen plates were stored at controlled temperature (293 K). However, increasing protein concentration did not help to achieve protein crystallization. Conditions that produce any form of crystals, including microcrystals and phase separation drops from the set up screens were optimized. Optimization involved varying

concentrations of precipitant reagents, pH and buffer composition and substituting metal salts in screening reagents with different ones.

In addition, sample quality was optimized by *in vitro* de-glycosylated of TrkA and TrkB ectodomains before ligand-protein incubation and then microseeding matrix screening was performed as previously described.

Prior to MMS, the TrkB-ECD (9 mg/mL) was incubated one hour at room temperature with ENT-C117 ligand at 10 K_d molar excess and with 5 K_d molar excess of ENT-A010 compound.

As regards as the co-crystallization of TrkA agonist compounds, STD-NMR studies showed that BNN27 binding to TrkA was enhanced in presence of NGF⁹², thus microseeding screening was conducted using TrkA-NGF complex, instead of TrkA-ECD alone. Moreover, measurements by grating coupled interferometry (see section 4.5) showed that ENT-A010 compound has micromolar affinities for both TrkA and TrkB ectodomains, so co-crystallization screening by MMS was conducted incubating the TrkA-NGF complex (7.5 mg/mL) with 5 K_d molar excess of ENT-A010 ligand and with BNN27 in a 10 fold K_d molar excess, for one hour at room temperature.

To date no crystal formation was observed from the co-crystallization screening of both TrkA and TrkB ectodomains. Only the co-crystallization of BNN27 and TrkA-NGF complex by MMS resulted in needles like crystals formed in 0.1 sodium citrate pH 5.5, 0.2 M sodium acetate and 10% PEG 4000 (figure 4.19).

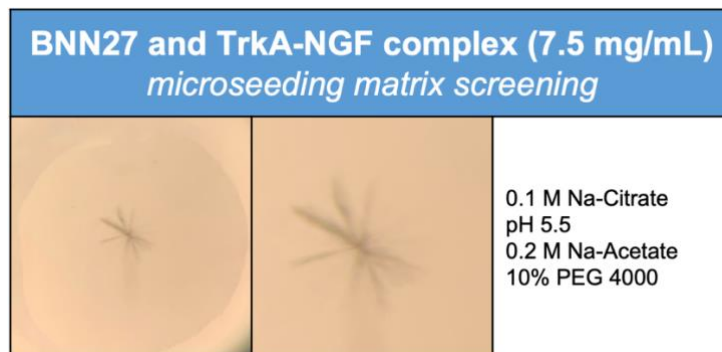


Figure 4.19. Crystal formations of BNN27 and TrkA-NGF complex co-crystallization screening by MMS.

The sitting drops consisted in 0.2 μ L of BNN27 and TrkA-NGF complex solution, 0.14 μ L of precipitant solution of Protein Complex Suite (Qiagen) and 0.06 μ L seed-stock obtained from TrkA-NGF complex needles. BNN27 was incubated for one hour at room temperature with 7.5 mg/mL TrkA-NGF complex in 0.1 M HEPES pH 7.4 and 0.15 M NaCl. Plates were stored at 20° C.

These results suggested that the *in vitro* de-glycosylation, as well as the complex formation, are critical for the crystallization of TrkA and TrkB ectodomains. Supporting this idea, the fact that the recently solved structure at 1.84 Å of TrkA-ECD was obtained using EndoF1 deglycosylated protein in complex with an interacting molecule at the d5 domain. Moreover, the final diffracting crystal was obtained by iterative optimization of precipitating conditions, starting from sea urchin-like crystals that were used for microseeding screening, which resulted in plate crystals that were further optimized and in turn used for final microseeding. Therefore, we could assume that in order to obtain a good diffracting crystal of the TrkA-NGF and TrkB-BDNF complex optimization of the hits obtained by MMS (figure 4.18 and 4.19) and a second microseeding screening were needed.

4.4. Cryo Electron Microscopy

In recent years, electron microscopy has become an important tool in structural biology. Through direct visualization and combination of images of different molecule orientations, single-particle cryo-EM makes possible to reconstruct the three-dimensional structure of monodispersed macromolecules in solution¹²⁴. The advent of new detectors and developments in sample preparation have exploded the use of this technique not only to determine at crystallographic resolution the structure of large macromolecular complexes, but also of protein below 200 kDa, opening up the structure determination to proteins not amenable to crystallization and not suitable for structural studies by NMR spectroscopy^{110,125,126}.

As described in section 4.2.4, the molecular weights of TrkA-NGF and TrkB-BDNF complex were calculated by extrapolation from the calibration curve of the gel filtration column. As the calculated weights were found to be 320 kDa and 319 kDa respectively, and thus to be large enough for analysis by SP cryo-EM, preliminary studies were conducted on service at the Cryo-EM Laboratory of the University of Milan.

Right after gel filtration, samples of TrkA-NGF and TrkB-BDNF complex were concentrated to 0.2 mg/mL and prepared for negative stain (NS) transmission electron microscopy (TEM). To remove organic contamination and create a hydrophilic surface, R1.2/1.3 Cu300 grids were prepared by glow discharge ionization before absorbing 3 μ L of complex samples. Grids were blotted by filter paper to remove liquid excess and thereafter stained with a heavy metal salt. For the TrkA-NGF complex, NS grids were prepared using 2 mg/mL protein concentration and dilutions at 1:10 and 1:100. As shown in figure 4.20-A, sample was highly heterogeneous in shape and width even at higher dilutions, probably due to different levels of particle aggregation in clusters. In comparison, the TrkB-BDNF complex sample was more homogeneous (figure 4.20-B), showing V-shaped particles, so TrkA-NGF complex was excluded from the analysis and vitrification screening was performed only for TrkB-BDNF complex.

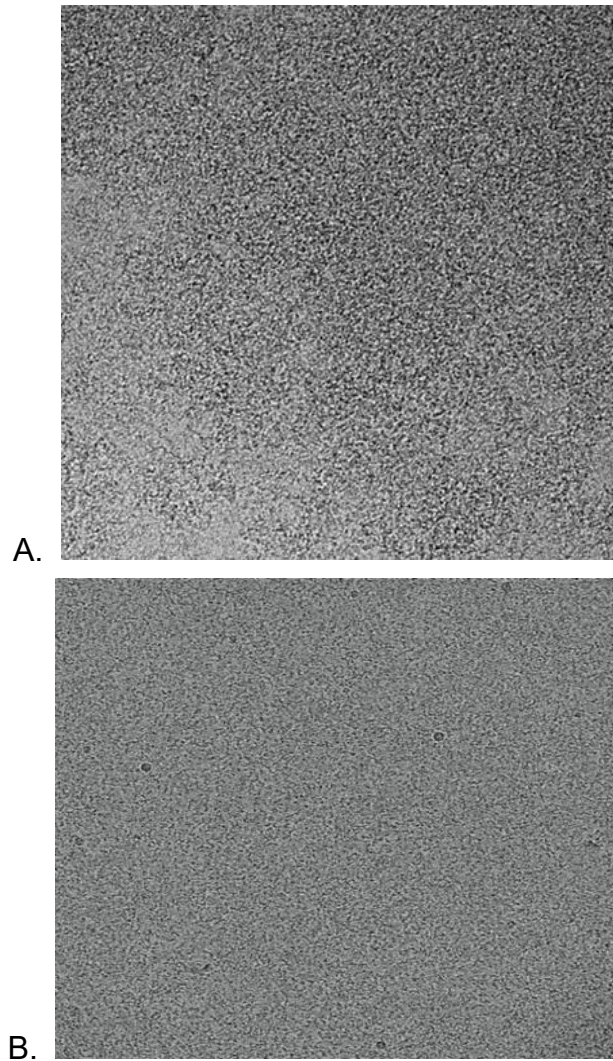


Figure 4.20. Negative staining Electron Microscopy preliminary analyses. **A)** Image taken at 73k magnification of NS grids of TrkA-NGF complex (0.002 mg/mL) and **B)** TrkB-BDNF complex at 0.2 mg/mL.

Using VitroBot Mark IV at 100% humidity and 4°C, grid screening was conducted testing different conditions as blotting time, drop size and sample concentration (0.2 mg/mL, 0.15 mg/mL and 0.015 mg/mL). Samples were applied onto glow-discharged grids and rapidly vitrified by plunge freezing in liquid ethane cooled by liquid nitrogen. Thereafter Cryo-EM images were recorded on FEI Talos Arctica 200 kV FEG, equipped with FEI Falcon 3EC direct detector and Volta Phase-plate. At lower concentration (0.015 mg/mL), the TrkB-BDNF complex specimen resulted more monodisperse showing V-like particles with limited size (highlighted in green rings in figure 4.19-B).

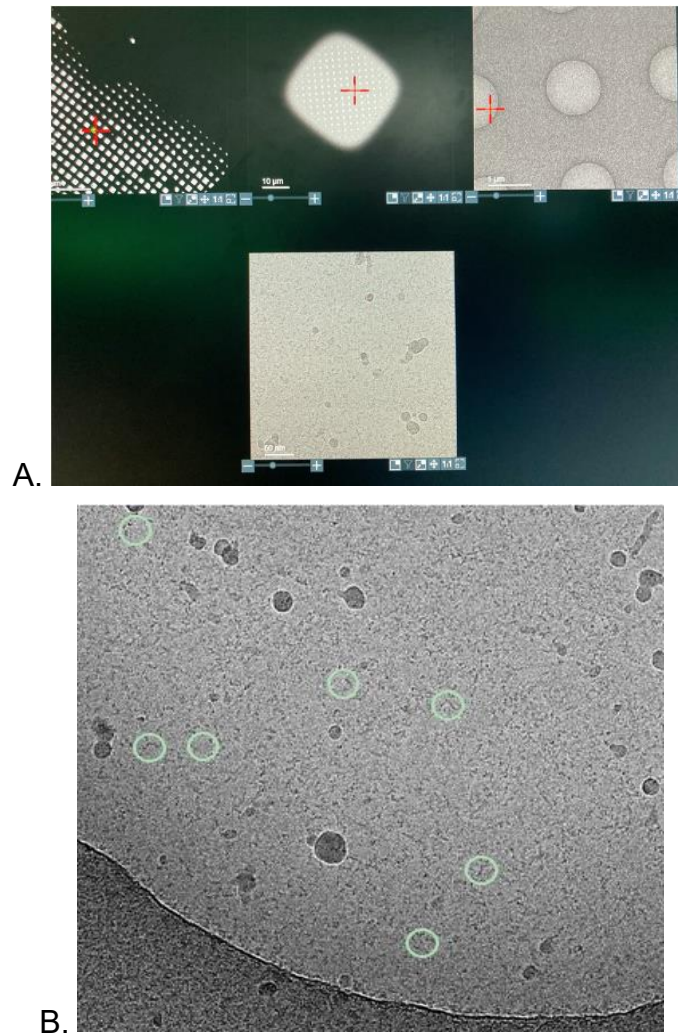


Figure 4.21. Preliminary study of TrkB-BDNF complex by single particle Cryo-EM. **A)** Images of cryo-EM grid at sequentially higher magnification taken during data collection. Starting with an image of the entire grid (left) and concluding with the visualized specimen in the carbon hole (bottom). **B)** Image of vitrified TrkB-BDNF complex sample at 0.015 mg/mL with the identified V-like particles shown in green.

To better understand the feasibility of structure reconstruction at high resolution, 3-days data collection was conducted and 1200 images were acquired with about 400 particle/image. Although the apparent molecular weight obtained from gel filtration, the particles in micrographs appeared smaller than a 320 kDa complex and still heterogenous to allow 2D classification.

In light of these results, we concluded the TrkB-BDNF complex was not a good candidate for structure determination by single particle Cryo-EM and that the apparent molecular weights did not indicate an oligomeric state of the target complexes, but these were likely due to longer hydrodynamic radii of the complexes resulting in early elution volume from analytical size exclusion.

4.5. Grating Coupled Interferometry

Grating Coupled Interferometry (GCI) is a label-free method based on waveguide interferometry used to characterize molecular interactions. The changes in mass of two interacting molecules are detected as refractive index changes within an evanescent field¹²⁷. Compared to other label-free techniques, as surface plasmon resonance (SPR), GCI is capable of providing kinetic rates (k_{on} and k_{off}) and affinity constants (K_D) of small molecules binding events with high sensitivity^{128,129}.

Therefore, GCI measurements were performed to provide qualitative and quantitative information of the intermolecular interactions between the purified TrkA and TrkB ectodomains and the ENT compounds developed within the EuroNeurotrophin consortium. Particularly, the interactions between BNN27, ENT-A005, ENT-A010 and TrkA-ECD and the interactions between ENT-A010, ENT-C117, ENT-C170, ENT-C171, ENT-C225 and TrkB-ECD were analysed. All GCI experiments were conducted at the laboratories of the Crystallography Institute of the National Research Center (IC-CNR) in Trieste (Italy).

4.5.1. Experimental design

GCI experiments were performed by two-channel Creoptic WAVE system (Creoptix AG, Switzerland). The two-channel design allows to reference the signal recorded on the target channel with a signal measured on a selected reference channel. In this experimental design, the TrkA and TrkB ectodomains were captured by ammine coupling on 4PCH WAVE chips (quasiplanar polycarboxylate surface, Creoptix) in channel 1 (Ch1), while channel 2 (Ch2) was used as reference. According to the manufacturer instructions, the 4PCH WAVE chips were previously conditioned in borate buffer (100 mM sodium borate pH 9.0, 1 M NaCl) and thereafter the TrkA and TrkB ectodomains were immobilized on the chip surface, using 50 $\mu\text{g}/\text{mL}$ protein solution in 10 mM sodium acetate pH 5.0 buffer and reaching a final density of 5000 pg/mm^2 and 5400 pg/mm^2 , respectively.

Dilution series were prepared in running buffer (PBS, 0.05% Tween 20, 0.2% dimethyl sulfoxide (DMSO) starting from 50 μM to 0.2 μM for each compound and single-cycle sequential injections were performed at 25°C, simultaneously into Ch1 and Ch2 flow cells and using a flow rate of 100 $\mu\text{L}/\text{min}$ (20 s association time, 45 s dissociation time), followed by a dissociation time of 600 s for the last higher concentration injection. Blank injections were used for double

referencing and a DMSO calibration curve for bulk correction. All the experiments have been performed in triplicate. Analysis and correction of the obtained data were performed using the Creoptix WAVE control software (correction applied: X and Y offset; DMSO calibration; double referencing). Mass transport binding models with bulk correction were used to fit all experiments.

4.5.2. Binding affinities and kinetics parameters by GCI

As previously described (chapter 2), *in vitro* studies showed the BNN27 was able to mimic the neuroprotective effects of NGF^{92,93} and based on this lead compound new small agonists have been developed within the Euroneurotrophin consortium. By GCI measurements, the binding kinetic profiles and the affinity constant values were defined for TrkA-ECD binding of BNN27 and ENT-A010, analog of BNN27 where C-17-spiro oxirane ring was replaced by a cyclopropane moiety¹³⁰, while ENT-A005 precipitated once diluted in running buffer and measurements were not performed.

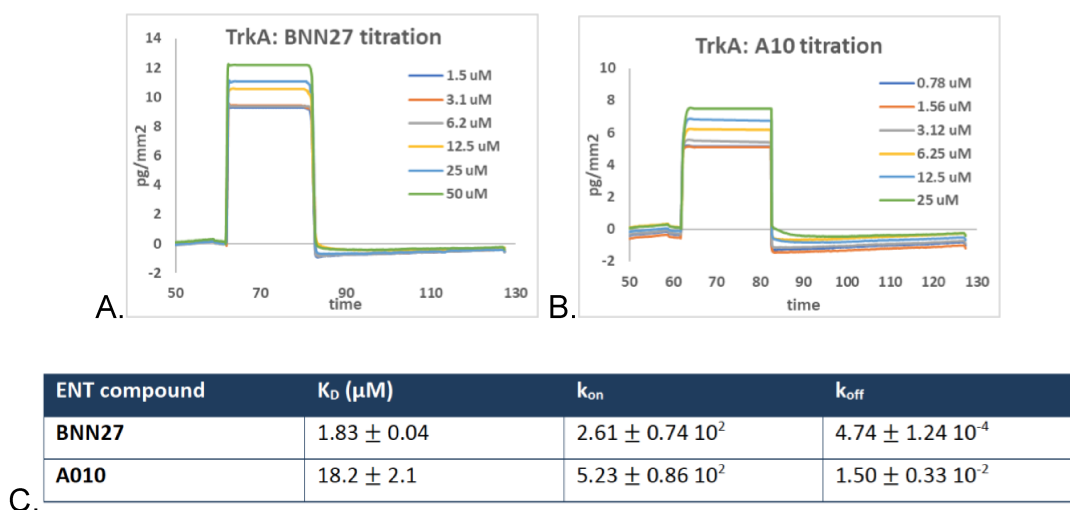


Figure 4.22. Quantitative binding kinetics of TrkA-ECD binders by GCI. A) Response curves of the 1:2 dilution series of ENT-A10 (25 μM - 0.78 μM range) and B) response curves of 1:2 serial dilutions of BNN27 (50 μM - 1.5 μM range) on a cell coated with 5000 pg/mm^2 of TrkA-ECD. C) Affinity constant K_d and kinetics parameters reported in table.

The affinity constant of BNN27 resulted in the low micro-molar range (1.83 μM), while K_D of ENT-A010 was 10 fold lower than BNN27 (table in figure 4.22-C). As expected, being related chemical analogs, and hence having close diffusion coefficients¹³¹, the association rate k_{on} of BNN27 and ENT-A010 were nearly comparable. On the other hand, the dissociation rate is dependent only on intermolecular interactions in the drug-receptor complex and typical k_{off} values are in the 10^{-6} to 1 s^{-1} range¹³¹. The measured k_{off} of BNN27 resulted in the order of 10^{-4} , versus the 10^{-2} of ENT-A010, reflecting in a longer residence time ($t_R=1/k_{\text{off}}$) of the BNN27-receptor complex compared to ENT-A010-receptor complex. Since longer residence times are critical for intrinsically slow biological process, such as receptor internalization or signal transduction¹³¹⁻¹³³, the higher affinity together with the lower dissociation rate identified the BNN27 as a more favorable TrkA agonist than ENT-A010.

With regard to TrkB-ECD binding measurements, ENT-117 and ENT-A010 resulted in closely kinetics profiles of k_{on} and k_{off} and affinity values of 17.2 μM and 12.3 μM , respectively. Showing comparable affinity for both receptor, these results confirmed the dual neurotrophin-like effect of ENT-A010 on TrkA and TrkB receptors, observed in the *in vitro* studies conducted within the EuroNeurotrophin consortium. However, the receptor selectivity of ENT-A010 could be still achieved kinetically by the resulting one-order difference in the dissociation constants between TrkA and TrkB binding (k_{off} : $1.5 \cdot 10^{-2}$ and k_{off} : $3.02 \cdot 10^{-3}$, respectively). As described above, the residence time of a ligand-protein complex is critical for receptor activation, so for similar K_D s the longer the residence time (lower k_{off}), the more selective it may be on one receptor over another.

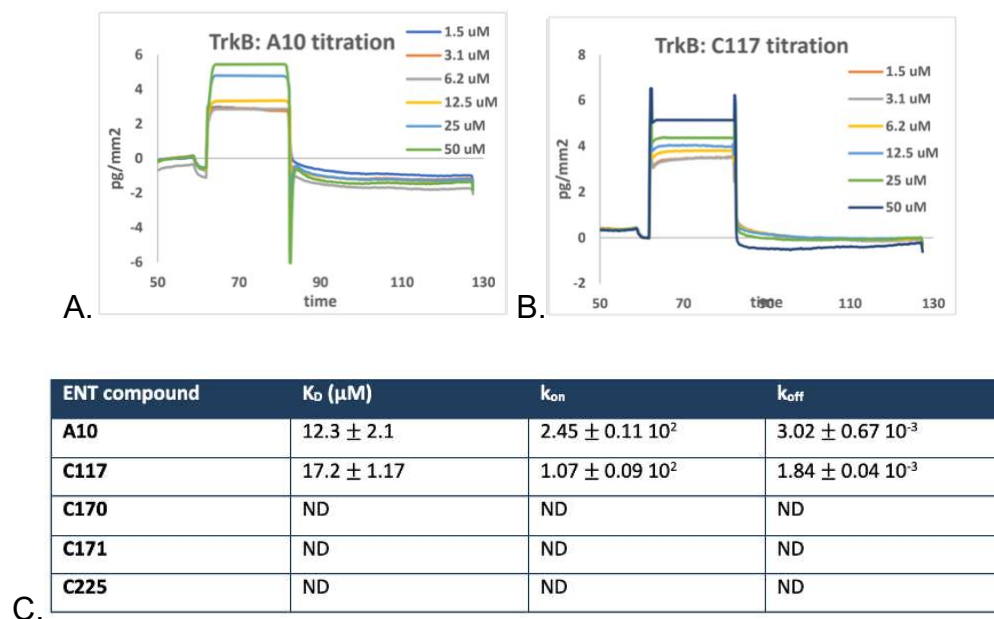


Figure 4.23: Quantitative binding kinetics of TrkB-ECD ligands by GCI. **A)** Response curves of 1:2 serial dilutions of ENT-A010 (50uM-1.5uM range) on a cell coated with 5400 pg/mm² of TrkB. **B)** Response curves of 1:2 serial dilutions of ENT-C117 (50uM-1.5uM range) on a cell coated with 5400 pg/mm² of TrkB. **C)** Affinity constant K_D and kinetics parameters reported in table.

On the contrary, no signal was detected in ENT-C170, ENT-C171 and ENT-C225 titrations, indicating that no binding event occurred. The ENT-C170 compound, also known as LM22A-4, was used as positive control for TrkB-ECD binding. Indeed, LM22A-4 was identified by pharmacophore modeling on BDNF and both *in vitro* and *in vivo* studies demonstrated neurotrophin mimetic effects and selective activation of TrkB receptor and downstream signaling proteins (AKT, ERK)⁹⁰. However, extensive series of cellular assays were performed by Boltaev et al., showing that either TrkB phosphorylation or AKT and ERK kinase activation by LM22A-4 were detected¹³⁴. In accordance with these results, the ND signal of ENT-C170/LM22A-4 obtained by GCI measurements supports the observations of Boltaev et al. on re-evaluating the agonist activity of the small compound¹³⁴.

5. Concluding remarks

The aim of this thesis was to provide the crystal structures of TrkA and TrkB receptors in complex with the neurotrophin mimetics, developed within the EuroNeurotrophin network, in order to drive the *in silico* ligand optimization, as well as to provide the first structure at atomic level of the extracellular domain of TrkB in complex with BDNF.

To address these goals, the research activities have been focused on the development of protocols for the production at high yields of pure target proteins. The bacterial *E. coli* expression system and the Hek293 mammalian system were used to produce the d5 domains, a 15 kDa subdomain of the extracellular domain involved in neurotrophin binding, and the whole ectodomains of TrkA and TrkB, respectively. Here, the results obtained are summarized and discussed.

First of all, we aimed to improve the production the d5 domains of TrkA and TrkB by varying intrinsic properties and extrinsic factors affecting the solubility of the recombinant proteins in *E. coli*. As described in section 1.3, the d5 domain adopts a characteristic immunoglobulin-like fold, consisting in two β -sheets where charged residues are solvent exposed, while hydrophobic patches packed against each other folding in a β -sandwich structure. This structural feature with extensive hydrophobic patches is prone to aggregate in inclusion bodies. Indeed, previous expressions of Trks d5 resulted in IBs accumulation and required protein recovery from IB pellet and refolding methods^{45,47,48,99,111}.

Essentially, during high level expression of heterologous proteins, nascent peptide chains form partially fold or misfolded intermediates, which aggregate through hydrophobic interactions and accumulate in inclusion bodies, visible as dense refractile deposits in the bacterial cytoplasm or periplasm¹³⁵. Recent experimental evidences showed that rather than amorphous structures, IBs are enriched with β -sheet elements that form ordered amyloid structures in a nucleation dependent-manner¹³⁶. Furthermore, amyloid-like IBs have the ability to seed aggregation of highly homologous proteins, resulting preferentially in fibrils of recombinant protein.

To minimize the tendency of the d5 β -sheets to aggregate into inclusion bodies, several constructs were designed to reduce the intrinsic propensity of the amino acid sequence by

adopting solubility tag, such as the MBP, and introducing monomer-stabilizing mutations (section 3.1.1).

At the same time, extrinsic factors affecting the solubility of the recombinant proteins were modified and tested for each construct in order to find out the best expression strategy. For example, lowering the growth temperature, as well as reducing the inducer concentration or changing culture medium were modified parameters in an attempt to reduce the transcription rate and thus the IBs formation. Furthermore, additives and engineered strains of *E. coli* were used to aid the protein folding process. The addition of low percentage of ethanol in culture media acts as an heat-shock-induction, eliciting a shock response and the production of chaperones, as well as the ArcticExpress strain constitutively expresses cold-adapted chaperones with high refolding activities at low temperature, combining the lowered transcription rate to chaperonin activity. Moreover, the formation of correct disulfide bridges is crucial to obtain stable and functional proteins, and requires an oxidative environment that is lacking in the bacterial cytoplasm. Therefore, to efficiently obtain the disulfide bond present in the d5 domains, connecting and stabilizing the β -sheets core, the engineered Rosetta-Gami cells were tested to promote correct disulfide bonds formation.

Nevertheless, all the different expression strategies resulted in accumulation of the d5 domain of TrkA into inclusion bodies, which required downstream approaches for protein purification. As described in section 3.2.3, the downstream approaches consisted in three different refolding strategies, plus an oxidative refolding, but the target protein mainly eluted in the void volume during gel filtration, suggesting that the TrkA-d5 did not refold correctly and the presence of other elements may be imperative to achieve proper folding. Only a small fraction eluted at the elution volume corresponding to TrkA-d5 monomer and CD data showed a characteristic β -strands spectrum. However, the final yield was not sufficient for structural studies by X-ray crystallography.

The only successful approach that enhanced the soluble production of the TrkB-d5 domain, but not TrkA-d5, was to co-express the target protein with the cognate neurotrophin. The co-expression strategy, together with optimized extrinsic factors, such as low growth temperature (18° C), rich growth medium (SB) and late induction time (OD_{600} :1.2), allowed to obtain a final yield of 5 mg/L of Trkb-d5. However, BDNF was expressed at lower yield respect to TrkB-d5 and it was not possible to purify TrkB-d5 and BDNF as a complex.

Gel filtration and mass spectrometry analyses validated the purification of the monomer conformation of the TrkB-d5 and CD analysis confirmed its secondary structure characterized by β -strand elements. These results showed that our developed purification protocol is the first to allow the soluble expression of the TrkB-d5 domain monomer in *E. coli* expression system.

Several crystallization screening were set up, using different concentration of TrkB-d5, but so far no crystals have been observed. The lack of crystallization hits could be due to the absence of interface contacts between the d5 domains, as previous crystal structures showed that intradomain interactions do not occur, as well as FRET experiments have shown that the extracellular domain has no thermodynamic contribution on dimer stability. Therefore, we could speculate that either higher concentrations of TrkB-d5 or the complex between TrkB-d5 and BDNF, or another bridging molecule, are required to obtain crystal formations.

Second of all, the entire extracellular domain of TrkA and TrkB receptors were produced in suspension-grown Hek293 cells.

Another factor affecting protein solubility in *E. coli*, particularly when expressing eukaryotic proteins, is the lack of an adequate host machinery for post-translational modifications (PTMs). PTMs play a key role in achieving native and biologically active conformation, indeed the presence of N-glycosylation of the Trks extracellular domain have been suggested to be critical for protein folding and structural integrity⁴⁶. In addition, the interaction between the d4 and d5 domains and the proper formation of disulfide bonds are critical elements for the d5 domain folding, such that whole extracellular domain has been expressed in an eukaryotic system.

As described in section 4.2.1, the protein constructs were designed with a translocation signal at the N-terminal to promote protein secretion, and an histidine-tag at the C-terminal to facilitate protein purification from the growth medium. Furthermore, the inhibitor of α -mannosidase I was added just prior to transfection to decrease the complexity and heterogeneity of the N-glycosylation, allowing PTMs only with oligomannose moieties. Thereafter, the produced ectodomains of TrkA and TrkB receptors were incubated with NGF and BDNF, respectively. The purified complexes were used for crystallization screening and for preliminary studies by single particle cryo-EM (sections 4.3-4.4). The images of negative-stained samples acquired for TrkA-NGF complex, as well as the images of the vitrified TrkB-BDNF complex showed heterogeneous specimen, with small particles, that did not allow 2D classification and hence structure reconstruction of the complex.

In addition, any crystals resulted from the crystallization set ups and, collectively, these results suggested that the remaining oligomannose chains still inserted a certain degree of flexibility and heterogeneity, hampering crystal formation. Thus, sample quality was improved by enzymatically removing the oligomannose moieties and new crystal screens were set up for both NT-Trk receptor complexes, as well as for co-crystallization screening of TrkA and TrkB ectodomains in complex with the neurotrophin mimetics developed within the EuroNeurotrophin network.

Several crystallization hits of the TrkA-NGF complex gave rise to needle-like and plate crystals. However, the diffraction was very poor and at low resolution and further optimization was required. Using bow-like crystal of the TrkA-NGF complex, microseeding matrix screening was performed in an attempt to promote crystal growth in metastable conditions, but only few precipitating conditions of TrkB-BDNF and TrkA-NGF complexes resulted in needle and rod formations.

Since no crystal formation was obtained for the TrkA and TrkB ectodomains set up, these results support the idea that complex formation is critical for ectodomain crystallization. Furthermore, the recent high-resolution crystal structure of TrkA-ECD was obtained using a similar approach for sample preparation, namely complete deglycosylation by treatment with EndoF1 and complex formation with an interacting molecule, and an iterative process of optimizing precipitating conditions by microseeding screening⁴⁹. Consequentially, we could conclude that further optimization and microseeding cycles were needed to obtain good diffracting crystals of TrkB-BDNF and TrkA-NGF complexes.

Lastly, the biophysical characterization of the binding between the TrkA and TrkB ectodomains and their respective agonist compounds was performed by GCI measurements. As previously described (section 4.5), the defined K_D and k_{off} values of BNN27 identified the lead compound as a more favorable TrkA agonist than ENT-A010, exhibiting a longer residence times (lower k_{off} value) and binding affinity in the low micromolar range. While of the five different Trk-B ligands, only ENT-C117 and ENT-A010 showed similar kinetics profiles and binding affinity values in micromolar range. Interestingly, no signals were detected for the ENT-C170/LM22A-4 compound, used as positive control, validating the observation to reconsider the selective agonist activity of the small compound on TrkB receptor¹³⁴.

Bibliography

1. Cohen, S., Levi-Montalcini, R. & Hamburger, V. A NERVE GROWTH-STIMULATING FACTOR ISOLATED FROM SARCOM AS 37 AND 180. *Proc. Natl. Acad. Sci. U. S. A.* **40**, 1014–8 (1954).
2. Cohen, S. & Levi-Montalcini, R. A NERVE GROWTH-STIMULATING FACTOR ISOLATED FROM SNAKE VENOM. *Proc. Natl. Acad. Sci. U. S. A.* **42**, 571–4 (1956).
3. Barde, Y. A., Edgar, D. & Thoenen, H. Purification of a new neurotrophic factor from mammalian brain. *EMBO J.* **1**, 549–553 (1982).
4. Hohn, A., Leibrock, J., Bailey, K. & Barde, Y. A. Identification and characterization of a novel member of the nerve growth factor/brain-derived neurotrophic factor family. *Nature* **344**, 339–341 (1990).
5. Ip, N. Y. *et al.* Mammalian neurotrophin-4: structure, chromosomal localization, tissue distribution, and receptor specificity. *Proc. Natl. Acad. Sci.* **89**, 3060–3064 (1992).
6. Berkemeier, L. R. *et al.* Neurotrophin-5: A novel neurotrophic factor that activates trk and trkB. *Neuron* **7**, 857–866 (1991).
7. Lin, M. I. *et al.* Trk C receptor signaling regulates cardiac myocyte proliferation during early heart development in vivo. *Dev. Biol.* **226**, 180–91 (2000).
8. Kashyap, M. *et al.* MP89-20 BDNF OVEREXPRESSION ALTERS THE PHENOTYPE OF CHOLINERGIC NEURONS IN RAT BLADDER. *J. Urol.* (2015). doi:10.1016/J.JURO.2015.02.1819
9. Kashyap, M. P., Roberts, C., Waseem, M. & Tyagi, P. Drug Targets in Neurotrophin Signaling in the Central and Peripheral Nervous System. *Molecular Neurobiology* **55**, 6939–6955 (2018).
10. Melamed, I. *et al.* Nerve growth factor signal transduction in human B lymphocytes is mediated by gp140trk. *Eur. J. Immunol.* **26**, 1985–92 (1996).
11. Deinhardt, K. & Chao, M. V. Trk receptors. *Handb. Exp. Pharmacol.* **220**, 103–119 (2014).
12. Chao, M. V. Neurotrophins and their receptors: A convergence point for many signalling pathways. *Nat. Rev. Neurosci.* **4**, 299–309 (2003).
13. Clary, D. O. & Reichardt, L. F. An alternatively spliced form of the nerve growth factor receptor TrkA confers an enhanced response to neurotrophin 3. *Proc. Natl. Acad. Sci. U. S. A.* **91**, 11133–7 (1994).
14. Yuan, W., Ibáñez, C. F. & Lin, Z. Death domain of p75 neurotrophin receptor: a structural perspective on an intracellular signalling hub. *Biol. Rev.* **94**, 1282–1293 (2019).

15. Caffino, L., Mottarlini, F. & Fumagalli, F. Born to Protect: Leveraging BDNF Against Cognitive Deficit in Alzheimer's Disease. *CNS Drugs* (2020). doi:10.1007/s40263-020-00705-9
16. Mufson, E. J. *et al.* Nerve growth factor pathobiology during the progression of Alzheimer's disease. *Front. Neurosci.* **13**, (2019).
17. Jin. Regulation of BDNF-TrkB Signaling and Potential Therapeutic Strategies for Parkinson's Disease. *J. Clin. Med.* **9**, 257 (2020).
18. Naegelin, Y. *et al.* Levels of brain-derived neurotrophic factor in patients with multiple sclerosis. *Ann. Clin. Transl. Neurol.* **7**, 2251–2261 (2020).
19. Wang, M., Xie, Y. & Qin, D. Proteolytic cleavage of proBDNF to mBDNF in neuropsychiatric and neurodegenerative diseases. *Brain Res. Bull.* **166**, 172–184 (2021).
20. Zhang, X. Y. *et al.* BDNF polymorphisms are associated with schizophrenia onset and positive symptoms. *Schizophr. Res.* **170**, 41–7 (2016).
21. Sklar, P. *et al.* Family-based association study of 76 candidate genes in bipolar disorder: BDNF is a potential risk locus. Brain-derived neurotrophic factor. *Mol. Psychiatry* **7**, 579–93 (2002).
22. Aref-Eshghi, E., Lin, F., Li, M. M. & Zhong, Y. The oncogenic roles of NTRK fusions and methods of molecular diagnosis. *Cancer Genet.* **258–259**, 110–119 (2021).
23. Rogers, C., Morrissette, J. J. D. & Sussman, R. T. NTRK point mutations and their functional consequences. *Cancer Genet.* **262–263**, 5–15 (2022).
24. Lawn, S. *et al.* Neurotrophin signaling via TrkB and TrkC receptors promotes the growth of brain tumor-initiating cells. *J. Biol. Chem.* **290**, 3814–24 (2015).
25. Johnston, A. L. M. *et al.* The p75 neurotrophin receptor is a central regulator of glioma invasion. *PLoS Biol.* **5**, e212 (2007).
26. Sinkevicius, K. W. *et al.* Neurotrophin receptor TrkB promotes lung adenocarcinoma metastasis. *Proc. Natl. Acad. Sci. U. S. A.* **111**, 10299–304 (2014).
27. Gibon, J. & Barker, P. A. Neurotrophins and Proneurotrophins: Focus on Synaptic Activity and Plasticity in the Brain. *Neuroscientist* **23**, 587–604 (2017).
28. Seidah, N. G. *et al.* Cellular processing of the nerve growth factor precursor by the mammalian pro-protein convertases. *Biochem. J.* **314** (Pt 3), 951–60 (1996).
29. Benicky, J., Sanda, M., Brnakova Kennedy, Z. & Goldman, R. N-Glycosylation is required for secretion of the precursor to brain-derived neurotrophic factor (proBDNF) carrying sulfated LacdiNAc structures. *J. Biol. Chem.* **294**, 16816–16830 (2019).
30. Rattenholl, A. *et al.* Pro-sequence assisted folding and disulfide bond formation of human nerve growth factor. *J. Mol. Biol.* (2001). doi:10.1006/jmbi.2000.4295

31. Suter, U., Heymach, J. V. & Shooter, E. M. Two conserved domains in the NGF propeptide are necessary and sufficient for the biosynthesis of correctly processed and biologically active NGF. *EMBO J.* **10**, 2395–2400 (1991).
32. Seidah, N. G. *et al.* Cellular processing of the nerve growth factor precursor by the mammalian pro-protein convertases. *Biochem. J.* **314 (Pt 3)**, 951–60 (1996).
33. Seidah, N. G., Benjannet, S., Pareek, S., Chrétien, M. & Murphy, R. A. Cellular processing of the neurotrophin precursors of NT3 and BDNF by the mammalian proprotein convertases. *FEBS Lett.* **379**, 247–50 (1996).
34. Gray, K. & Ellis, V. Activation of pro-BDNF by the pericellular serine protease plasmin. *FEBS Lett.* **582**, 907–910 (2008).
35. Lee, R., Kermani, P., Teng, K. K. & Hempstead, B. L. Regulation of cell survival by secreted proneurotrophins. *Science (80-)*. **294**, 1945–1948 (2001).
36. Tauris, J. *et al.* Proneurotrophin-3 may induce Sortilin-dependent death in inner ear neurons. *Eur. J. Neurosci.* **33**, 622–31 (2011).
37. Zanin, J. P., Unsain, N. & Anastasia, A. Growth factors and hormones pro-peptides: the unexpected adventures of the BDNF prodomain. *J. Neurochem.* **141**, 330–340 (2017).
38. Dieni, S. *et al.* BDNF and its pro-peptide are stored in presynaptic dense core vesicles in brain neurons. *J. Cell Biol.* **196**, 775–88 (2012).
39. Yang, J. *et al.* Neuronal release of proBDNF. *Nat. Neurosci.* **12**, 113–5 (2009).
40. Nagappan, G. *et al.* Control of extracellular cleavage of ProBDNF by high frequency neuronal activity. *Proc. Natl. Acad. Sci. U. S. A.* **106**, 1267–72 (2009).
41. Yan, R. *et al.* The Structure of the Pro-domain of Mouse proNGF in Contact with the NGF Domain. *Structure* **27**, 78-89.e3 (2019).
42. Mizui, T., Ohira, K. & Kojima, M. BDNF pro-peptide: A novel synaptic modulator generated as an N-terminal fragment from the BDNF precursor by proteolytic processing. *Neural Regen. Res.* **12**, 1024–1027 (2017).
43. McDonald, N. Q. *et al.* New protein fold revealed by a 2.3-Å resolution crystal structure of nerve growth factor. *Nature* **354**, 411–414 (1991).
44. Robinson, R. C. *et al.* The structures of the neurotrophin 4 homodimer and the brain-derived neurotrophic factor 0 neurotrophin 4 heterodimer reveal a common Trk-binding site. 2589–2597 (1999).
45. Robertson, A. G. S. *et al.* Identification and structure of the nerve growth factor binding site on TrkA. *Biochem. Biophys. Res. Commun.* **282**, 131–141 (2001).
46. Wehrman, T. *et al.* Structural and Mechanistic Insights into Nerve Growth Factor Interactions with the TrkA and p75 Receptors. *Neuron* **53**, 25–38 (2007).
47. Wlesmann, C., Ultsch, M. H., Bass, S. H. & De Vos, A. M. Crystal structure of nerve

- growth factor in complex with the ligand- binding domain of the TrkA receptor. *Nature* **401**, 184–188 (1999).
48. Banfield, M. J. *et al.* Specificity in Trk receptor:neurotrophin interactions: The crystal structure of TrkB-d5 in complex with neurotrophin-4/5. *Structure* **9**, 1191–1199 (2001).
 49. Cao, L. *et al.* Design of protein binding proteins from target structure alone. *Nature* 1–1 (2022). doi:10.1038/s41586-022-04654-9
 50. Theillet, F.-X. *et al.* The alphabet of intrinsic disorder. *Intrinsically Disord. Proteins* **1**, e24360 (2013).
 51. Kot, E. F. *et al.* Intrinsically disordered regions couple the ligand binding and kinase activation of Trk neurotrophin receptors. *iScience* **25**, 104348 (2022).
 52. Strohmaier, C., Carter, B. D., Urfer, R., Barde, Y. A. & Dechant, G. A splice variant of the neurotrophin receptor trkB with increased specificity for brain-derived neurotrophic factor. *EMBO J.* **15**, 3332–7 (1996).
 53. Franco, M. L. *et al.* Structural basis of the transmembrane domain dimerization and rotation in the activation mechanism of the TRKA receptor by nerve growth factor. *J. Biol. Chem.* **295**, 275–286 (2020).
 54. Bertrand, T. *et al.* The crystal structures of TrkA and TrkB suggest key regions for achieving selective inhibition. *J. Mol. Biol.* **423**, 439–453 (2012).
 55. Hubbard, S. R. Structural analysis of receptor tyrosine kinases. *Prog. Biophys. Mol. Biol.* **71**, 343–358 (1999).
 56. Bertrand, T. *Crystal Structures of Neurotrophin Receptors Kinase Domain.* *Vitamins and Hormones* **104**, (Elsevier Inc., 2017).
 57. McTigue, M. A. *et al.* Crystal structure of the kinase domain of human vascular endothelial growth factor receptor 2: a key enzyme in angiogenesis. *Structure* **7**, 319–330 (1999).
 58. Shen, J. & Maruyama, I. N. Nerve growth factor receptor TrkA exists as a preformed, yet inactive, dimer in living cells. *FEBS Lett.* **585**, 295–299 (2011).
 59. Ahmed, F. & Hristova, K. Dimerization of the Trk receptors in the plasma membrane: Effects of their cognate ligands. *Biochem. J.* **475**, 3669–3685 (2018).
 60. Bibel, M. & Barde, Y. A. Neurotrophins: key regulators of cell fate and cell shape in the vertebrate nervous system. *Genes Dev.* **14**, 2919–37 (2000).
 61. Levi-Montalcini, R. The nerve growth factor thirty-five years later. *In Vitro Cell. Dev. Biol.* **23**, 227–38 (1987).
 62. Davies, A. M. Regulation of neuronal survival and death by extracellular signals during development. *EMBO J.* **22**, 2537–45 (2003).
 63. Tauszig-Delamasure, S. *et al.* The TrkC receptor induces apoptosis when the

- dependence receptor notion meets the neurotrophin paradigm. *Proc. Natl. Acad. Sci.* **104**, 13361–13366 (2007).
64. Nikolettou, V. *et al.* Neurotrophin receptors TrkA and TrkC cause neuronal death whereas TrkB does not. *Nature* **467**, 59–63 (2010).
 65. Cellerino, A. & Kohler, K. Brain-derived neurotrophic factor/neurotrophin-4 receptor TrkB is localized on ganglion cells and dopaminergic amacrine cells in the vertebrate retina. *J. Comp. Neurol.* **386**, 149–60 (1997).
 66. Krause, S., Schindowski, K., Zechel, S. & von Bohlen und Halbach, O. Expression of trkB and trkC receptors and their ligands brain-derived neurotrophic factor and neurotrophin-3 in the murine amygdala. *J. Neurosci. Res.* **86**, 411–21 (2008).
 67. Ringstedt, T., Lagercrantz, H. & Persson, H. Expression of members of the trk family in the developing postnatal rat brain. *Brain Res. Dev. Brain Res.* **72**, 119–31 (1993).
 68. Sobreviela, T. *et al.* TrkA-immunoreactive profiles in the central nervous system: colocalization with neurons containing p75 nerve growth factor receptor, choline acetyltransferase, and serotonin. *J. Comp. Neurol.* **350**, 587–611 (1994).
 69. McAllister, K., Kats, L. & Lo c., D. Neurotrophins and synaptic plasticity. *Annu. Reviv Neurosci.* **22**, 295–318 (1999).
 70. Thoenen, H. Neurotrophins and neuronal plasticity. *Science (80-)*. **270**, 593–598 (1995).
 71. Mowla, S. J. *et al.* Differential Sorting of Nerve Growth Factor and Brain-Derived Neurotrophic Factor in Hippocampal Neurons. *J. Neurosci.* **19**, 2069–2080 (1999).
 72. Andreska, T., Lüningschrör, P. & Sendtner, M. Regulation of TrkB cell surface expression—a mechanism for modulation of neuronal responsiveness to brain-derived neurotrophic factor. *Cell Tissue Res.* **382**, 5–14 (2020).
 73. Chao, M. V., Rajagopal, R. & Lee, F. S. Neurotrophin signalling in health and disease. *Clin. Sci. (Lond)*. **110**, 167–73 (2006).
 74. Mitre, M., Mariga, A. & Chao, M. V. Neurotrophin signalling: novel insights into mechanisms and pathophysiology. *Clin. Sci. (Lond)*. **131**, 13–23 (2017).
 75. Weissmiller, A. M. & Wu, C. Current advances in using neurotrophic factors to treat neurodegenerative disorders. *Transl. Neurodegener.* **1**, 14 (2012).
 76. Ginty, D. D. & Segal, R. A. Retrograde neurotrophin signaling: Trk-ing along the axon. *Curr. Opin. Neurobiol.* **12**, 268–274 (2002).
 77. Bonni, A. & Greenberg, M. E. Neurotrophin regulation of gene expression. *Can. J. Neurol. Sci.* **24**, 272–283 (1997).
 78. Scott-Solomon, E. & Kuruvilla, R. Mechanisms of neurotrophin trafficking via Trk receptors. *Mol. Cell. Neurosci.* **91**, 25–33 (2018).

79. Lehigh, K. M., West, K. M. & Ginty, D. D. Retrogradely Transported TrkA Endosomes Signal Locally within Dendrites to Maintain Sympathetic Neuron Synapses. *Cell Rep.* **19**, 86–100 (2017).
80. Arévalo, J. C. & Wu, S. H. Neurotrophin signaling: Many exciting surprises! *Cell. Mol. Life Sci.* **63**, 1523–1537 (2006).
81. Reichardt, L. F. Neurotrophin-regulated signalling pathways. *Philos. Trans. R. Soc. B Biol. Sci.* **361**, 1545–1564 (2006).
82. York, R. D. *et al.* Role of phosphoinositide 3-kinase and endocytosis in nerve growth factor-induced extracellular signal-regulated kinase activation via Ras and Rap1. *Mol. Cell. Biol.* **20**, 8069–83 (2000).
83. Brunet, A., Datta, S. R. & Greenberg, M. E. Transcription-dependent and -independent control of neuronal survival by the PI3K–Akt signaling pathway. *Curr. Opin. Neurobiol.* **11**, 297–305 (2001).
84. Allen, S. J. & Dawbarn, D. Clinical relevance of the neurotrophins and their receptors. *Clinical Science* **110**, 175–191 (2006).
85. Saragovi, H. U., Galan, A. & Levin, L. A. Neuroprotection: Pro-survival and anti-neurotoxic mechanisms as therapeutic strategies in neurodegeneration. *Front. Cell. Neurosci.* **13**, 1–12 (2019).
86. Covaceuszach, S. *et al.* Development of a Non Invasive NGF-Based Therapy for Alzheimers Disease. *Curr. Alzheimer Res.* **6**, 158–170 (2009).
87. Tian, L. *et al.* Intranasal administration of nerve growth factor ameliorate β -amyloid deposition after traumatic brain injury in rats. *Brain Res.* **1440**, 47–55 (2012).
88. Eriksson Jönhagen, M. *et al.* Intracerebroventricular infusion of nerve growth factor in three patients with Alzheimer's disease. *Dement. Geriatr. Cogn. Disord.* **9**, 246–57 (1998).
89. Apfel, S. C. Neurotrophic factors and pain. *Clin. J. Pain* **16**, S7-11 (2000).
90. Massa, S. M. *et al.* Small molecule BDNF mimetics activate TrkB signaling and prevent neuronal degeneration in rodents. *J. Clin. Invest.* **120**, 1774–85 (2010).
91. Gudasheva, T. A., Povarnina, P. Y., Tarasiuk, A. V. & Seredenin, S. B. Low-molecular mimetics of nerve growth factor and brain-derived neurotrophic factor: Design and pharmacological properties. *Med. Res. Rev.* **41**, 2746–2774 (2021).
92. Pediaditakis, I. *et al.* Selective and differential interactions of BNN27, a novel C17-spiroepoxy steroid derivative, with TrkA receptors, regulating neuronal survival and differentiation. *Neuropharmacology* **111**, 266–282 (2016).
93. Pediaditakis, I. *et al.* BNN27, a 17-spiroepoxy steroid derivative, interacts with and activates p75 neurotrophin receptor, rescuing cerebellar granule neurons from apoptosis. *Front. Pharmacol.* **7**, 1–14 (2016).

94. Yilmaz, C. *et al.* ENT-A010, a Novel Steroid Derivative, Displays Neuroprotective Functions and Modulates Microglial Responses. *Biomolecules* **12**, (2022).
95. Ultsch, M. H. *et al.* Crystal structures of the neurotrophin-binding domain of TrkA, TrkB and TrkC. *J. Mol. Biol.* **290**, 149–159 (1999).
96. Shoemark, D. K., Williams, C., Fahey, M. S., Watson, J. J. & Sue, J. Design and Nuclear Magnetic Resonance (NMR) S tructure D etermination of the S econd E xtracellular I mmunoglobulin T yrosine K inase A (TrkAlg2) D omain C onstruct for B inding S ite D etermination in D rug D iscovery. 1–7
97. Mészáros, B., Erdős, G. & Dosztányi, Z. IUPred2A: context-dependent prediction of protein disorder as a function of redox state and protein binding. *Nucleic Acids Res.* **46**, W329–W337 (2018).
98. Wiedemann, C., Bellstedt, P. & Görlach, M. CAPITO—a web server-based analysis and plotting tool for circular dichroism data. *Bioinformatics* **29**, 1750–1757 (2013).
99. Shoemark, D. K. *et al.* Design and nuclear magnetic resonance (NMR) structure determination of the second extracellular immunoglobulin tyrosine kinase A (TrkAlg2) domain construct for binding site elucidation in drug discovery. *J. Med. Chem.* **58**, 767–77 (2015).
100. Gasteiger, E. *et al.* Protein Identification and Analysis Tools on the ExPASy Server. in *The Proteomics Protocols Handbook* 571–607 (Humana Press, 2005). doi:10.1385/1-59259-890-0:571
101. Bondos, S. E. & Bicknell, A. Detection and prevention of protein aggregation before, during, and after purification. *Anal. Biochem.* **316**, 223–231 (2003).
102. Studier, F. W. Protein production by auto-induction in high-density shaking cultures. *Protein Expr. Purif.* **41**, 207–234 (2005).
103. Chhetri, G., Kalita, P. & Tripathi, T. An efficient protocol to enhance recombinant protein expression using ethanol in Escherichia coli. *MethodsX* **2**, 385–391 (2015).
104. Ferrer, M., Chernikova, T. N., Yakimov, M. M., Golyshin, P. N. & Timmis, K. N. Chaperonins govern growth of Escherichia coli at low temperatures [2]. *Nat. Biotechnol.* **21**, 1266–1267 (2003).
105. Uversky, V. N. Natively unfolded proteins: A point where biology waits for physics. *Protein Sci.* **11**, 739–756 (2002).
106. Wang, L., Wang, X. & Wang, C. C. Protein disulfide-isomerase, a folding catalyst and a redox-regulated chaperone. *Free Radic. Biol. Med.* **83**, 305–313 (2015).
107. Tu, B. P. & Weissman, J. S. Oxidative protein folding in eukaryotes: mechanisms and consequences. *J. Cell Biol.* **164**, 341 (2004).
108. Arakawa, T. *et al.* Suppression of protein interactions by arginine: A proposed mechanism of the arginine effects. *Biophys. Chem.* **127**, 1–8 (2007).

109. Tsumoto, K. *et al.* Role of arginine in protein refolding, solubilization, and purification. *Biotechnol. Prog.* **20**, 1301–1308 (2004).
110. Healthcare, G. E. Purifying Challenging Proteins. *Gen. Electr. Co.* **28-9095-3**, 1–107 (2007).
111. Ultsch, M. H. *et al.* Crystal structures of the neurotrophin-binding domain of TrkA, TrkB and TrkC 1 1 Edited by I. A. Wilson. *J. Mol. Biol.* **290**, 149–159 (1999).
112. Lennon, G., Auffray, C., Polymeropoulos, M. & Soares, M. B. The I.M.A.G.E. Consortium: An Integrated Molecular Analysis of Genomes and Their Expression. *Genomics* **33**, 151–152 (1996).
113. Frenkel, L. & Bremer, H. Increased Amplification of Plasmids pBR322 and pBR327 by Low Concentrations of Chloramphenicol. *Dna* **5**, 539–544 (1986).
114. Aricescu, A. R., Lu, W. & Jones, E. Y. A time- and cost-efficient system for high-level protein production in mammalian cells. *Acta Crystallogr. Sect. D Biol. Crystallogr.* **62**, 1243–1250 (2006).
115. Nelson, C. A., McCoy, W. H. & Fremont, D. H. Eukaryotic expression systems for structural studies. *Methods Mol. Biol.* **1140**, 107–116 (2014).
116. Bhatwa, A. *et al.* Challenges Associated With the Formation of Recombinant Protein Inclusion Bodies in *Escherichia coli* and Strategies to Address Them for Industrial Applications. *Front. Bioeng. Biotechnol.* **9**, 630551 (2021).
117. E., J. Structural Biology of Glycoproteins. in *Glycosylation* (InTech, 2012). doi:10.5772/48154
118. Elbein, A. D., Tropea, J. E., Mitchell, M. & Kaushal, G. P. Kifunensine, a potent inhibitor of the glycoprotein processing mannosidase I. *J. Biol. Chem.* **265**, 15599–15605 (1990).
119. Chang, V. T. *et al.* Glycoprotein Structural Genomics: Solving the Glycosylation Problem. *Structure* **15**, 267–273 (2007).
120. Trimble, R. B. & Tarentino, A. L. Identification of distinct endoglycosidase (endo) activities in *Flavobacterium meningosepticum*: Endo F1, endo F2, and endo F3. Endo F1 and endo H hydrolyze only high mannose and hybrid glycans. *J. Biol. Chem.* **266**, 1646–1651 (1991).
121. Tarentino, A. L. & Plummer, T. H. Enzymatic deglycosylation of asparagine-linked glycans: Purification, properties, and specificity of oligosaccharide-cleaving enzymes from *Flavobacterium meningosepticum*. *Methods Enzymol.* **230**, 44–57 (1994).
122. Struwe, W. B. & Robinson, C. V. Relating glycoprotein structural heterogeneity to function – insights from native mass spectrometry. *Curr. Opin. Struct. Biol.* **58**, 241–248 (2019).
123. E., J. Structural Biology of Glycoproteins. *Glycosylation* (2012). doi:10.5772/48154

124. Milne, J. L. S. *et al.* Cryo-electron microscopy - A primer for the non-microscopist. *FEBS J.* **280**, 28–45 (2013).
125. Cheng, Y. Single-particle Cryo-EM at crystallographic resolution. *Cell* **161**, 450–457 (2015).
126. Nakane, T. *et al.* Single-particle cryo-EM at atomic resolution. (2020).
127. Kozma, P., Hamori, A., Cottier, K., Kurunczi, S. & Horvath, R. Grating coupled interferometry for optical sensing. *Appl. Phys. B* **97**, 5–8 (2009).
128. Kozma, P., Hámori, A., Kurunczi, S., Cottier, K. & Horvath, R. Grating coupled optical waveguide interferometer for label-free biosensing. *Sensors Actuators, B Chem.* **155**, 446–450 (2011).
129. Jankovics, H. *et al.* Grating-coupled interferometry reveals binding kinetics and affinities of Ni ions to genetically engineered protein layers. *Sci. Rep.* **10**, 22253 (2020).
130. Yilmaz, C. *et al.* ENT-A010, a Novel Steroid Derivative, Displays Neuroprotective Functions and Modulates Microglial Responses. *Biomolecules* **12**, 424 (2022).
131. Núñez, S., Venhorst, J. & Kruse, C. G. Target-drug interactions: First principles and their application to drug discovery. *Drug Discov. Today* **17**, 10–22 (2012).
132. Pan, A. C., Borhani, D. W., Dror, R. O. & Shaw, D. E. Molecular determinants of drug-receptor binding kinetics. *Drug Discov. Today* **18**, 667–673 (2013).
133. Corzo, J. Time, the forgotten dimension of ligand binding teaching. *Biochem. Mol. Biol. Educ.* **34**, 413–416 (2006).
134. Boltaev, U. *et al.* Multiplex quantitative assays indicate a need for re-evaluating reported small-molecule TrkB agonists. *Sci. Signal.* **10**, (2017).
135. Upadhyay, A. K., Murmu, A., Singh, A. & Panda, A. K. Kinetics of Inclusion Body Formation and Its Correlation with the Characteristics of Protein Aggregates in *Escherichia coli*. *PLoS One* **7**, e33951 (2012).
136. Sabate, R., Groot, N. S. De, Villaverde, A., Garcı, E. & Ventura, S. Biological role of bacterial inclusion bodies : a model for amyloid aggregation. **278**, 2419–2427 (2011).